DOCUMENTATION PAGE

Form Approved
OMB No 0704-0188

1. AGENCY USE ONLY (Leave blank)	2. REPORT DATE	3. REPORT TYPE AND DATES COVERED
	1992	THESIS/~~DISSERTATION~~

4. TITLE AND SUBTITLE
Radar Based Case Study of a Northeast Colorado Winter Storm

5. FUNDING NUMBERS

6. AUTHOR(S)
Nicolas S. Powell, Captain

7. PERFORMING ORGANIZATION NAME(S) AND ADDRESS(ES)
AFIT Student Attending: Colorado State University

8. PERFORMING ORGANIZATION REPORT NUMBER
AFIT/CI/CIA- 92-099

9. SPONSORING/MONITORING AGENCY NAME(S) AND ADDRESS(ES)
AFIT/CI
Wright-Patterson AFB OH 45433-6583

10. SPONSORING/MONITORING AGENCY REPORT NUMBER

11. SUPPLEMENTARY NOTES

12a. DISTRIBUTION/AVAILABILITY STATEMENT
Approved for Public Release IAW 190-1
Distributed Unlimited
ERNEST A. HAYGOOD, Captain, USAF
Executive Officer

12b. DISTRIBUTION CODE

13. ABSTRACT *(Maximum 200 words)*

14. SUBJECT TERMS

15. NUMBER OF PAGES
163

16. PRICE CODE

17. SECURITY CLASSIFICATION OF REPORT	18. SECURITY CLASSIFICATION OF THIS PAGE	19. SECURITY CLASSIFICATION OF ABSTRACT	20. LIMITATION OF ABSTRACT

Capt Nicolas S. Powell
3530 Beechwood Ct.
Colorado Springs, CO. 80918
1 June 1992

AFIT/CIR
Wright-Patterson AFB OH 45422-6583

Dear Major Smith,
As required by AFITR 53-1, enclosed you will find:

1. One unbound copy of my thesis
2. Two Copies of the abstract
3. Two copies of the bibliography.

Also, here is the additional title page information required by AFITR 53-1, para 7-7:

Author: Nicolas S. Powell
Title: Radar Based Case Study of a Northeast Colorado Winter Storm
Rank: Captain, USAF
Date: 1992
Pages: 163
Degree: Master of Science, Atmospheric Science
Institution: Colorado State University

Please contact me at the above address or at the Air Force Space Forcast Center, Falcon AFB CO 80912, if you have any questions or I may be of assistance. Thank you for all your assistance.

Respectfully,

Nicolas S. Powell
Captain, USAF

THESIS

RADAR BASED CASE STUDY OF A NORTHEAST COLORADO SNOWSTORM

Submitted by

Nicolas S. Powell

Department of Atmospheric Science

In partial fulfillment of the requirement

for the degree of Master of Science

Colorado State University

Fort Collins, Colorado

Summer 1992

COLORADO STATE UNIVERSITY

May 15, 1992

WE HEREBY RECOMMEND THAT THE THESIS PREPARED UNDER OUR SUPERVISION BY NICOLAS S. POWELL ENTITLED RADAR BASED CASE STUDY OF A NORTHEAST COLORADO SNOWSTORM BE ACCEPTED AS FULFILLING IN PART REQUIREMENTS FOR THE DEGREE OF MASTER OF SCIENCE.

Committee on Graduate Work

Advisor

Department Head

ABSTRACT

RADAR BASED CASE STUDY OF A NORTHEAST COLORADO SNOWSTORM

Radar and conventional meteorological data collected during the 19-20 January 1991 winter storm over Northeast Colorado as part of WISP-91 (Winter Icing and Storm Project) were analyzed to describe observations of snow bands and possible band formation mechanisms. A review of the synoptic situation led to classification of this storm as an anticyclonic type of upslope storm. Single and dual-Doppler radar analyses showed well organized mesoscale snow bands oriented west-southwest to east-northeast, parallel to the 800-400 mb thermal wind, formed during upslope conditions several hours after passage of an arctic cold front over the research area. Embedded within the bands were precipitation cores that propagated along the band with the upper level winds and nearly stationary (band relative) trapped mountain waves. The evolution and structure of snowband kinematic properties were studied by analysis of horizontal and vertical velocity profiles and reflectivity distributions using PPI scans and Extended Velocity Azimuth Display (EVAD) techniques. Various mechanisms were examined for their potential role in formation and maintenance of snow bands. These mechanisms included: conditional instability, Conditional Symmetric Instability (CSI), ducted and internal gravity waves, jet streak circulations, seeder-feeder cloud structures, and terrain induced phenomena such as trapped mountain waves, low level barrier jets, and cold air damming.

Nicolas Stuart Powell
Atmospheric Science Department
Colorado State University
Fort Collins, CO 80523
Summer 1992

ACKNOWLEDGEMENTS

I would like to express my gratitude to my advisor Dr. Steven A. Rutledge, for his advice, and encouragement during this study without which this thesis would not have been possible. I also thank my other committee members, Dr. T. McKee, Dr. R. Rasmussen, and Dr. V. Chandrasekar for their contributions.

Thanks are in order for the Colorado State University CHILL radar staff: Pat Kennedy, Dave Brunkow, Gene Meuller, and Ken Pattison for their unending patience and willingness to answer my questions, as well as act as my hosts during the data collection phase of WISP-91. Doug Burks, Research Associate, CSU Department of Atmospheric Science, provided invaluable assistance to help me learn the computer system and software that was used to analyze and display the data. Ben Bernstein of NCAR/RAP was instrumental in retrieving almost all the other non CSU-CHILL data from NCAR. Dr. Doug Wesley provided many helpful comments and insight into northeast Colorado winter storms. My office mates, Walt Petersen and Rob Cifelli, were the source of much information and were always willing to discuss my research. Jamie Golden of the CSU Visualization Lab helped me put together a videotape radar loop that included terrain data. John Weaver provided the 30 second topographic data. Kim Elmore helped get MHR data from the NCAR Mass Storage System.

Non salary support for this research was provided by National Science Foundation grant ATM-9016798 under the Mesoscale Dynamics Program. Salary and tuition were paid by the U.S. Air Force under the Air Force Institute of Technology Graduate Meteorology program.

Finally, special thanks are due to my wife, Jane, who not only provided constant support and encouragement during study and research, but also accepted with grace the irony that my presence was required at CSU-CHILL on her birthday, the same day as the case described in this thesis.

TABLE OF CONTENTS

LIST OF FIGURES

LIST OF TABLES

Chapter 1

INTRODUCTION

Northeast Colorado winter storms bring a wide range of snowfall amounts with accompanying beneficial to detrimental economic and social impacts. The effects of a heavy snowfall are far reaching and may have national in addition to local impacts when the role of Denver - Stapleton Airport (and the new Denver Airport when completed) as a major airline hub in the nation's air transportation system is considered (Schlatter *et al.* 1983, Reinking and Boatman 1986, Dunn 1988). Though the consequences of a heavy snowfall may be far reaching, the actual distribution of snow can be highly localized. For example, during the Christmas Blizzard of 1982 snow depths varied between over 76 cm (30 in) in the Denver Metropolitan area to less than 5 cm (2 in) over a distance of less than 60 km to the north (Schlatter *et al.* 1983). The orientation of low level winds with respect to topographical features as well as precipitation bands are significant factors in snowfall distribution and amounts (Wesley 1991, Wesley and Pielke 1990).

In view of the important nature of winter storms in the region, the Winter Icing and Storms Project (WISP) was initiated in 1990. In this thesis, data from the WISP-91 (15 January through 31 March, 1991) experiment were used to examine a snowstorm that occurred 19-20 January 1991 with the goals of discussing observations of snow band activity and evaluate formation and maintenance mechanisms. Chapter 2 provides the synoptic and mesoscale meteorological overview incorporating the many assets deployed during WISP-91. Radar data and their analyses, important elements in observation of storm structure and snow bands, is the subject of Chapter 3. Possible

mechanisms for the creation and maintenance of snow bands and a conceptual model are discussed in Chapter 4. Chapter 5 presents conclusions and recommendations for future research.

1.1 General Background

Until recently intense field experiments of winter storms in the United States have been concentrated over the coastal areas of the Pacific Northwest, and Eastern Seaboard with only a small number of experiments, limited in scope, conducted over the mid-continent (Ramamurthy et al. 1991). Hobbs et al. (1980) described the objectives, facilities, and operations of the CYCLonic Extratropical Storms Project (CYCLES), which took place over coastal Washington State and adjacent ocean areas. Numerous papers on a wide variety of topics related to winter storms, including storm kinematics and microphysics, were published under the umbrella of CYCLES research. Similarly, Dirks et al. (1988) and Raman and Riordan (1988) discussed the Genesis of Atlantic Lows Experiment (GALE) occurring off the Mid-Atlantic States.

Literature on major mid-continent winter storm research projects is more limited. Ramamurthy *et al.* (1991) described goals and objectives of the University of Illinois Winter Precipitation Program (UNIWIPP) and listed other important studies on mid-continent winter storm research including works by Carbone and Bohne (1975), Bohne (1975), Heymesfield (1979), Byrd (1989), Moore and Blakeley (1988), and Agee and Gilbert (1989). These authors discussed winter storm activity, including kinematics and microphysics, in the Great Lakes Region and relatively flat land areas of the central plains of the United States.

Winter field projects conducted over the intermountain western United States have been even more limited in scope, and in general were concerned with gaining an understanding of the processes that would lead to precipitation enhancement through weather modification (Rasmussen *et al.*, 1992). The Colorado River Basin Pilot Project

(Marwitz 1980), conducted during the five winter seasons between 1970-75, was designed to evaluate precipitation enhancement potential over the San Juan Mountains of southern Colorado. The Sierra Cooperative Pilot Project (Reynolds and Dennis 1986) was a weather modification experiment performed from 1976 to the late 1980's over the American River Basin in the Sierra Nevada of California. The Colorado Orographic Seeding Experiment (Rauber *et al.* 1986) studied winter clouds over the Park Range of northern Colorado with the goal of developing a weather modification hypothesis. The State of Utah Division of Water Resources and the National Oceanic and Atmospheric Administration (NOAA) Tushar Mountains Cooperative Weather Modification program (Long *et al.* 1990, Sassen *et al.* 1990) is an ongoing study of weather systems over mountainous regions of southern Utah designed to gain more insight into conditions favorable for weather modification. All of the above studies were focused on research into conditions and weather systems favorable for precipitation enhancement. Since the storms most likely to fall into this category would have Pacific origins, these projects were located on the western side of the Continental Divide thus did not address conditions over eastern Colorado.

Despite the lack of large scale field projects over eastern Colorado prior to WISP-91, research has been conducted by several investigators on winter storms over northeast Colorado. Wesley (1991) provides a good summary of significant research on winter storms over the region. Briefly, winter storms generally fall into two categories, deep cyclonic and shallow anticyclonic (Reinking and Boatman, 1986). Deep cyclonic systems encompass easterly flow to levels above 700 mb in response to a deep, stacked low pressure area typically centered over the four corners region of the southwest United States. Anticyclonic systems are characterized by shallow easterly upslope flow over the eastern plains of Colorado occurring in the anticyclonic flow associated with a post-frontal arctic high pressure area. Hybrid systems encompassing

features of both may also occur (i.e. anticyclonic easterly surface flow, low pressure and cyclonic easterly flow aloft; Wesley 1991). Alternatively, climatological studies of heavy snow over eastern Colorado in progress at Colorado State University (CSU) suggest this classification scheme might need modification. The location of a surface low pressure area in the vicinity of the Colorado-New Mexico border, which is a common occurrence in all cases, is a significant factor in snowfall distribution and is a better descriptor of weather type, rather than the cyclonic and anticyclonic classification described above (personal communication, Prof. T. McKee). For the purposes of this paper however, the classification scheme described by Reinking and Boatman (1986) will be used.

1.2 WISP-91 and Data Sources

The Winter Icing and Storms Project in 1991(WISP-91) was the first intensive, highly instrumented field experiment to investigate winter storms and aircraft icing over northeast Colorado. The project evolved from a need to conduct aircraft icing research and a general desire for winter storm study by the research community to an experiment with these two broad goals: "1) *to improve our understanding of the processes involved in the production and depletion of supercooled liquid water content in winter storms and* 2) *to improve forecasts of aircraft icing in winter storms*" (Rasmussen and Politovich 1990). Rasmussen *et al.* (1992) provide an overview of the experiment goals, operations, organization, participation, and instrument platforms. Figure 1.1 shows the location of facilities including the Colorado State University (CSU) CHILL and National Oceanic and Atmospheric Administration (NOAA) Mile High (MHR) radars, forming a dual-Doppler pair used during the experiment, and for this research. Appendix A lists station location information including station callsign, name, latitude,

longitude, and elevation. More details on data collection platforms are available in the WISP-91 Data Catalog (NCAR 1991).

Surface data were collected every minute at the 39 National Center for Atmospheric Research (NCAR) Portable Automated Mesonet (PAM) stations and every 5 minutes at the NOAA Prototype Regional Operational Forecast System (PROFS) surface mesonet stations in addition to the hourly and special observations taken at National Weather Service (NWS), Department of Defense, and Federal Aviation Administration weather stations. Complementing the twice daily NWS rawinsonde network observations were those taken at 3 hour intervals at the NCAR Cross-chain Loran Atmospheric Sounding System (CLASS) sites between 1800 UTC 19 January and 2100 UTC 20 January. Radar volume scans were completed about every 10 minutes. Wind profiler data were available every 20 minutes. Given the large variety of meteorological sensors used during the experiment and the volume of data obtained for this case study, many analyses and display techniques were used to evaluate the data. Appendix B describes some of those techniques and software used or developed.

Participation in the data collection phase of WISP-91 at the recently installed CSU CHILL 10 cm Doppler radar just north of the Greeley airport, offered the chance to view each case and make an immediate estimation of its suitability for further study. The case of 19-20 January 1991 was selected on the basis of data quality and the highly banded structure of the observed echoes. Using the Boatman and Reinking (1986) scheme, this case is best classified an anticyclonic upslope event since precipitation did not begin until well after passage of the surface cold front where the region was under the influence of an arctic high pressure area. Chapter 2 provides a detailed meteorological overview of the storm using the WISP-91 data set collected for those days.

1.3 Northeast Colorado Topography and Climate Controls

The WISP 91 data set provided a unique opportunity to examine in detail the role of terrain features on winter storms over northeast Colorado. Previous studies by Dunn (1988), Wesley and Pielke (1990), Wesley (1991), Wesley *et al.* (1990), and Toth (1987) made use of the NOAA Prototype Regional Operational Forecast System (PROFS) surface mesonet which has greater resolution than the standard airport observing networks. As Figure 1.1 shows, the addition of 39 PAM stations extended the network and filled gaps in the coverage with respect to the complex terrain found in the region.

The rapid terrain rise of the Rocky Mountain Front Range coupled with arctic airmass outbreaks over the central United States create a climatology unique from that of the rest of the United States. Figure 1.2 is a topographical map of eastern Colorado showing the complicated terrain variations from the eastern plains to the Continental Divide. Several features merit notice: the major west-east extensions of higher terrain embodied by the Cheyenne Ridge near the Wyoming border and the Palmer Divide south of Denver, and the rapid increase of terrain elevations found along the Front Range. The two west-east divides separate three major river drainage basins. The North Platte River flows north of the Cheyenne ridge, the South Platte River Basin lies between the Cheyenne Ridge and Palmer Divide, while the Arkansas River runs south of the Palmer Divide. These extensions of elevated terrain significantly modify precipitation distribution over eastern Colorado. The Christmas Blizzard of 1982 is an excellent example of how these extensions can affect snowfall over the region (Schlatter *et al.* 1983).

Climate controls for the eastern plains and Front Range of Colorado differ significantly from those governing the Piedmont on the eastern approach to the Appalachian Mountains (Lilly 1981). Foremost in these differences is the lack of a

relatively warm ocean and maritime airmass to the east. Continental arctic air can plunge southward out of Canada into the central United States unhampered by terrain barriers. Colorado terrain is significantly higher both over the plains to the east and the mountains to the west than comparable regions of the Appalachians and adjacent Piedmont. In general, snow over eastern Colorado occurs after a cold front passes or development of low pressure near the Colorado-New Mexico border and requires easterly flow to lift moist air having origins in the Gulf of Mexico against the Front Range of the Rocky Mountains. The depth of the easterlies combined with the location and speed of storm scale dynamics, with respect to terrain, governs the location, duration, and amount of snow (Reinking and Boatman 1986). However, there are cases where strong, moist westerly flow aloft over a deep, extremely cold arctic airmass with weak easterly surface flow can cause prolonged heavy snow, contrary to the popularly held opinion that heavy snows result from deep easterly flow (Wesley *et al.* 1990).

1.4 Precipitation Bands

Precipitation bands are a commonly observed mesoscale feature of nearly all winter storms, including those of northeast Colorado (Rasmussen *et al.* 1992). Extensive studies of precipitation bands were conducted during CYCLES. Six types of rainbands were identified and classified as: warm frontal, warm sector, wide cold frontal, narrow cold frontal, prefrontal cold surge, and post frontal (Matejka *et al.* 1980). Prefrontal cold surge bands need not be considered here since snow bands discussed later occurred after the cold front passage. Studies of precipitation bands were also published as part of GALE (Emanuel 1988) and the UNIWIPP experiment (Shields *et al.* 1991). Discussion of precipitation bands over northeast Colorado has been limited to a few studies described below.

Hobbs *et al.* (1980) discussed the organization of cold front precipitation bands. They identified three types of bands, the warm sector (or prefrontal) band, wide cold-frontal bands, tens of kilometers in width straddling the front, and narrow cold-frontal bands, approximately 4 km wide, located at the surface frontal boundary. As before, the warm sector band is of no interest here since this study focused on the period after cold front passage. All wide cold-frontal bands observed by Hobbs *et al.* (1980) were oriented parallel to the front and moved in the same direction as the front though at a greater speed. Occasionally wide cold-frontal bands were observed to overtake the surface front.

The mesoscale and microscale organization and structure of narrow cold-frontal rain bands observed during CYCLES were described in detail by Hobbs and Persson (1982). They found the band was comprised of heavy precipitation cores, ellipsoidal in shape, with an average orientation angle of 29° between the synoptic scale cold front and the long axis of the precipitation core, and gap regions of lighter precipitation. The cores moved with the speed of the front but also had a component of velocity parallel to the frontal boundary. Leading edges of core regions were also marked by strong low level convergence and upward vertical motions on the order of 1-10 ms^{-1}. Modeling studies by Rutledge and Hobbs (1984) indicate that rapid growth of ice crystals by riming in the strong updraft of the narrow cold-frontal rainband is responsible for precipitation (which can exceed 100 mm h^{-1}).

Wave-like warm-frontal rain bands observed during CYCLES were found in advance of and parallel to the warm front (Herzegh and Hobbs 1980). Typically, these bands are the result of a seeder-feeder mechanism where ice crystals fall from shallow, upper level convective cells located in potentially unstable air ($\partial\theta_w/\partial z < 0$, where θ_w is wet-bulb potential temperature, and z is height), and scavenge cloud water in lower level stable cloud layers (Matejka *et al.* 1980, Houze *et al.* 1981). Simulations by

Rutledge and Hobbs (1983) of two warm-frontal types (extensive area of weak vertical velocities and strong mesoscale ascent over a more limited area, respectively) indicate that in the first case seed crystals grow by vapor deposition, while in the second they grow by riming.

Studies of precipitation bands from other regions have been more limited in scope than the CYCLES experiment. Furthermore, more attention was given to the role of conditional symmetric instability (CSI), first proposed by Bennetts and Hoskins (1979) and investigated further by Emanuel (1983a, b). Reuter and Yau (1990) examined seven cases of banded precipitation during the Canadian Atlantic Storms Program and concluded that slantwise convection may have been a factor in producing precipitation bands in the vicinity of Atlantic low pressure areas passing south of Nova Scotia. Wolfsberg *et al.* (1986) studied precipitation bands on the order of 50-100 km in width that occurred in a New England winter storm and found that they paralleled the thermal wind, characteristic of CSI. However, they concluded that other factors also contributed to CSI in forming and maintaining the bands including frontogenetical forcing. Mesoscale bands were observed in the coastal front during a GALE case study conducted by Riordan (1990). These bands were attributed to frontogentic forcing, differential heating, and differences in land-sea friction. Shields *et al.* (1991) identified three types of snow bands in a winter storm over east-central Illinois during UNIWIPP. They concluded that two narrow intense bands early in the storm were the result of surface convergence along a narrow confluence zone associated with the remnants of a weak surface warm front. The second type of band was a result of surface convergence in the vicinity of an inverted pressure trough. Multiple parallel bands forming in the later stages of the observation period were the result of CSI from destabilization caused by frontogenetic forcing. Byrd (1989) performed a composite analysis for 27 winter overrunning precipitation events over the southern Great Plains and found CSI could be

a forcing mechanism in the majority of the cases he classified as banded and strongly banded. Lindzen and Tung (1976) proposed ducted gravity waves have a roll in the development and maintenance of precipitation bands observed in association with convective storms.

Within widespread precipitation regions of northeast Colorado winter storms, heavier snowfall has been observed to coincide with mesoscale bands having an assortment of orientations (Rasmussen et al. 1992). Lilly (1981), presented radar observations of bands parallel to the mean wind vector. Dunn (1988) examined a large band associated with a September snowstorm over northeast Colorado. He found that orographic influences were unimportant in this case and that CSI coupled with ageostrophic jet streak and frontogenetical circulations led to the conditions necessary for formation of the band. Wesley and Pielke (1990) observed banded structure in two cases. Similarities in the data between their cases and that of Wolfsberg *et al.* (1986) (i.e. bands parallel to the thermal wind vector, similar sounding structure, and radar observations) lead them to conclude that CSI could have been a factor in band formation. However, they also raised the question of the roles played by other mechanisms such as low level convergence zones, mountain-induced gravity waves, and lee waves. Rasmussen *et al.* (1990) documented a case of snow bands that were not parallel to the thermal wind thus failing one of the qualitative tests for CSI. Their modeling studies indicate that a density current propagating southward with a cold front was the mechanism responsible for band growth.

In summary, mesoscale precipitation bands are frequently observed in winter storms. A large body of evidence suggests that CSI may play significant role in the formation and maintenance in these bands. However, other mechanisms might also be important contributors to snow bands over northeast Colorado. They include: low level convergence zones, low level barrier jets (Wesley 1991), conditional instability, ducted

gravity waves, mountain or lee waves, upslope induced vertical motions, density currents, and upper level jet streaks. These phenomena will be evaluated in greater detail for their role in band formation with respect to this case in Chapter 4.

1.5 Radar Data

Radar has played a vital role in the observation and analysis of winter precipitation bands, including the studies cited above. Several other studies merit attention here. Szoke (1991) described the use of the MHR in an operational setting where snow bands were observed over the Denver metropolitan area and corresponded to regions of heavier precipitation. Heckman and Dulong (1989) showed there was a good relationship between northeast Colorado snow band orientation and movement with the 500 mb height and wind fields respectively. Sanders (1986) investigated a major New England snow band associated with rapid development of an offshore low pressure area. He found frontogenetic forcing was the most important factor in band development.

Radar data analysis techniques vary from simple, qualitative examination of Plan Position Indicator (PPI) and Range Height Indicator (RHI) displays to dual-Doppler studies and are summarized by Battan (1973) and Doviak and Zrnic (1984). Most existing studies of snow bands used single-Doppler analysis techniques. However, Heymsfield (1979) performed a dual-Doppler analysis of precipitation bands parallel to a warm front moving over Chicago to investigate the three dimensional structure of the bands. The bands were oriented perpendicular to the mid level flow, contrary to bands examined in this case where they paralleled the upper level winds. Dual-Doppler study of snow bands near Champaign, Ill was conducted by Bohne (1979). The bands formed in the rear of a cyclone and in general were perpendicular to the flow, but moved in the direction of the flow. Kessinger and Lee (1991) describe an operational dual-

Doppler analysis technique used during WISP. In general, the literature contains little on dual-Doppler studies of snow bands, especially over northeast Colorado. Dual-Doppler analysis was performed on one volume scan in this case to examine the kinematic structure of small scale snow bands.

In this study single-Doppler analysis provided information on the larger scale organization and the movement of the storm system, major snow bands, and precipitation cores. The velocity-azimuth (VAD) display developed by Browning and Wexler (1968) has been used to investigate the kinematic structure of horizontal wind fields in winter storms (Lilly 1981, Wolfsberg *et al.* 1986, Sanders and Bosart 1985b, Sassen *et al.* 1990). Here, an attempt was made to use the extended velocity-azimuth display (EVAD) technique (Srivastava *et al.* 1986, Matejka and Srivastava, 1991) to retrieve estimates of mesoscale vertical motion. The results of radar observations and analyses are presented in Chapter 3.

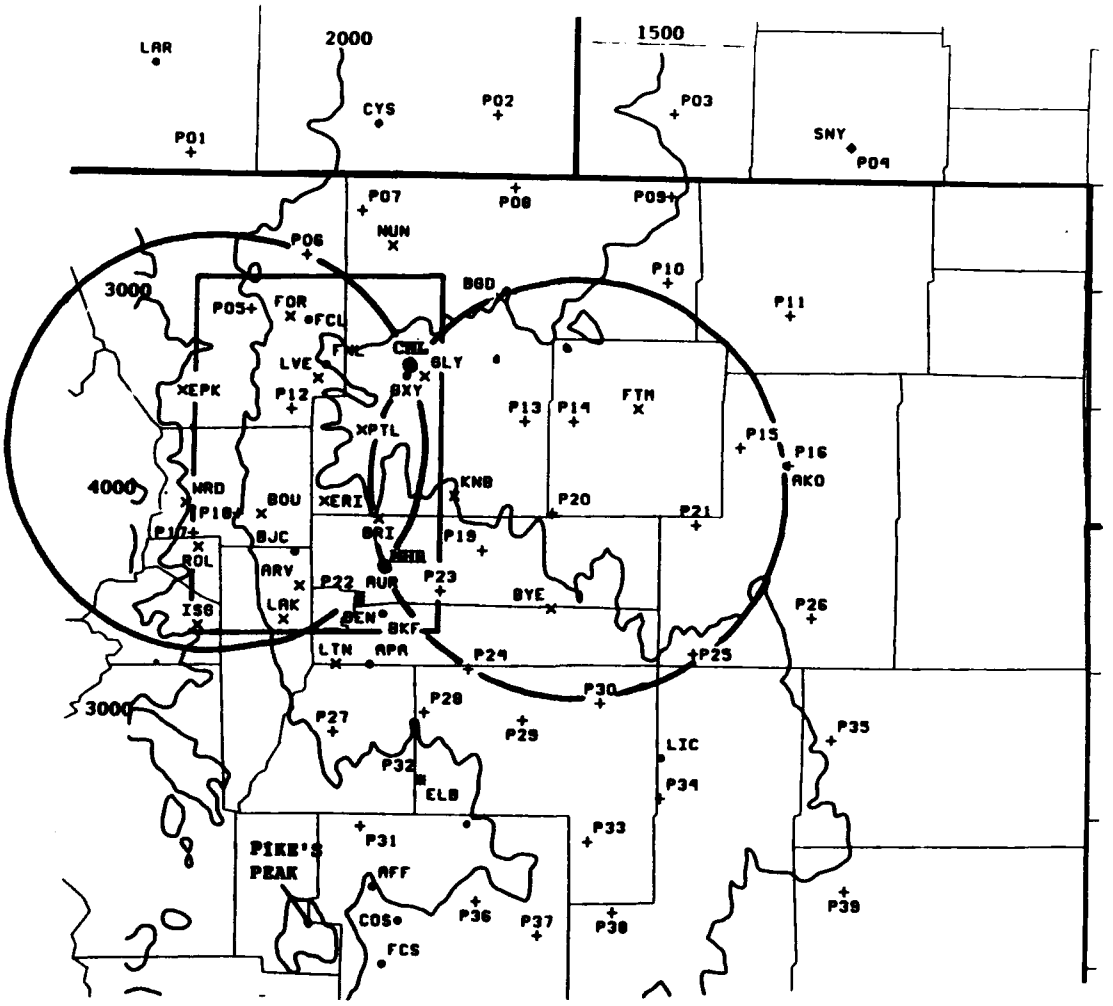

Figure 1.1: WISP-91 Instrumentation locator map. Dots, crosses, and X's represent Surface Airway Observation network stations, PAM stations, and PROFS stations. respectively. CSU-CHILL and Mile High radars (indicated by CHL and MHR) dual-Doppler 30 degree crossing angle lobes are the large circles. Dual-Doppler analysis is the rectangular region. CLASS soundings were taken at PTL, P03, P12, P14, P16, P32, P35, and near P10. Wind Profilers and microwave radiometers were located at PTL and DEN and PTL, DEN and P32 respectively. Terrain contours are in meters.

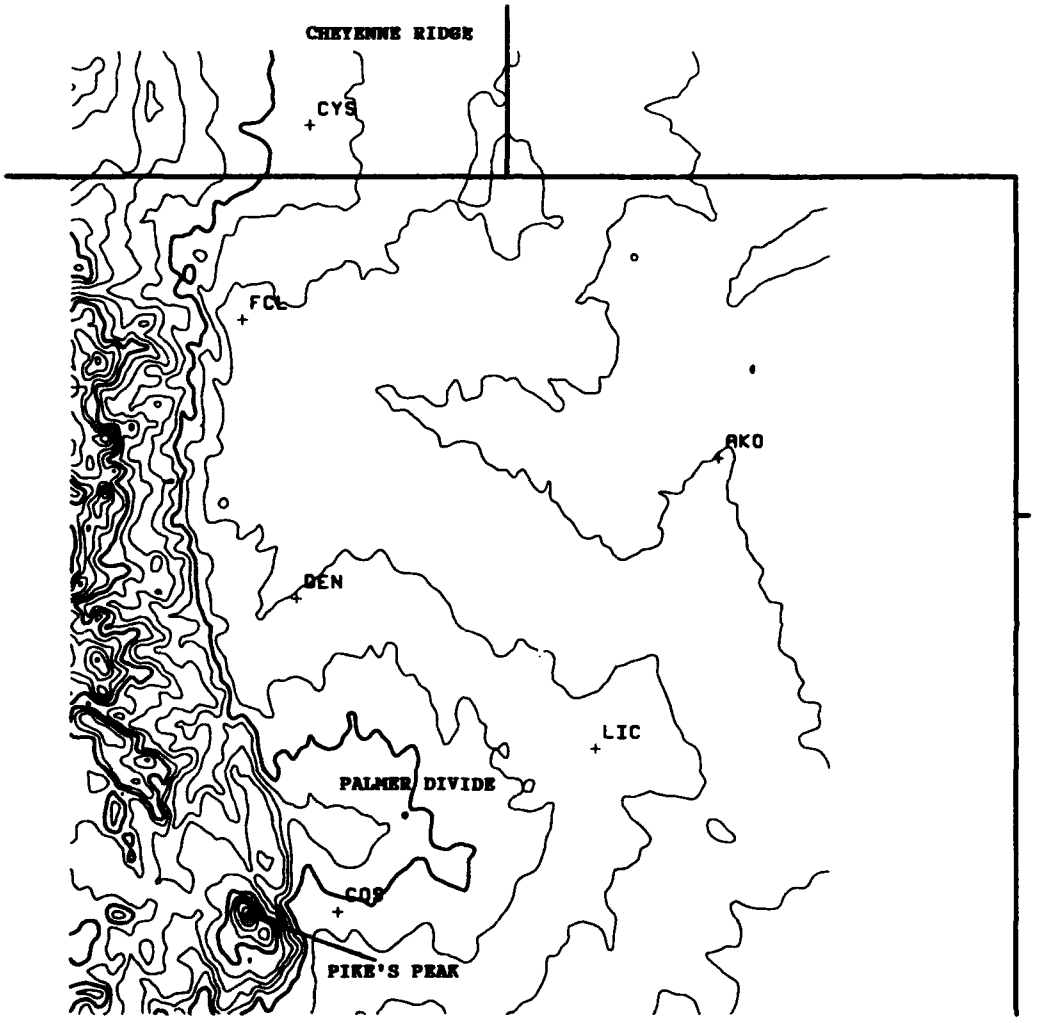

Figure 1.2: Terrain height contours every 200 m for northeastern Colorado. The 2000, 3000, and 4000 meter contours are indicated by bold lines. Major Surface Airway Observation network stations are also shown.

Chapter 2

METEOROLOGICAL ANALYSIS

This chapter describes the synoptic and mesoscale situation prior to and during the snowstorm of 19-20 January 1991. In general, an arctic cold front moved through eastern Colorado leaving anticyclonic upslope flow conditions favorable for the initiation of snow (Boatman and Reinking 1984, Reinking and Boatman 1987, Toth 1991, Wesley 1991). Observations showed snow started over most of northeast Colorado around 2100 UTC 19 January and ended by 1200 UTC 20 January. Total snowfall ranged between less than 2.5 cm (1.0 in) to more than 15 cm (6.0 in) with liquid water equivalents between .03 cm (0.01 in) and .75 cm (0.30 in). Figures 2.1 and 2.2 show snowfall and liquid water equivalent contours respectively, obtained from the special WISP-91 snow spotter observer network sites (Wesley 1991), and National Weather Service, Federal Aviation Administration, and Department of Defense weather stations. Note the three distinct snowfall maxima: the tongue extending from the Fort Collins area across Weld County and into Morgan County, the region north of Denver, and area over the eastern Palmer Divide. A radar loop of Mile High radar scans and surface observations suggest that topographic influences on the low level flow regime played a significant role in the initiation and maintenance of heavier snowfall over the Denver region and the maximum near Fort Collins. For the other region, the upper level flow regime played a more important role, particularly over the Palmer Divide where a well defined snow band was present. More discussion of these two flow regimes and radar observations will be given in chapter 3.

Unlike the arctic outbreak case examined by Wesley (1991) which occurred over 5 days, no more than 18 hours elapsed from frontal passage until the end of the upslope generated snow. Also, there were other departures from the anticyclonic upslope situation described by Boatman and Reinking (1984). These differences are addressed below and in Chapter 3.

2.1. Upper Air

A strong, vigorous shortwave in the upper atmosphere and associated arctic surface cold front moved southeast out of Canada on 19 January passing to the east of Colorado by 1200 UTC 20 January. The upper level shortwave trough had its origins over the North Pacific but came in phase with a polar low pressure area west of northern Greenland that had a southeast extension over Hudson Bay. National Meteorological Center (NMC) 500 mb analyses (Figs. 2.3a-d) for 19 and 20 January revealed the evolution and movement of the upper level trough. During this period, the Denver 500 mb height decreased 180 meters, while the 1000-500 mb thickness decreased from over 5520 to less than 5280 meters. Thermal wind analyses were constructed for various combinations of sounding levels. Figure 2.4 is representative of these analyses and indicated a southwest to northeast orientation to the 800-400 mb thermal wind. Radar observed precipitation bands (described in Chapter 3), particularly above the boundary layer, paralleled the thermal wind, characteristic of conditional symmetric instability (CSI) (Sanders and Bosart 1985).

NMC vorticity analyses for the period (not shown) indicated a well defined vorticity maximum associated with the shortwave trough moved across the state from the northwest corner to the southeast corner between 0000 and 1200 UTC 20 January. Northeast Colorado was in an area of positive vorticity advection by 0000 UTC 20

January. The 500 mb temperatures over Denver decreased 12°C from -18 to -30°C, during the period which indicated strong cooling aloft.

Winds increased and backed with time as the jet stream migrated over the region between 0000 UTC 19 January and 1200 UTC 20 January and was reflected in the NMC 300 mb analysis for the period (Figs 2.5a-d). Two branches of the jet stream were visible at 0000 UTC 19 January 1991 with split flow around the low pressure area over Texas. A strong jet streak at 1200 UTC 19 January 1991 associated with the shortwave over Idaho and western Washington weakened and shifted eastward by 0000 UTC 20 January 1991. Meanwhile, the southern branch of the jet stream shifted northward and merged with the northern portion of the split flow as the 500 mb low pressure area weakened over Oklahoma. At 0000 UTC, during the height of the storm, northeast Colorado was not in either the classic left-exit or right-entrance quadrant region of a well defined jet streak, the favored region for heavy snow (Dunn 1988). Examination of the higher temporal and spatial resolution offered by the 300 mb CLASS sounding plots (Fig. 2.6a-d) supports this conclusion. Reinking and Boatman (1986) suggest that precipitation generated by terrain induced upward vertical motions of the arctic airmass can occur, despite subsidence associated with the left-entrance region of jet streaks. Furthermore, temperature advection can modify the favored locations of jet streak induced midtropospheric vertical motion (Keyser and Shapiro 1986).

Time series of the Platteville and Denver windprofilers (Figs. 2.7a-b) depict the vertical structure of horizontal winds at every hour between 1200 UTC 19 January and 0600 UTC 20 January 1991. Several features can be seen:

1. A wind maximum was present in the lower levels of the Platteville profiler in the early observations prior to passage of the surface cold front, indicating the presence of moderate downslope winds. This was confirmed by surface observations at Fort Collins where a gust of 25 ms^{-1} from the west was recorded at 1255 UTC.

2. An upper level wind maximum crossed the region between 2000 UTC 19 January and 0300 UTC 20 January.

3. The 20 minute resolution Denver profiler plot (Figure 2.7b) showed deepening and backing of low level northeasterlies associated with the surface arctic airmass. This was also visible in the CLASS time series (Figures 2.14a-d).

4. Winds increased with height and had very little directional shear above the boundary layer. Both these conditions are qualitative indicators of conditional symmetric instability (Snook 1992; Wolfsberg *et al.* 1986).

Examination of the 700 mb moisture field (see Figs 2.8a-c) showed a significant portion of the storm moisture was carried along with the upper level trough. Dewpoint depressions at 0000 UTC 19 January (Fig. 2.8a) over most of the western U. S. were greater than 12°C while those in the vicinity of the upper level trough, while variable over space, were less than 10°C. These lower dewpoint depressions associated with the trough could be traced back to even earlier NMC analyses (not shown). Figs. 2.8b-c show the moisture at 700 mb moved with the trough. Dewpoint depressions were slightly lower at 500 mb and were probably the result of moisture advected from the upper level low pressure area that moved over California (see Figs 2.3a-d). Minimum mid-level dewpoint depressions were actually above the 500 mb mandatory reporting level on the Denver and Grand Junction 1200 UTC 19 January soundings (Figs 2.9a-b). This elevated moisture region was also visible on the 1800 UTC 19 January Berthoud CLASS sounding (Fig 2.10a). Boatman and Reinking (1984) point out the need for relatively moist Pacific air to cross the Rocky Mountains and Colorado Front Range for cloud enhancement (and greater snowfall) above the shallow arctic airmass over the Eastern Plains. In this case, the cross mountain moisture requirement was actually satisfied by complex interaction of the two distinct sources described above.

By 0000 UTC 20 January the entire airmass had approached saturation up to the tropopause, which lowered nearly 70 mb in 6 hours at Berthoud (see Figs. 2.10a-b). Similar reductions in the tropopause height occurred at all CLASS stations. The 0000 UTC Akron and Elbert CLASS soundings (Figs, 2.10c-d) resembled the Berthoud sounding with the exception of a shallower cold air depth at Elbert. Comparison of the pressure at the top of the arctic airmass inversion recorded in the Berthoud and Akron soundings suggested observational verification of Wesley's (1991) description of a vertical bulge in the western edge of the arctic air mass. A greater easterly wind component in the boundary layer would have made this feature more pronounced and possibly enhanced precipitation near the Front Range (see Wesley 1991).

Auer and White (1982) found that a 600 mb temperature between -12 and -16°C was a common characteristic in 75 heavy snow events. They deduced heavy snow will occur when the temperature regime of maximum crystal growth by vapor deposition in a water saturated environment (between -12 and -16°C) coincides with maximum vertical velocities associated with the level of nondivergence (approximately 600 mb). All 0000 UTC 20 January CLASS soundings had 600 mb temperatures between -12 and -16°C which agreed with the findings of Auer and White. While heavy snow did occur in this case, the distribution was uneven (see Fig 2.1) reflecting the role of other processes (e.g. snow bands, terrain effects, etc.) in local snowfall amounts.

2.2 Vertical Cross Sections

Cross sections in space and time of various data and parameters were constructed to gain understanding of the thermodynamic structure of the atmosphere during this precipitation event. Figure 2.11 shows the two 0000 UTC 20 January vertical cross section transects discussed in this section as well as the low level winds at the stations in Northeast Colorado. The arctic airmass was visible as the tighter packing of isentropes

in the lower levels of Fig. 2.12a , and between DEN and LBF (see Appendix A for a listing of station identifiers, names, and location information) in Fig. 2.12b. The cross section planes in Figures 2.12a and 2.12b were oriented approximately perpendicular and within 30 degrees of parallel to the low level winds respectively. In the lower levels these cross sections were similar to those of Boatman and Reinking (1984), with the exception that isentropes sloped downwards between BTD and DEN. Additionally, above the arctic airmass, a tendency towards lower potential stability values reflected a more vigorous shortwave aloft than observed by Boatman and Reinking (1984). Figure 2.12a also shows that the arctic airmass had just passed Dodge City as reflected in the position of the surface front in Fig. 2.15b.

Examination of the time series plots of equivalent potential temperature at the CLASS stations Akron (AKR), Wiggins (WIG), Berthoud (BTD), and Flagler (FLA) (Figs. 2.13a-d) showed conditional instability near the surface at BTD and FLA, and a trend towards instability above 600 mb in all cross sections. Increasing relative humidities in the cross sections were more the result of cold air advection rather than significant moisture advection. The CLASS sounding data showed only slight increases in the dewpoint temperature profiles, whereas there was significant cooling through the depth of the atmosphere with the passage of the surface cold front and subsequent arrival of arctic air in the low levels, and cold air advection associated with the upper level trough above the arctic airmass.

Whiteman (1973) states that over the high plains, relative humidities near 85% define regions of cloudiness and anticyclonic storms are often characterized by abrupt decreases in humidity (increased dewpoint depressions) at cloud top as opposed to the more gradual dewpoint depression increases in height associated with deep cyclonic storms. Dewpoint depressions in the CLASS soundings (Figs. 2.10b-d) increased dramatically at the tropopause above the 400 mb level indicating a distinct cloud top,

lending support to the conclusion that this storm can be classified as anticyclonic (Rasmussen *et al.* 1992).

It has been proposed that given the proper orientation of the upper level flow with respect to the frontal boundary aloft, upward vertical motion may occur in the flow just above the boundary up to several hours after passage of a shallow sloped surface cold front (personal communication, Dr. R. Rasmussen, 1992). This might help explain the lag in cloudiness and precipitation after passage of the surface cold front often observed with winter storms over northeast Colorado. A rough approximation of the frontal slope in this case was obtained by taking an average of the vertical displacements of equivalent potential temperature surfaces near the top of the arctic airmass from the New Raymer and Elbert 0000 UTC 20 January CLASS sounding data. The New Raymer Elbert axis is approximately parallel to the direction of movement experienced by the low level arctic airmass. The average vertical displacement was 500 m across a horizontal distance of 165 km. This yields a slope of approximately 3.03×10^{-3} or an angle of 0.17° for the arctic airmass which had an approximate depth of 1500 m and top between 3400-3900 m MSL over northeast Colorado. If the winds above the top of the boundary were from 260 degrees at 15 ms^{-1} (see Fig. 2.10b-d), and the axis of the frontal slope was oriented 030-210° (increasing in height towards 030°), then 15 ms^{-1} x cos 50°, or 9.6 ms^{-1} will represent the component of the wind forced upward along the frontal surface. If the frontal surface was moving at a speed of 17 ms^{-1} (see section 2.3), then the vertical velocity induced by the upper level wind flowing up the arctic airmass boundary will be (9.6 + 17) x sin 0.17°, or 0.08 ms^{-1} (8 cm s^{-1}). This is probably close to a theoretical maximum as it is likely that the airmass had slowed to less than 17 ms^{-1}. As described in section 2.3, the surface front was well through northeast Colorado by 0000 UTC. Thus, the data suggest that conditions were favorable for weak vertical ascent of the upper level winds which may help explain the lag in the onset of cloudiness and precipitation.

2.3 Surface

In response to the advance of the upper level trough of low pressure described above, a surface low pressure area and associated frontal system developed in Alberta. The low pressure area skirted the northern tier states while the cold front moved rapidly south out of Canada, through the northern plains states, and into Northeast Colorado over an 18 hour period. This represents an average speed of nearly 60 km hr^{-1} (or ~17 ms^{-1}). According to Reinking and Boatman (1987) this sequence of events is typical for anticylconic upslope conditions over Northeast Colorado. However, at the same time a trough of low pressure over eastern Colorado and the subsequent development of a surface low pressure area over southeast Colorado in response to the upper level trough, strengthened the post frontal pressure gradient over the eastern plains. This aided in the development of upslope flow rather than having to rely on post frontal anticyclonic flow alone. Figs. 2.15a-b show the surface synoptic situation as analyzed by the National Meteorological Center (NMC) at 1200 UTC 19 January and 0000 UTC 20 January 1991. They illustrate the speed with which the front moved and development of the southeast Colorado low pressure area. Prior to frontal passage northern portions of the Colorado front range experienced downslope wind conditions with gusts to 25 ms^{-1} in response to the surface pressure gradient between high pressure over Utah and a lee side trough over eastern Colorado and western Kansas.

Time cross sections were plotted for all PAM and PROFS stations used in the experiment. The Greeley cross section (Fig. 2.15) is typical of conditions experienced at most stations before, during, and after frontal passage. In this case there was no dramatic rise in pressure and only a moderate temperature decrease, which contrasts with the cases described by Marwitz and Day (1991), Wesley (1991), and the dramatic example of Shapiro (1984) where rapid temperature decreases occurred shortly after

frontal passage. A similar gradual surface temperature decrease occurred in the case described by Dunn (1987). However, in that case surface winds had a much greater easterly component which lead to cold air damming and the development of a strong convergence zone, or meso-front, some distance away from the rapidly rising terrain of the Front Range. The greatest temperature falls in the case studied here took place over an hour after the 1900 UTC frontal passage, as indicated by a wind shift and increased windspeeds. Snow began around the time that the temperature - dewpoint spread decreased significantly. The Greeley Airport weather observer took a special observation for snow at 2124 UTC which is shortly after the large dewpoint rise. At 2146 UTC the Denver Airport National Weather Service Forecast Office reported snow. It continued there until 1041 UTC 20 January with the heaviest amounts falling between 2200 UTC 19 January and 0600 UTC 20 January. Radar data showed that the onset of snow was rapid, occurring over most of Northeast Colorado within a short time around 2100 UTC, except for a region in the northeast portion of the radar coverage area where snow began shortly after frontal passage. Surface data indicated that dewpoints decreased at a slower rate than the temperature after frontal passage which suggests that cold air advection rather than influx of moisture laden air from some other region was the cause for increasing low level humidities after frontal passage. This cooling process, in conjunction with similar cooling described in section 2.1, took several hours which offers a partial explanation for the lag in precipitation after passage of the surface front..

Unlike the cases described by Wesley and Pielke (1990), Dunn (1987), and Wesley (1991), there was no evidence to support an argument for cold air damming. No distinct cold pool along the foothills and adjacent plains was present in the isotherm analyses (see Fig 2.16 for example). However, colder temperatures occurred over the higher, mountainous terrain to the west and well into the arctic airmass to the north. Also, there was no indication of a barrier jet, common in extreme cases of cold air

damming (Wesley and Pielke 1990, Wesley 1991), in the wind profiler (see Figs. 2.7a-b) or surface wind data.

Figure 2.17 shows a typical streamline and isotach pattern over the region during the storm. Note the only evidence of a confluence zone, and thus meso-front as described by Wesley and Pielke (1990), Wesley (1991), Boatman and Reinking (1984), and Dunn (1987) was over the area south of Denver and near the western portions of the Palmer Divide. Pure upslope flow was a significant factor in low-level upward vertical motion, especially over the Palmer Divide (and a small region near Fort Collins). Assuming there is an average 700 m rise in terrain over a distance of approximately 125 km from the Platte River Valley east of Greeley to the ridge of the Palmer Divide near PAM station P31, upslope winds with an upslope component of 7 ms^{-1} (or ~25 km hr^{-1}) would lead to a vertical velocity of nearly 4 cms^{-1}. Therefore, upslope flow and low-level convergence may partially explain the higher precipitation over the region south of Denver. Also, easterly flow in the vicinity of Fort Collins provided strong upslope flow and probably played an important role in causing heavier snowfall in that region. Other factors (e.g. seeder-feeder mechanism, CSI, etc.) that may have also been responsible for the formation and maintenance of snow bands observed by radar and responsible for the uneven distribution of precipitation will be explored in later chapters.

2.4 Summary

Anticyclonic upslope flow in the wake of an upper level trough of low pressure and associated frontal system, and enhanced by the development of a surface low pressure area in southeastern Colorado, brought 5-10 cm of snow (over 15 cm in few locations) to Northeast Colorado. The system appeared to have two distinct moisture sources in the upper atmosphere, one near 700 mb that traveled with the trough and the other having origins in an upper level low pressure area over California. Cold air

damming and a barrier jet were not present during this storm. There was some confluence in the wind south of Denver, as well as upslope conditions near Fort Collins, but this does not fully explain the precipitation distribution pattern or the highly banded structure of the precipitation observed by radar.

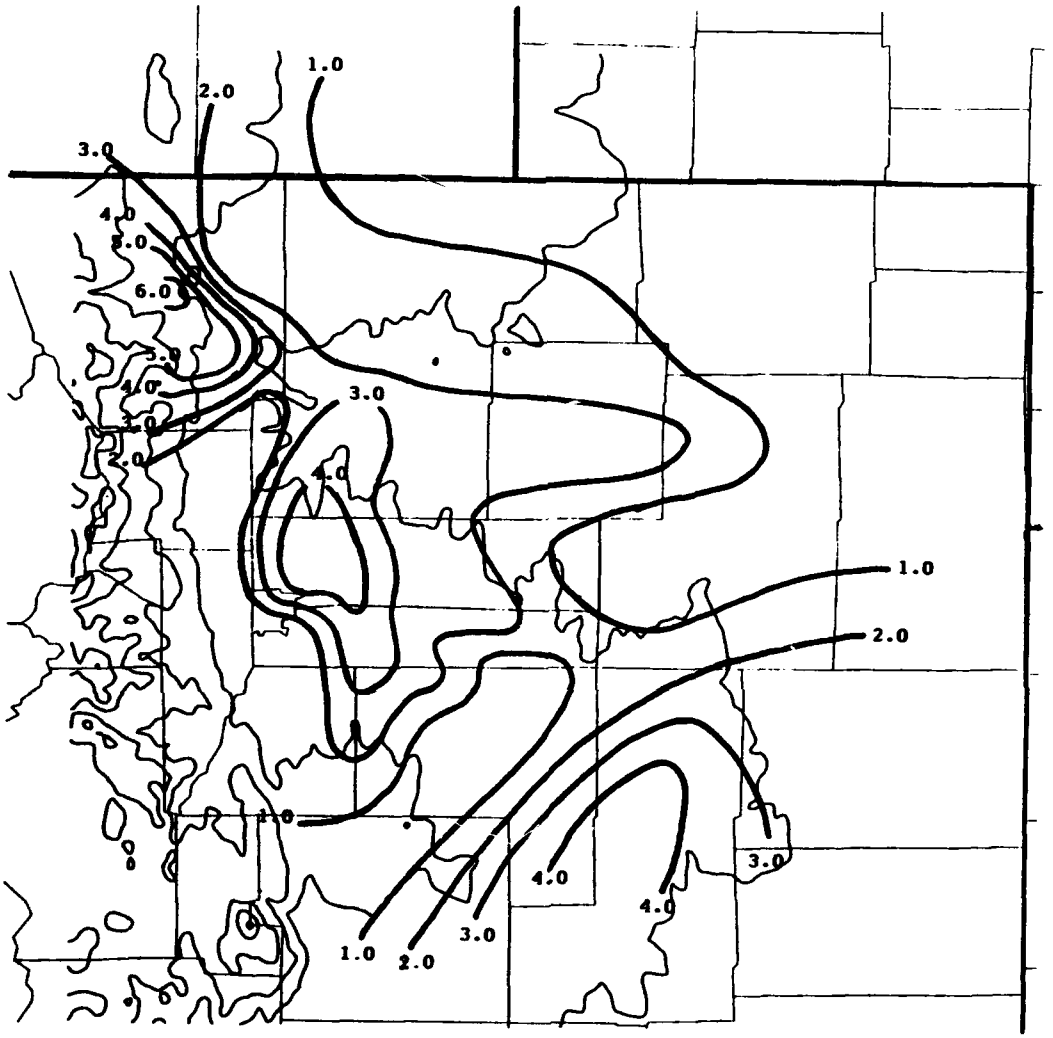

Figure 2.1: Total snowfall distribution (in) over Northeast Colorado 19-20 January 1991. Terrain height contours are every 500 m.

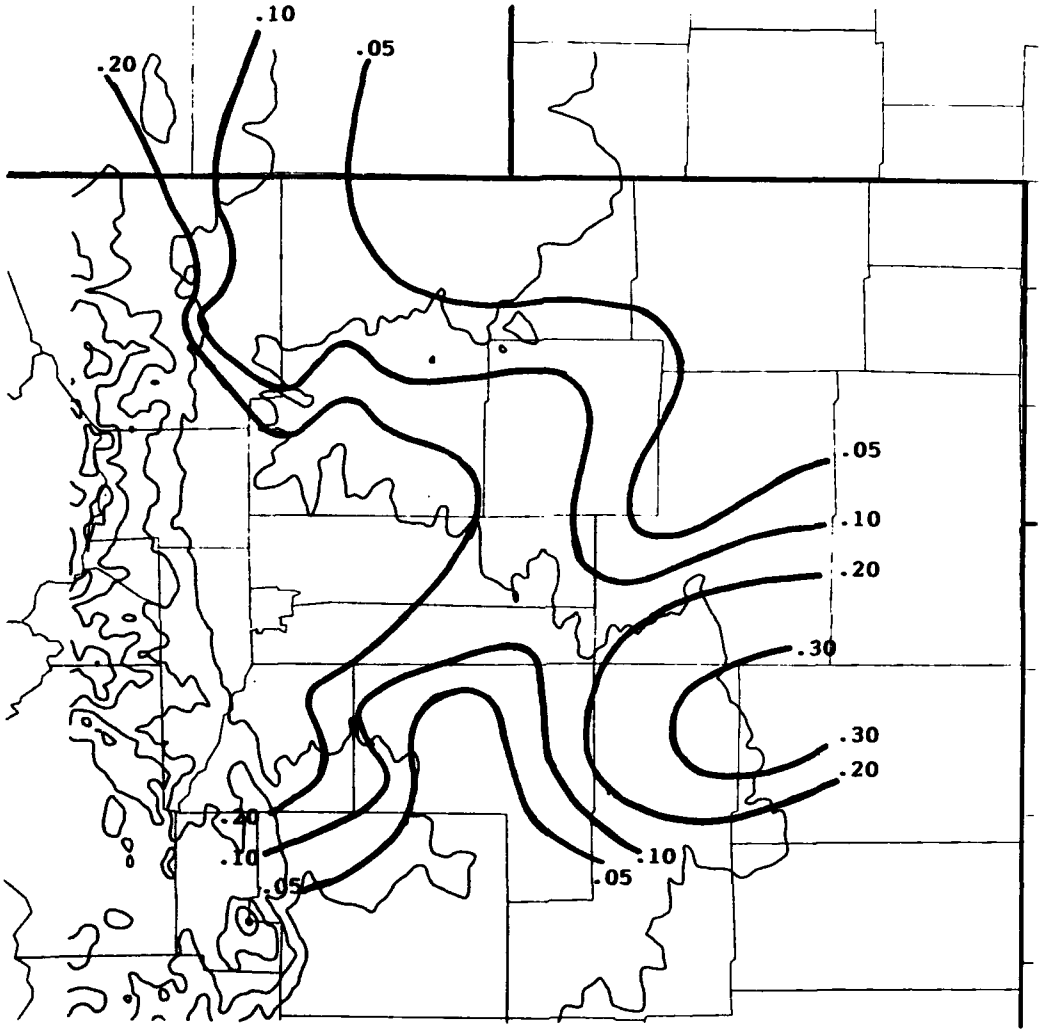

Figure 2.2: Total liquid water equivalent (in) over Northeast Colorado 19-20 January 1991. Terrain height contours are every 500 m.

Figure 2.3: (a) National Meteorological Center (NMC) 500 mb analysis for 0000 UTC 19 January 1991. Solid lines are height contours in dm and dashed lines are isotherms in °C. Full barbs and half barbs on wind shafts represent 5 ms^{-1} and 2.5 ms^{-1} respectively.

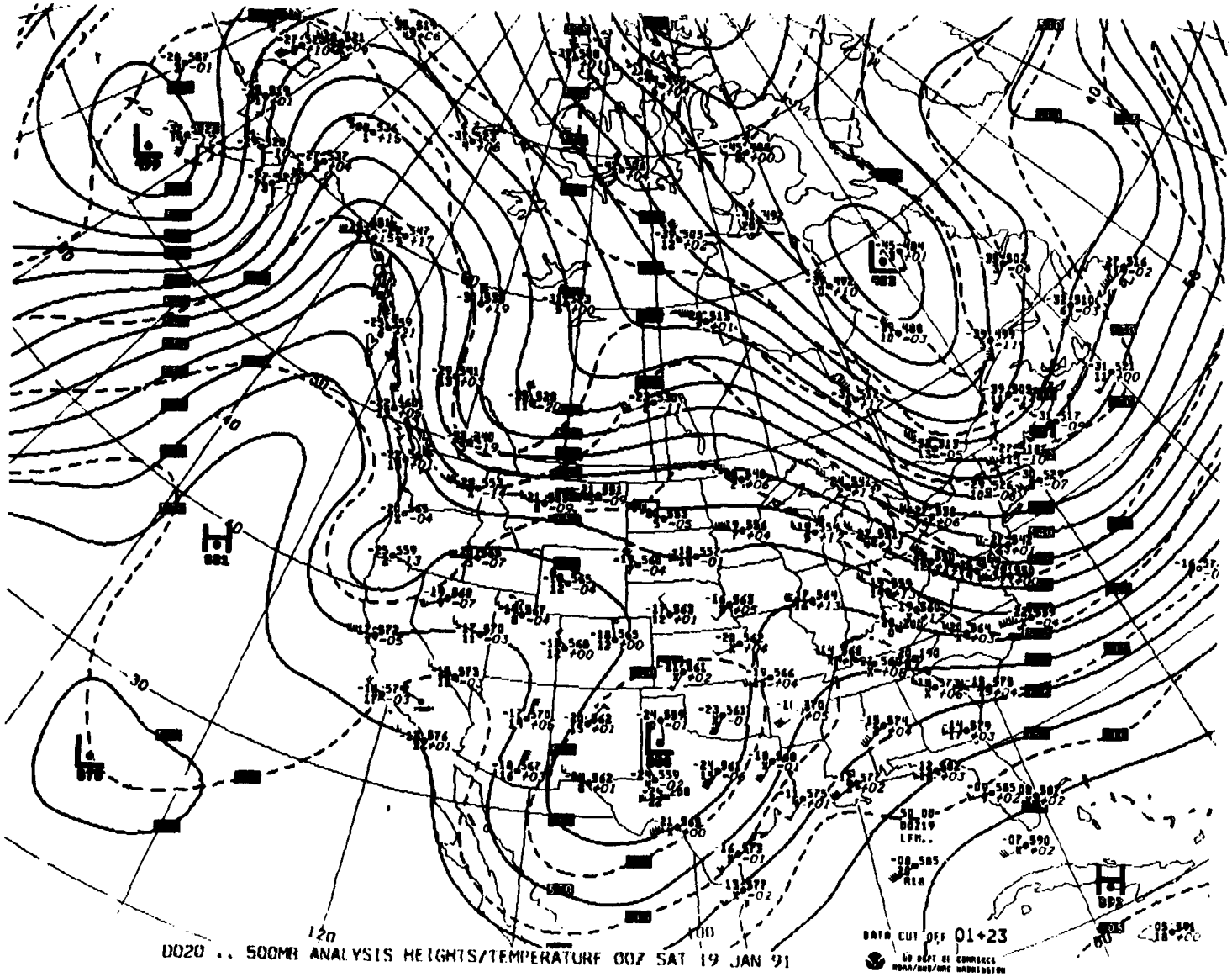
0020 .. 500MB ANALYSIS HEIGHTS/TEMPERATURE 00Z SAT 19 JAN 91
DATA CUT OFF 01+23

Figure 2.3: (b) Same as (a) except for 1200 UTC 19 January 1991.

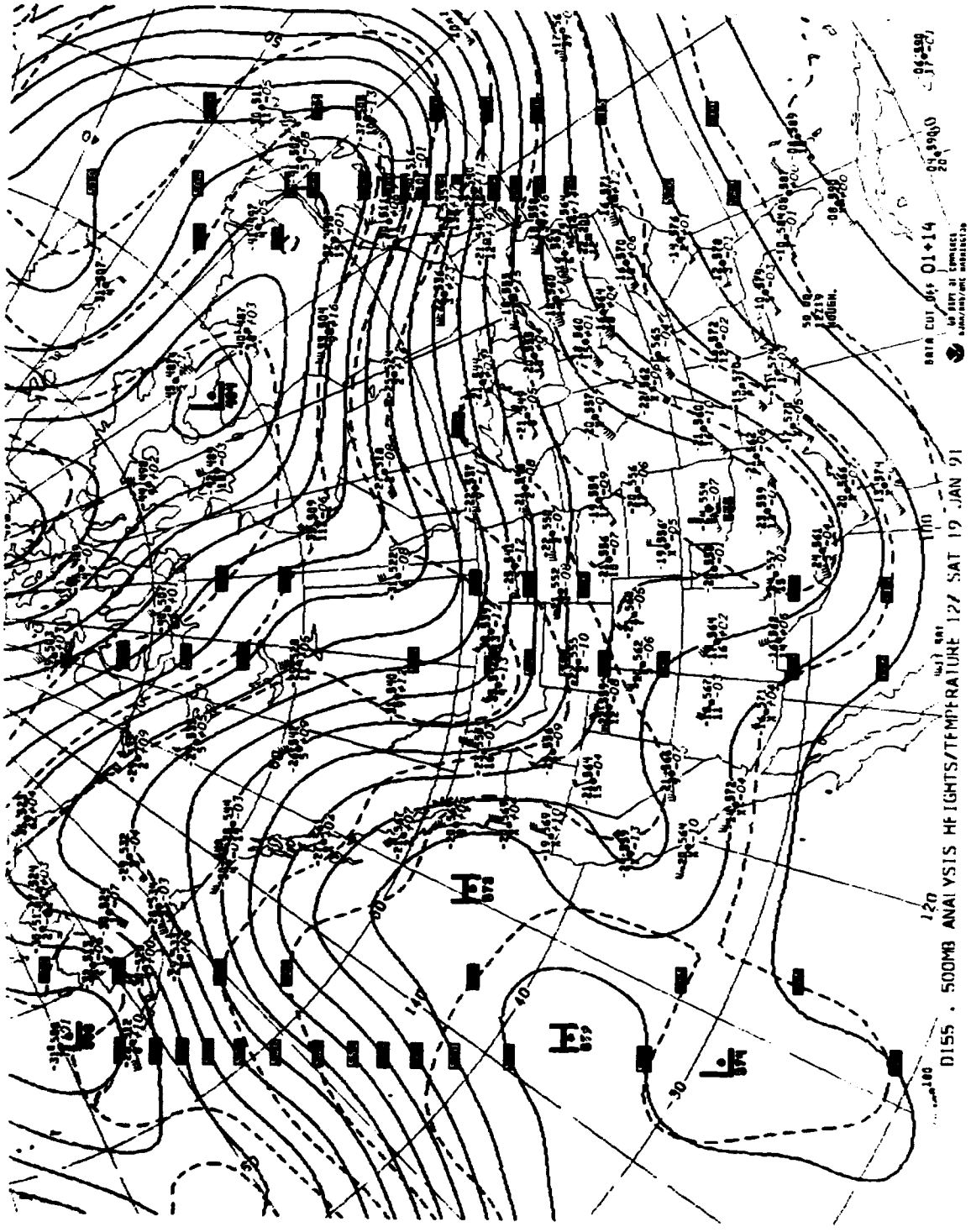
0155 . 500MB ANALYSIS HEIGHTS/TEMPERATURE 12Z SAT 19 JAN 91

Figure 2.3: (c) Same as (a) except for 0000 UTC 20 January 1991.

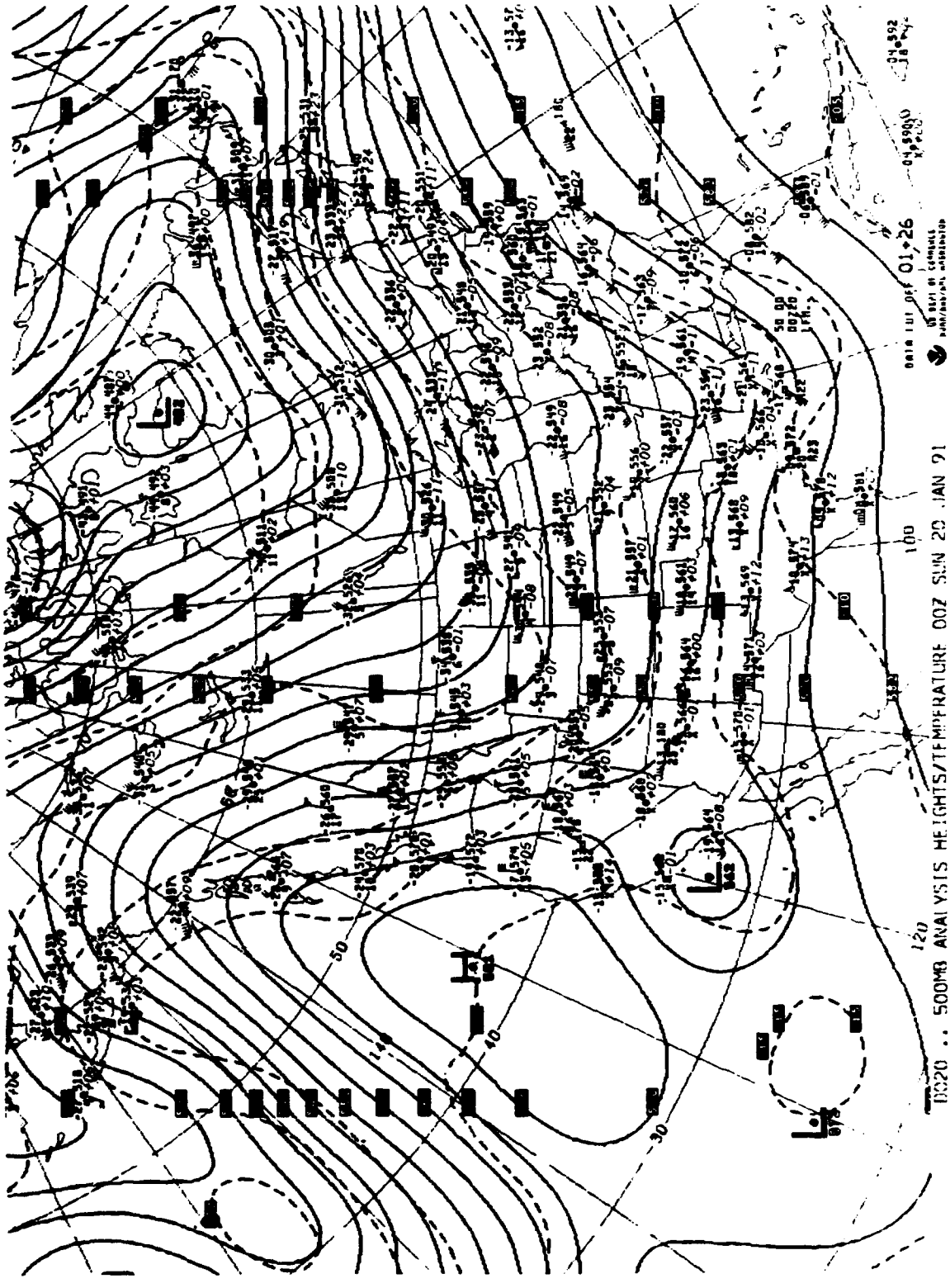
0320 .. 500MB ANALYSIS HEIGHTS/TEMPERATURE 00Z SUN 20 JAN 91
120
100
50
40
30

Figure 2.3: (d) Same as (a) except for 1200 UTC 20 January 1991.

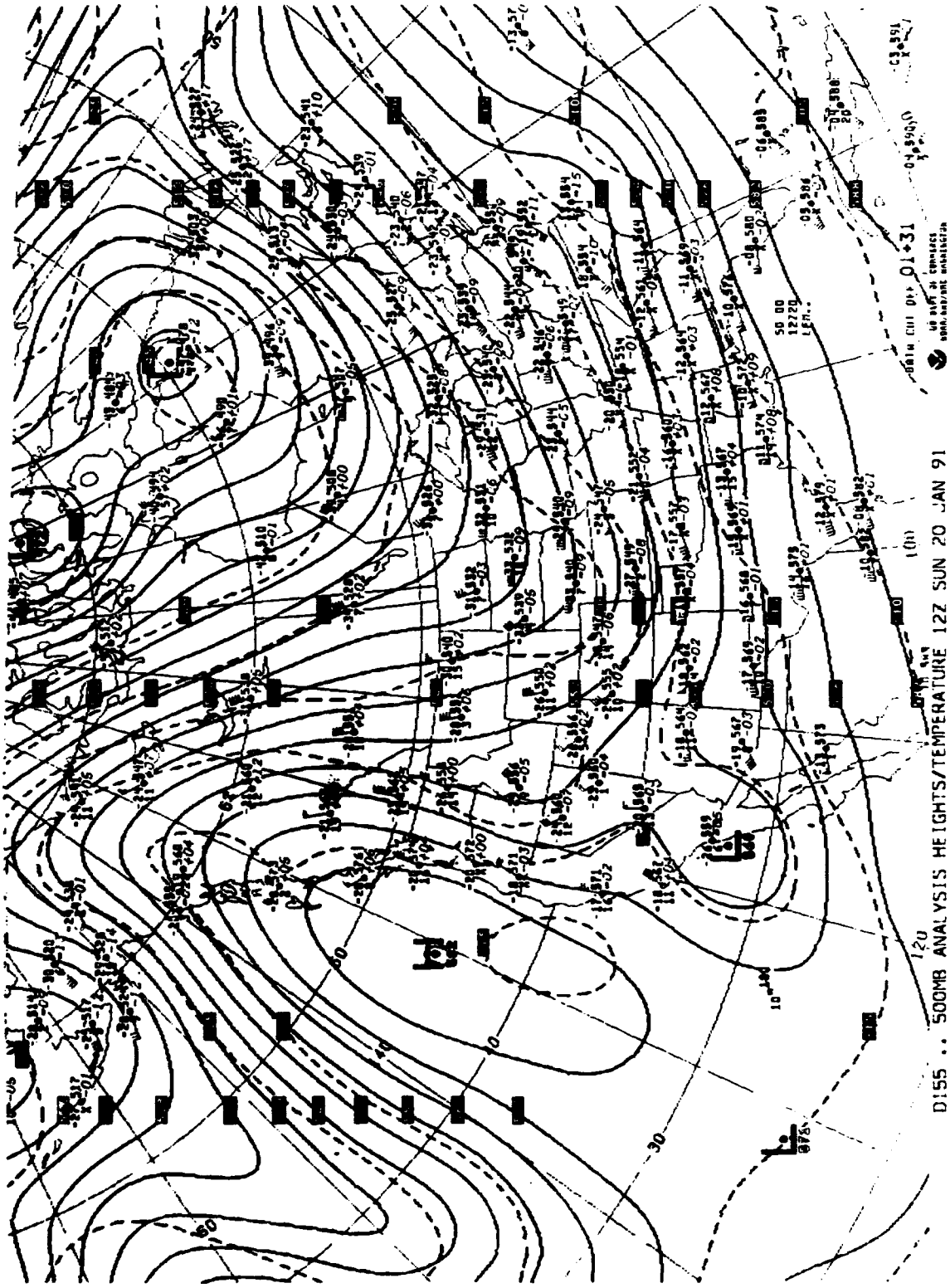
D155 .. 500MB ANALYSIS HEIGHTS/TEMPERATURE 12Z SUN 20 JAN 91

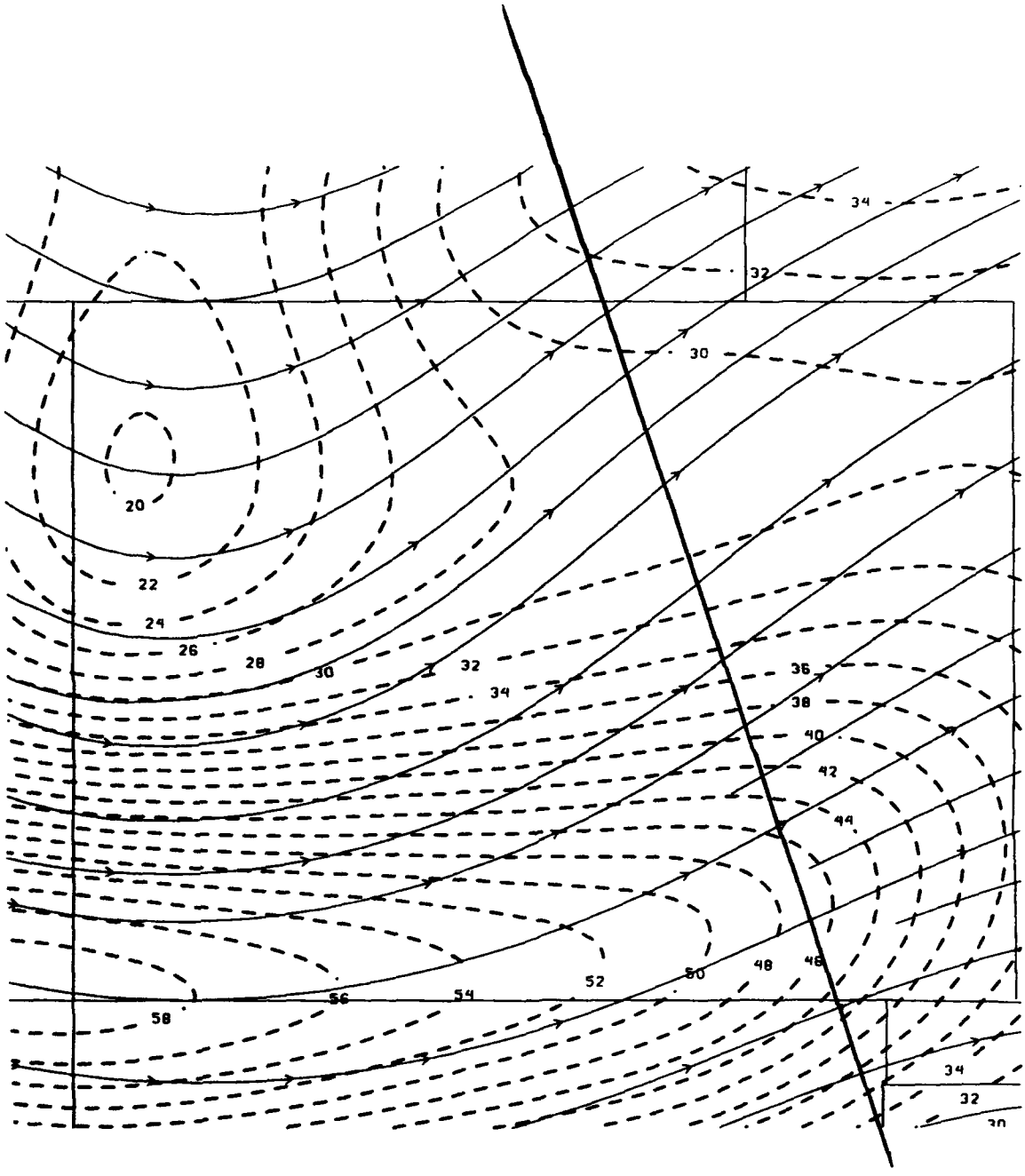

Figure 2.4: 0000 UTC 800-400 mb thermal wind streamlines (solid lines) and isotachs (dashed lines) in ms^{-1}. Line represents axis along which CSI profile was computed in Fig. 4.3.

Figure 2.5: (a) NMC 300 mb analysis for 0000 UTC 19 January 1991. Solid lines are height contours in dm, thick dashed lines are isotherms in °C, thin dashed lines are isotachs in ms^{-1}. Pennants, full barbs, and half barbs on wind shafts represent 25 ms^{-1}, 5 ms^{-1}, and 2.5 ms^{-1} respectively.

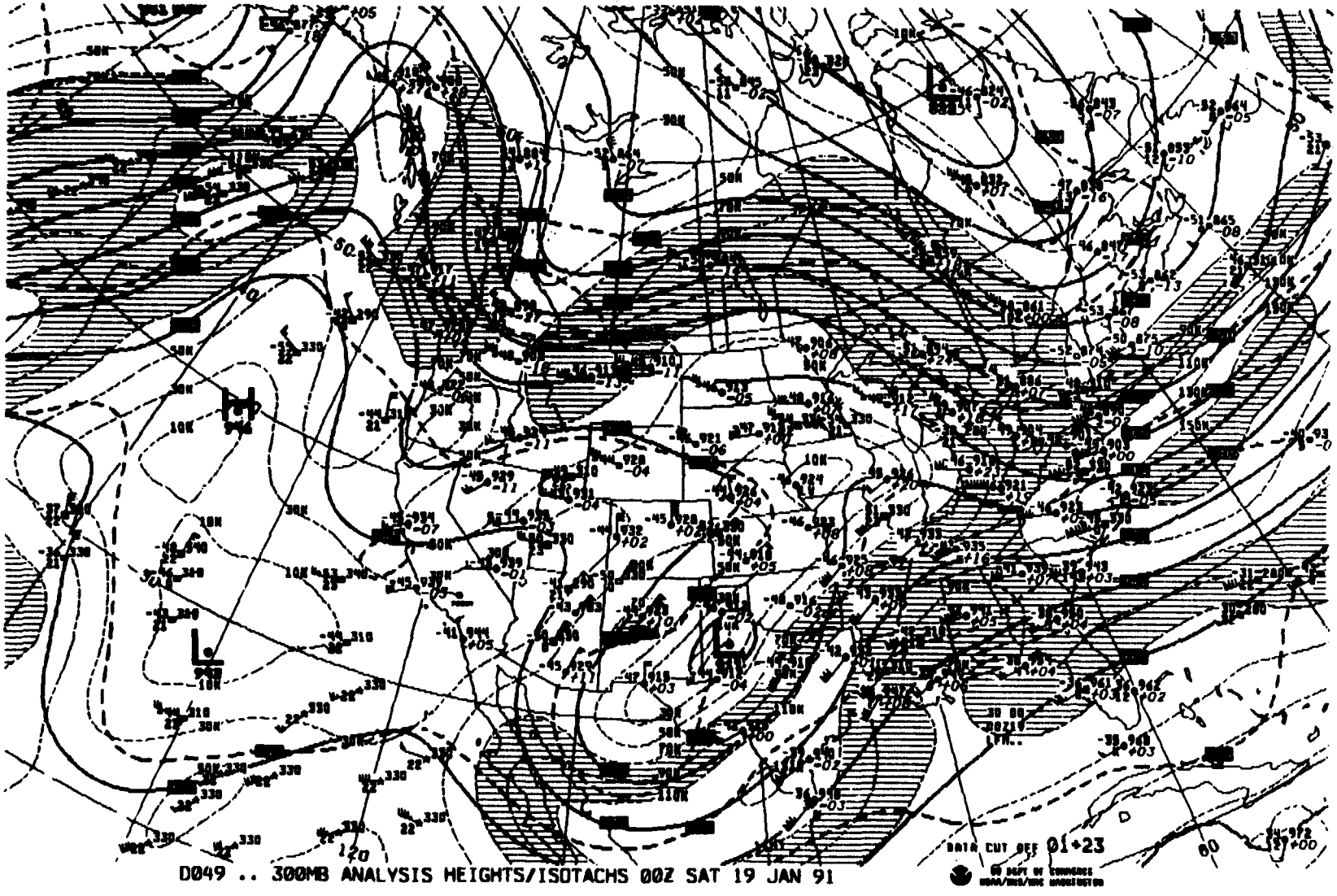
D049 .. 300MB ANALYSIS HEIGHTS/ISOTACHS 00Z SAT 19 JAN 91
DATA CUT OFF 01+23

Figure 2.5: (b) Same as (a) except for 1200 UTC 19 January 1991.

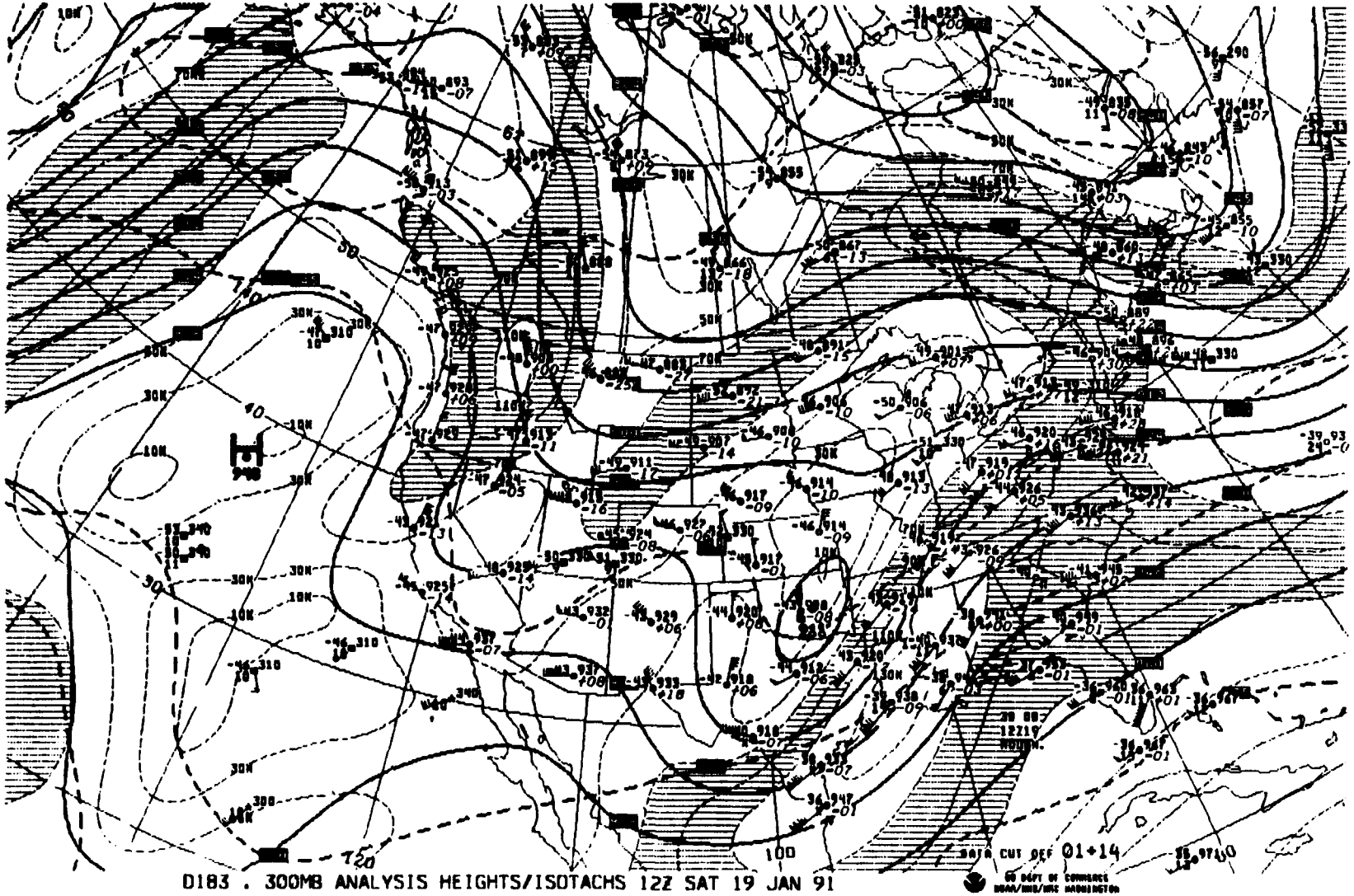

D183 . 300MB ANALYSIS HEIGHTS/ISOTACHS 12Z SAT 19 JAN 91

Figure 2.5: (c) Same as (a) except for 0000 UTC 20 January 1991.

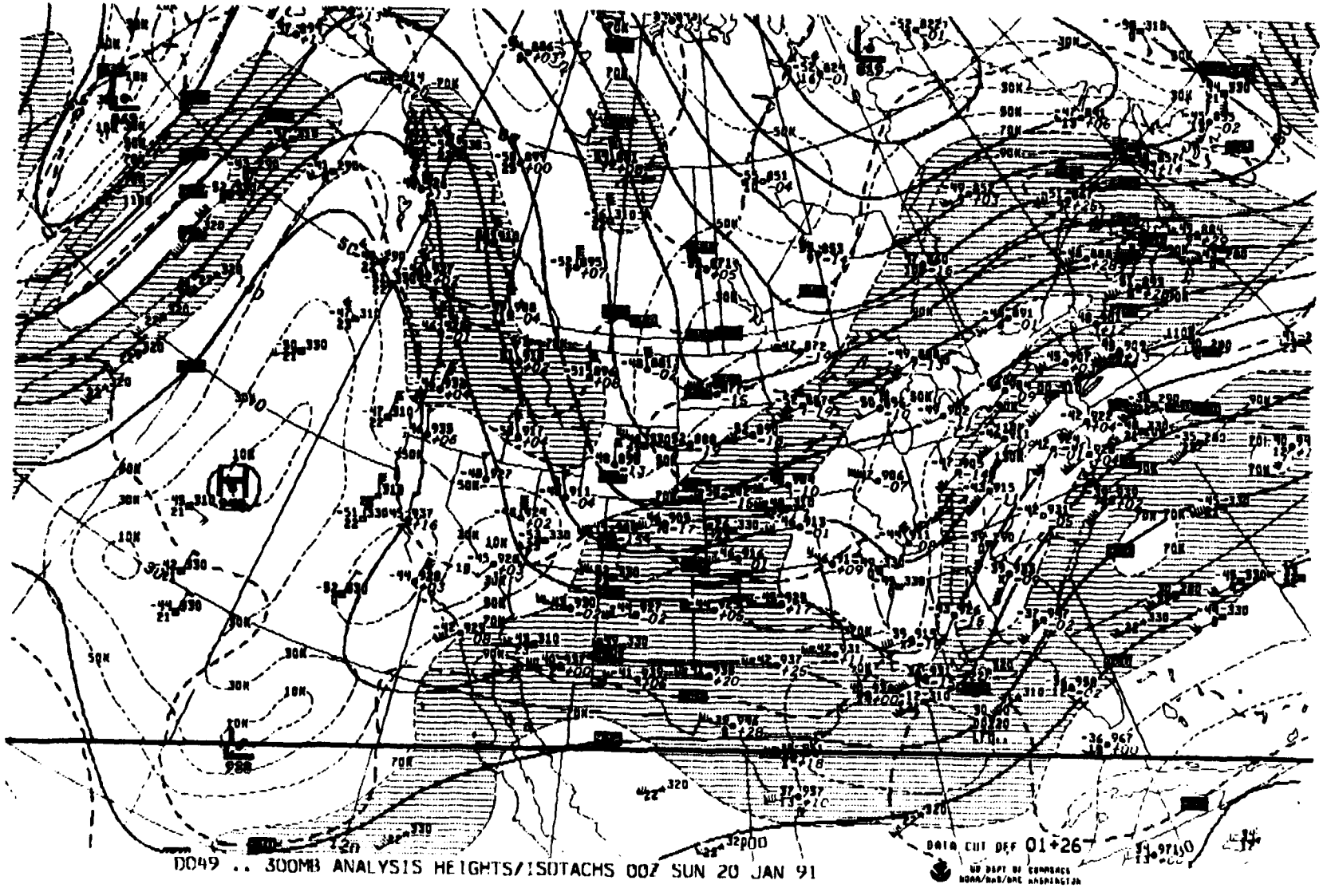

D049 .. 300MB ANALYSIS HEIGHTS/ISOTACHS 00Z SUN 20 JAN 91

Figure 2.5: (d) Same as (a) except for 1200 UTC 20 January 1991.

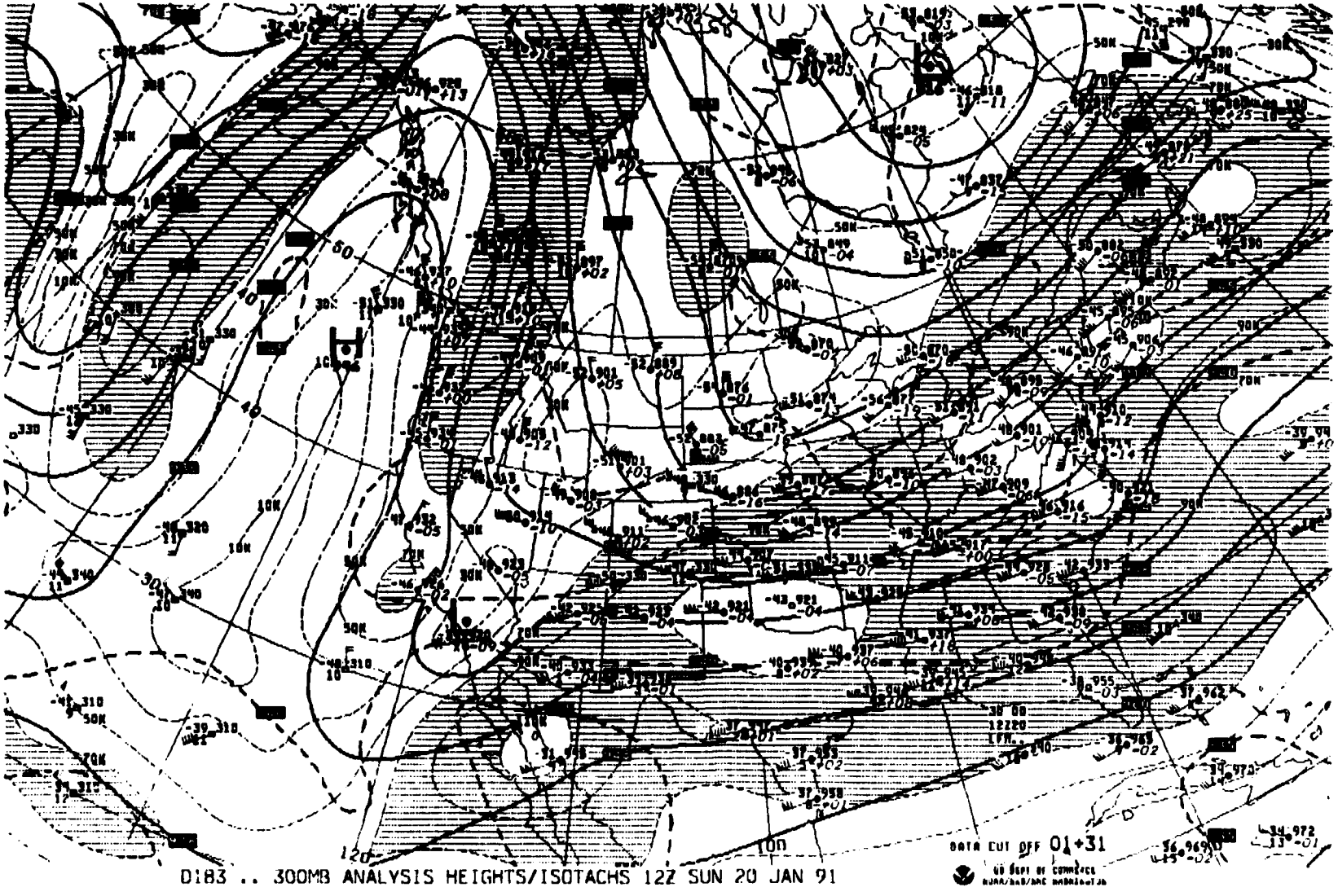
D183 .. 300MB ANALYSIS HEIGHTS/ISOTACHS 12Z SUN 20 JAN 91
DATA CUT OFF 01+31

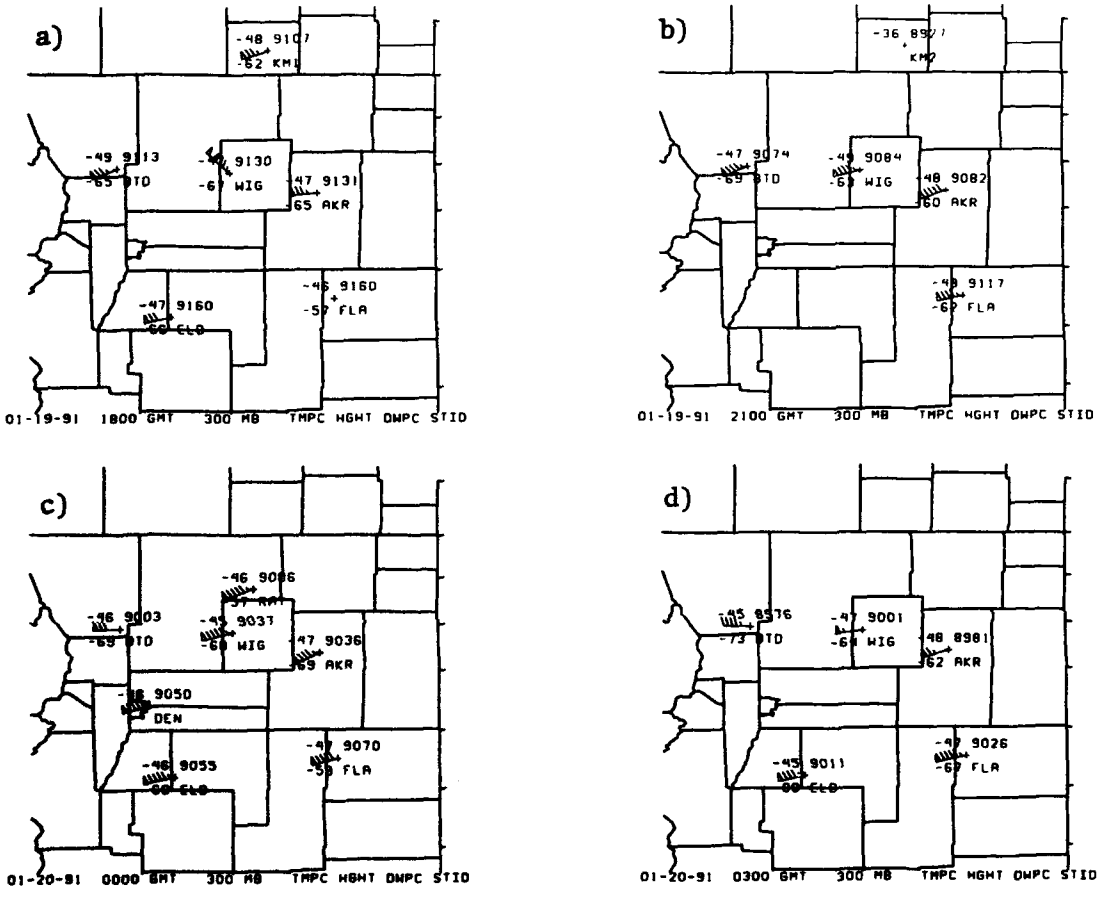

Figure 2.6: CLASS 300 mb station plots over Northeast Colorado for a) 1800 UTC 19 January 1991, b) 2100 UTC, c) 0000 UTC 20 January, and d) 0300 UTC. From upper left corner of plot working clockwise, plots show temperature in °C, height in dm, station identifier, and dewpoint in °C. Pennants, long barbs, and short barbs on wind shafts represent 25 ms^{-1}, 5 ms^{-1}, and 2.5 ms^{-1} respectively.

Figure 2.7: (a) Platteville wind profiler horizontal winds 1200 UTC 19 January to 0600 UTC 20 January 1991. Pennants, long barbs, and short barbs on wind shafts represent 25 ms^{-1}, 5 ms^{-1}, and 2.5 ms^{-1} respectively.

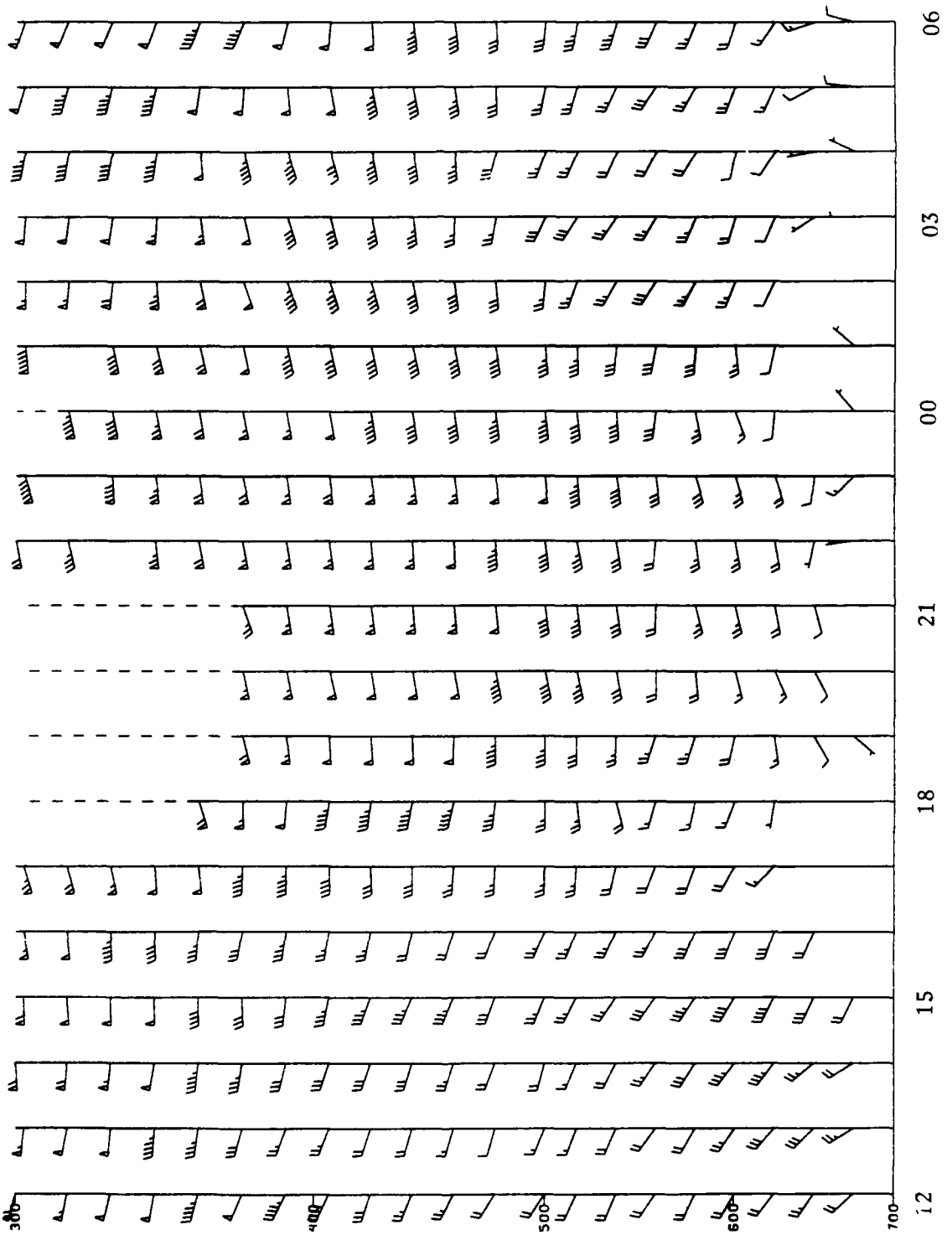
06
03
00
21
18
15
12
300
400
500
600
700

Figure 2.7: (b) Denver wind profiler horizontal winds between 2100 UTC 19 January to 0300 UTC 20 January 1991. Long barbs and short barbs on the shafts represent 10 ms^{-1} and 5 ms^{-1} respectively.

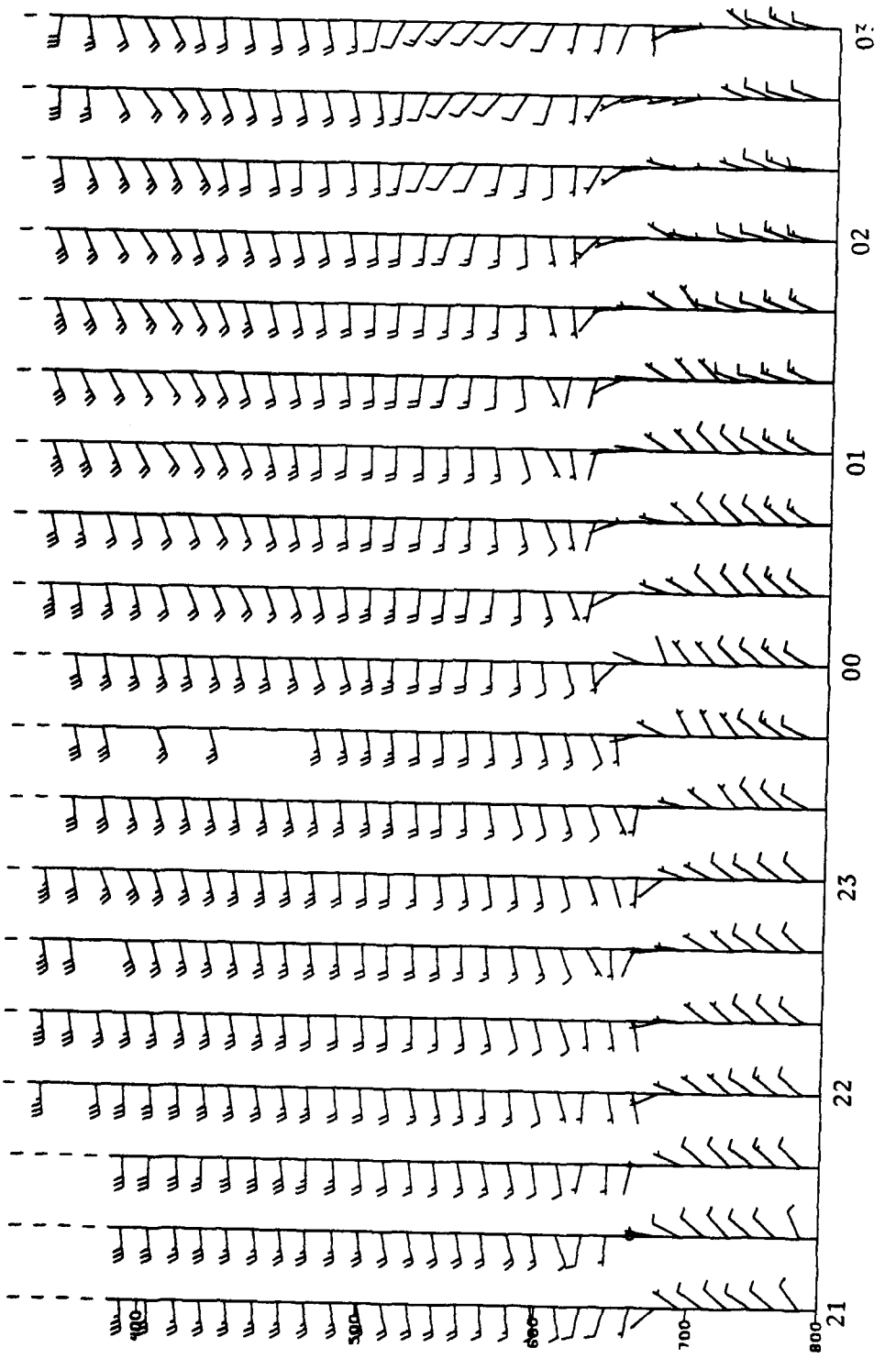
20
02
01
00
23
22
21
100
300
600
700
800

Figure 2.8: (a) NMC 700 mb analysis for 0000 UTC 19 January 1991. Solid lines are height contours in dm and dashed lines are isotherms in °C. Pennants, long barbs, and short barbs on wind shafts represent 25 ms^{-1}, 5 ms^{-1}, and 2.5 ms^{-1} respectively.

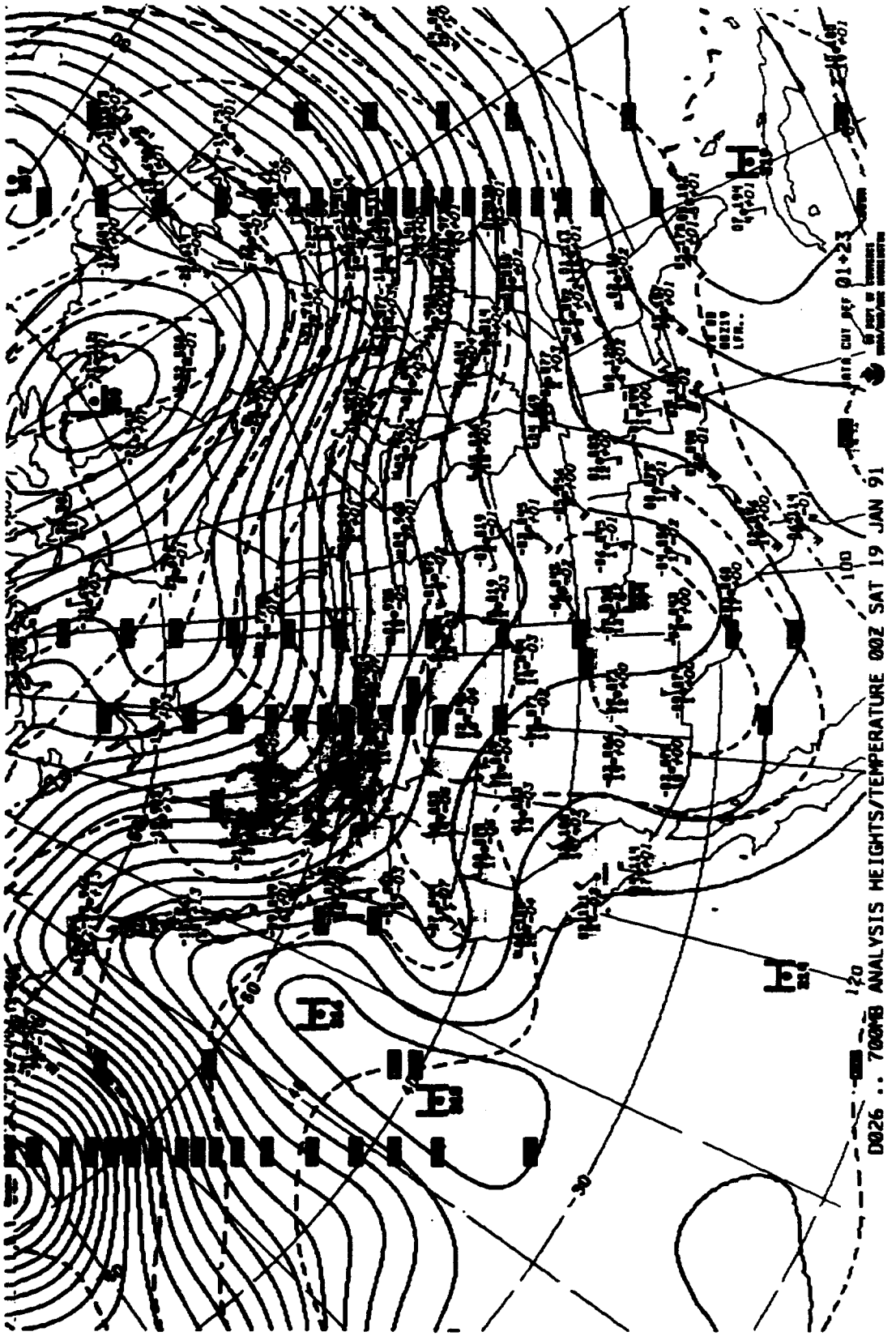
D026 .. 700MB ANALYSIS HEIGHTS/TEMPERATURE 00Z SAT 19 JAN 91

Figure 2.8: (b) Same as (a) except for 1200 UTC 19 January 1991.

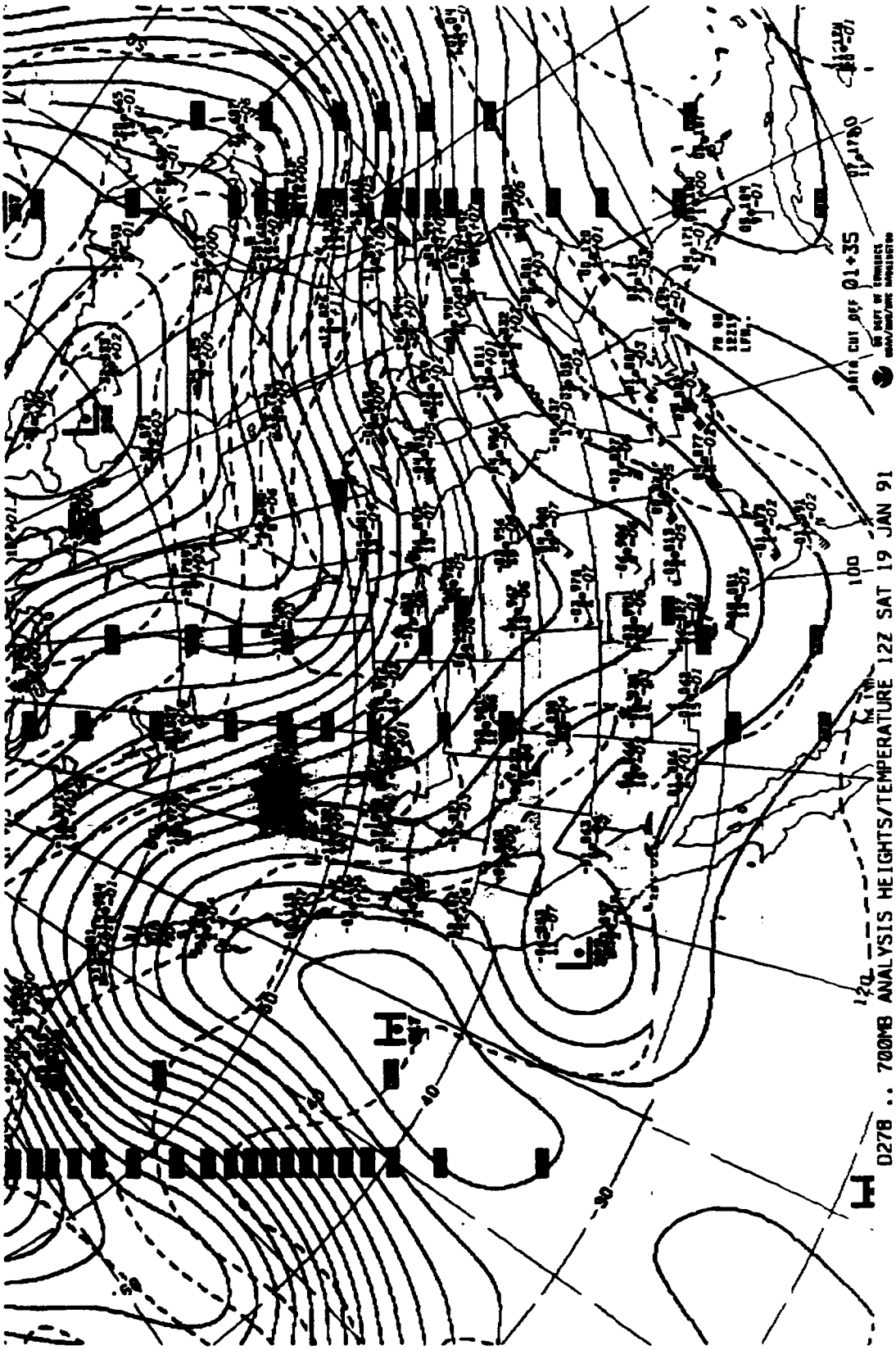
0278 .. 700MB ANALYSIS HEIGHTS/TEMPERATURE 12Z SAT 19 JAN 91

Figure 2.8: (c) Same as (a) except for 0000 UTC 20 January 1991.

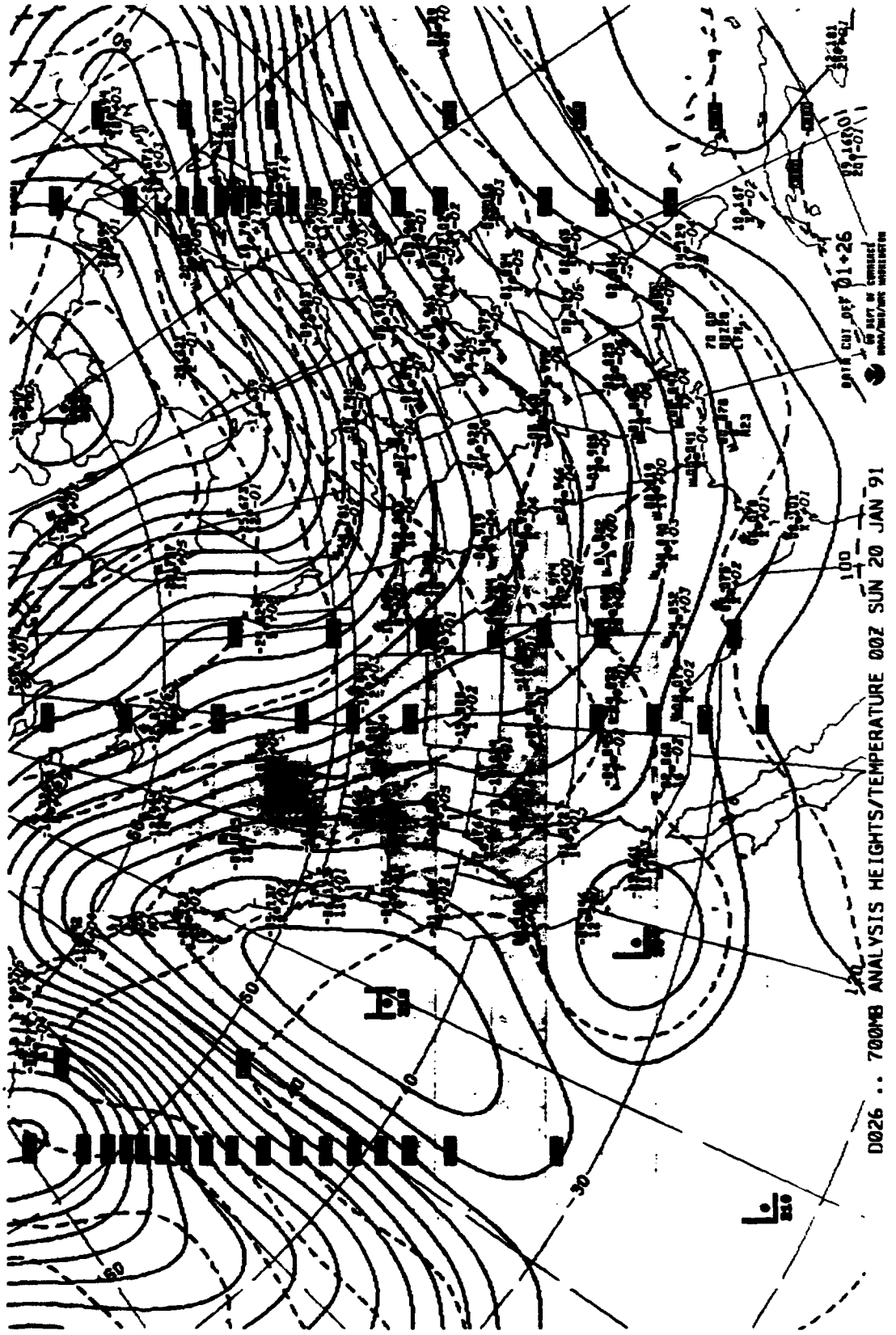
D026 .. 700MB ANALYSIS HEIGHTS/TEMPERATURE 00Z SUN 20 JAN 91

a)

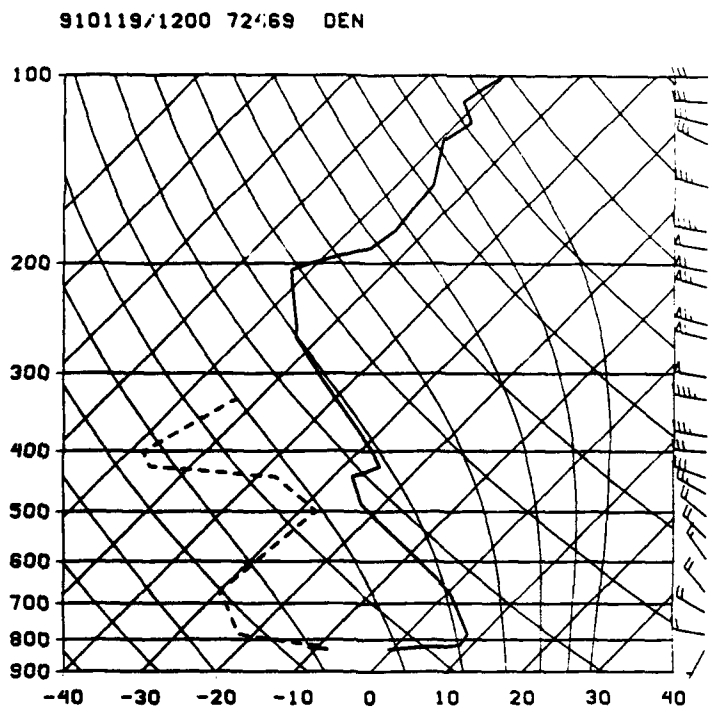

b)

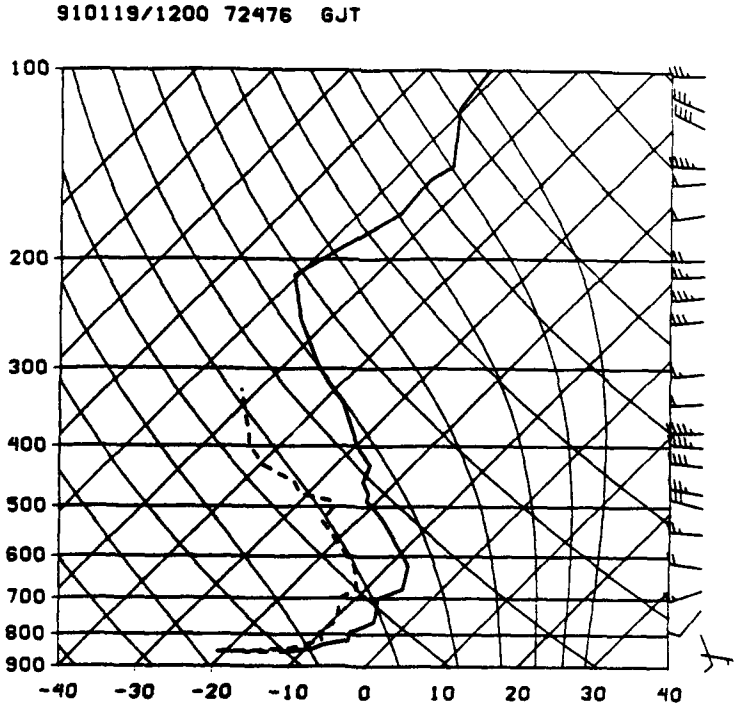

Figure 2.9: 1200 UTC 19 January 1991 rawinsonde sounding for a) Denver and b) Grand Junction. Heavy solid line, heavy dashed line, horizontal solid line, straight diagonal lines, slightly curved lines and heavily curved lines represent temperature trace, dewpoint trace, isobars (mb), isotherms (°C), dry adiabats, and moist adiabats respectively. The same wind barb notation as Fig. 2.7a is used here.

a)

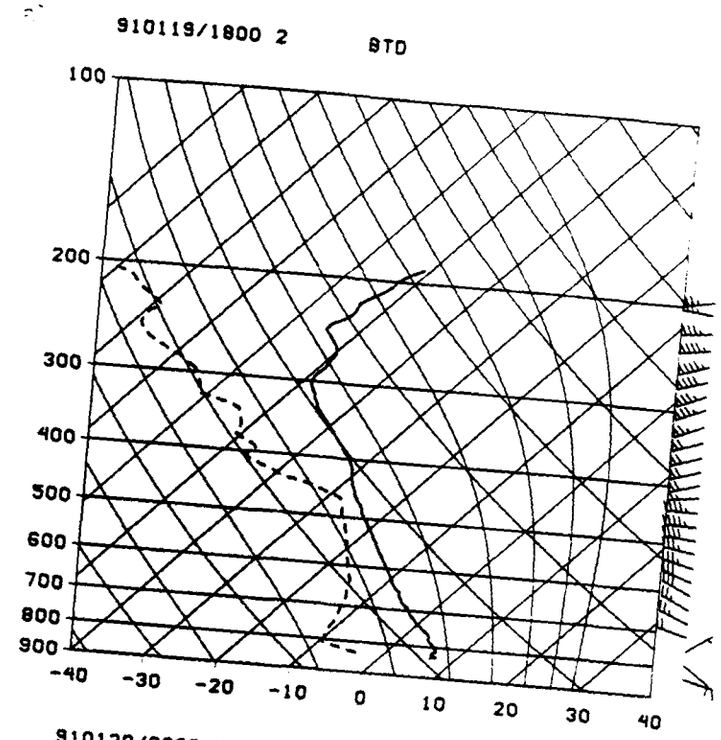

b)

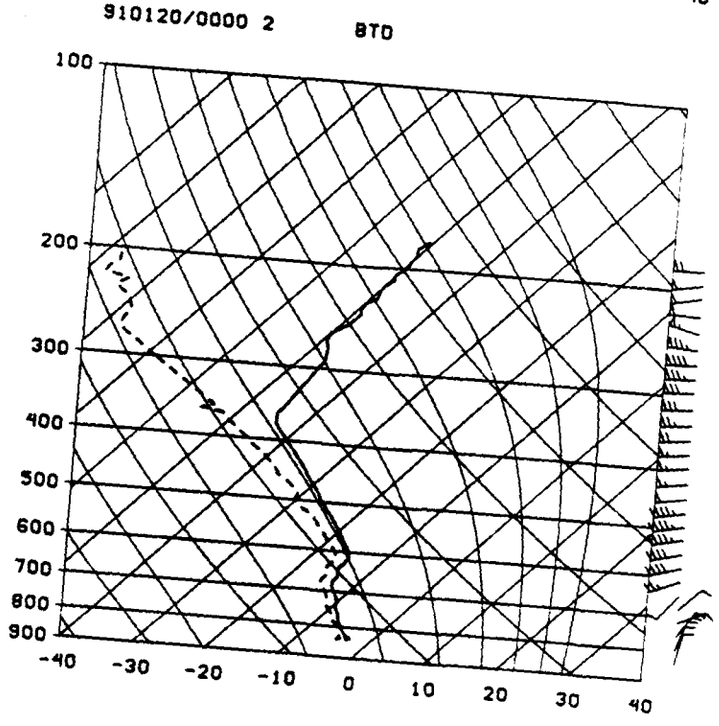

Figure 2.10: Berthoud CLASS rawinsonde soundings for a) 1800 UTC 19 January and b) 0000 UTC 20 January 1991. The same line convention is used here as in Figure 2.9.

c)

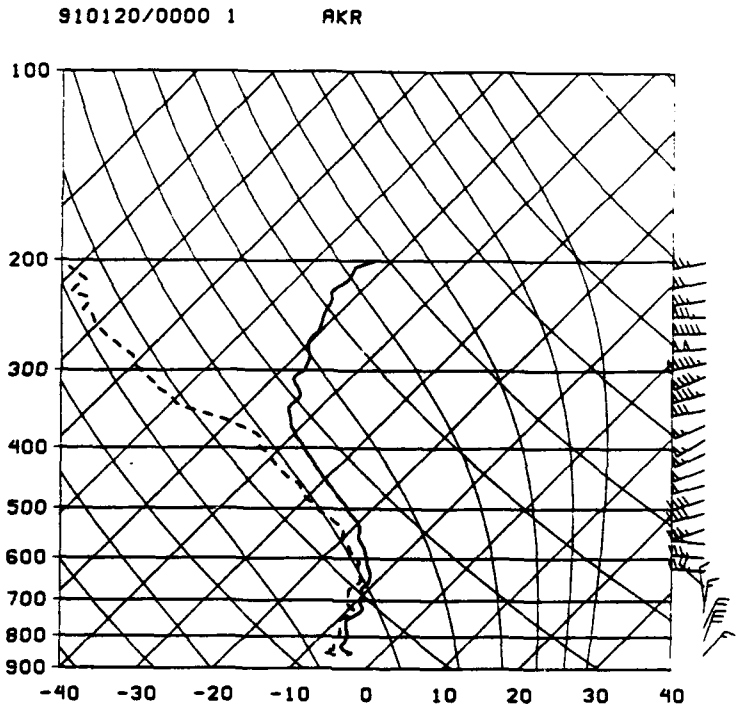

d)

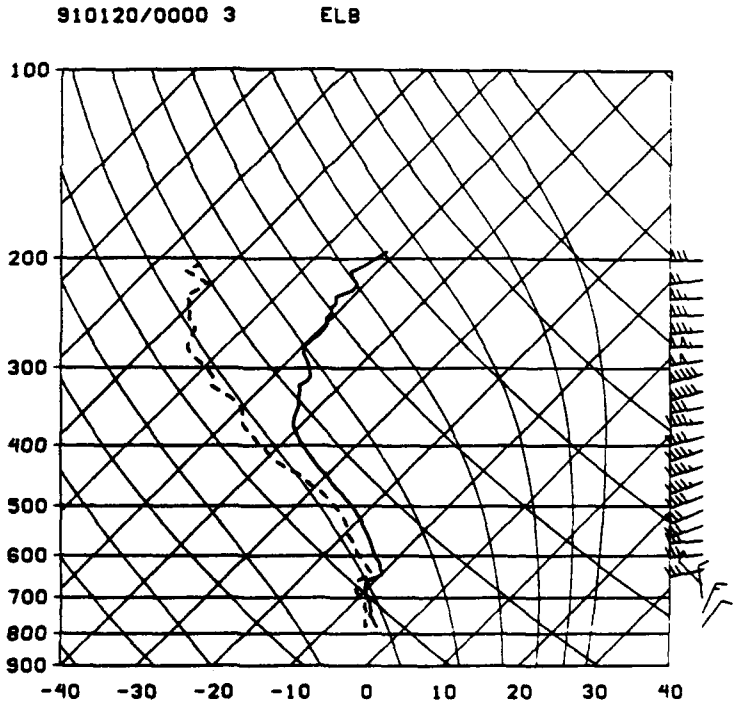

Figure 2.10: 0000 UTC 20 January 1991 CLASS rawinsonde soundings for c) Akron and d) Elbert.

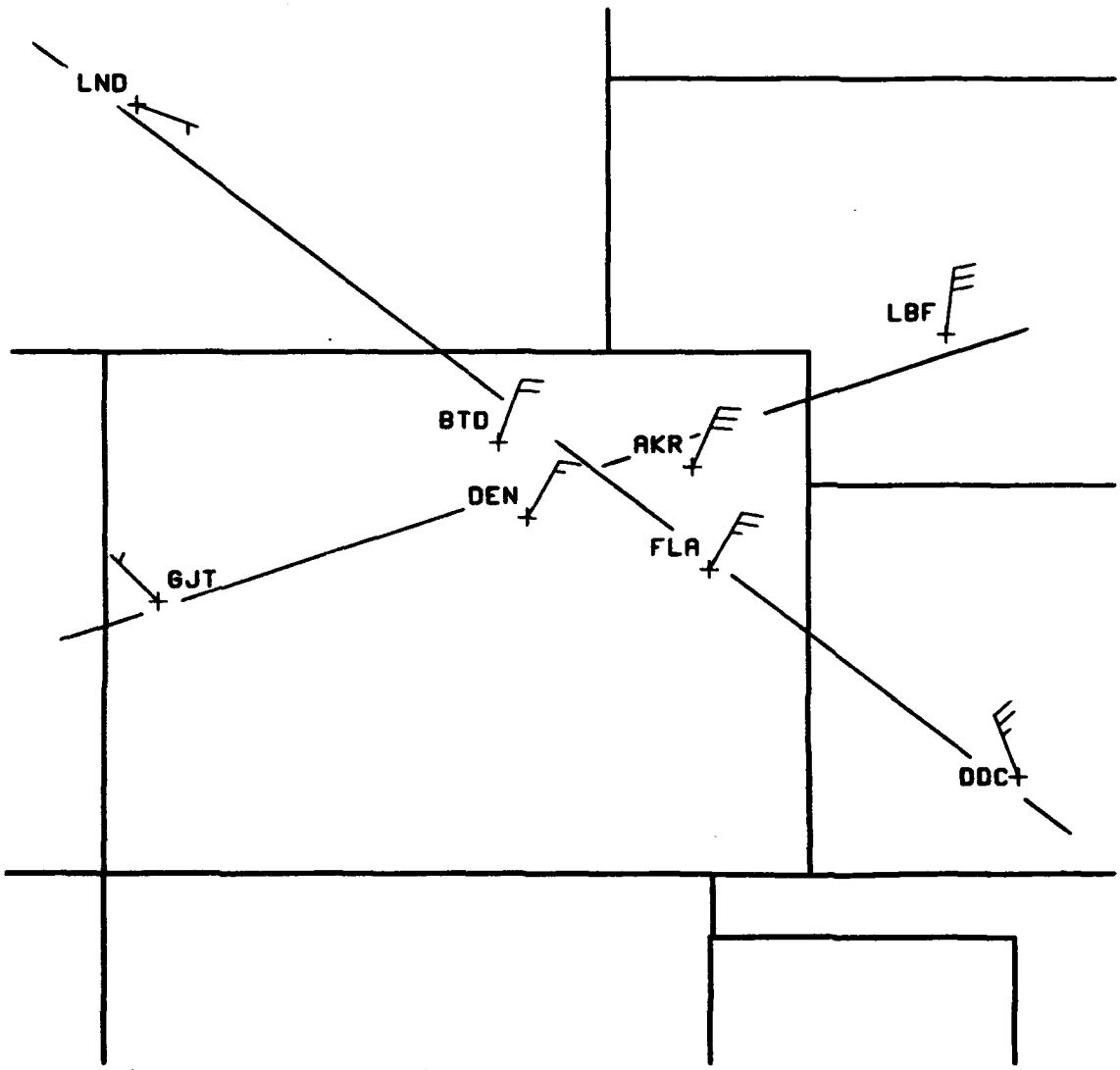

Figure 2.11: Cross section transects and representative low level winds. Long barbs on wind shafts represent 5 ms^{-1}, and short barbs 2.5 ms^{-1}.

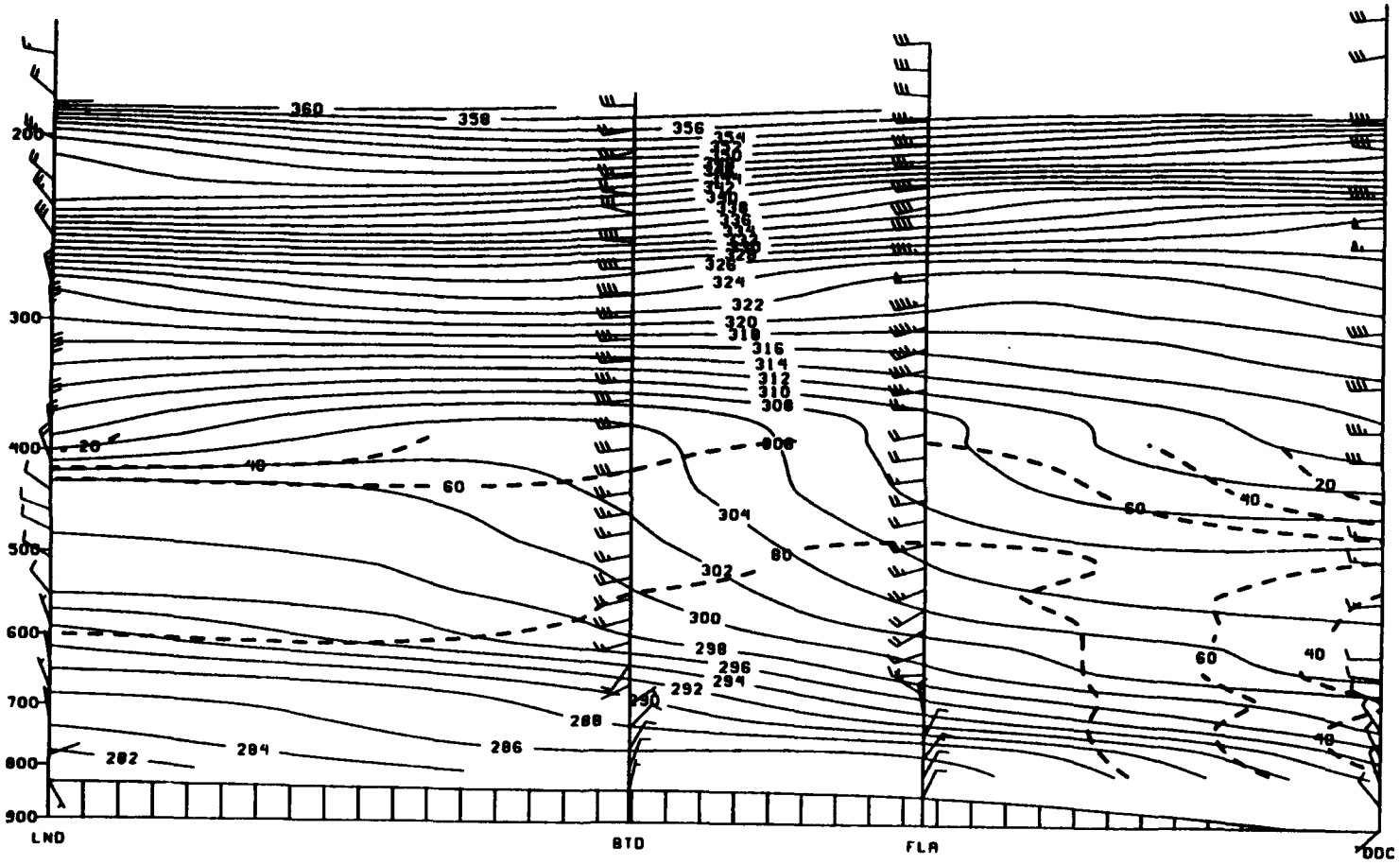

Figure 2.12: (a) 0000 UTC 20 January 1991 Lander, WY to Dodge City, KS cross section. Solid lines are isentropes (°K) and dashed lines are relative humidities (percent). Pennants, long barbs, and short barbs on wind shafts represent 50 ms^{-1}, 10 ms^{-1}, and 5 ms^{-1} respectively.

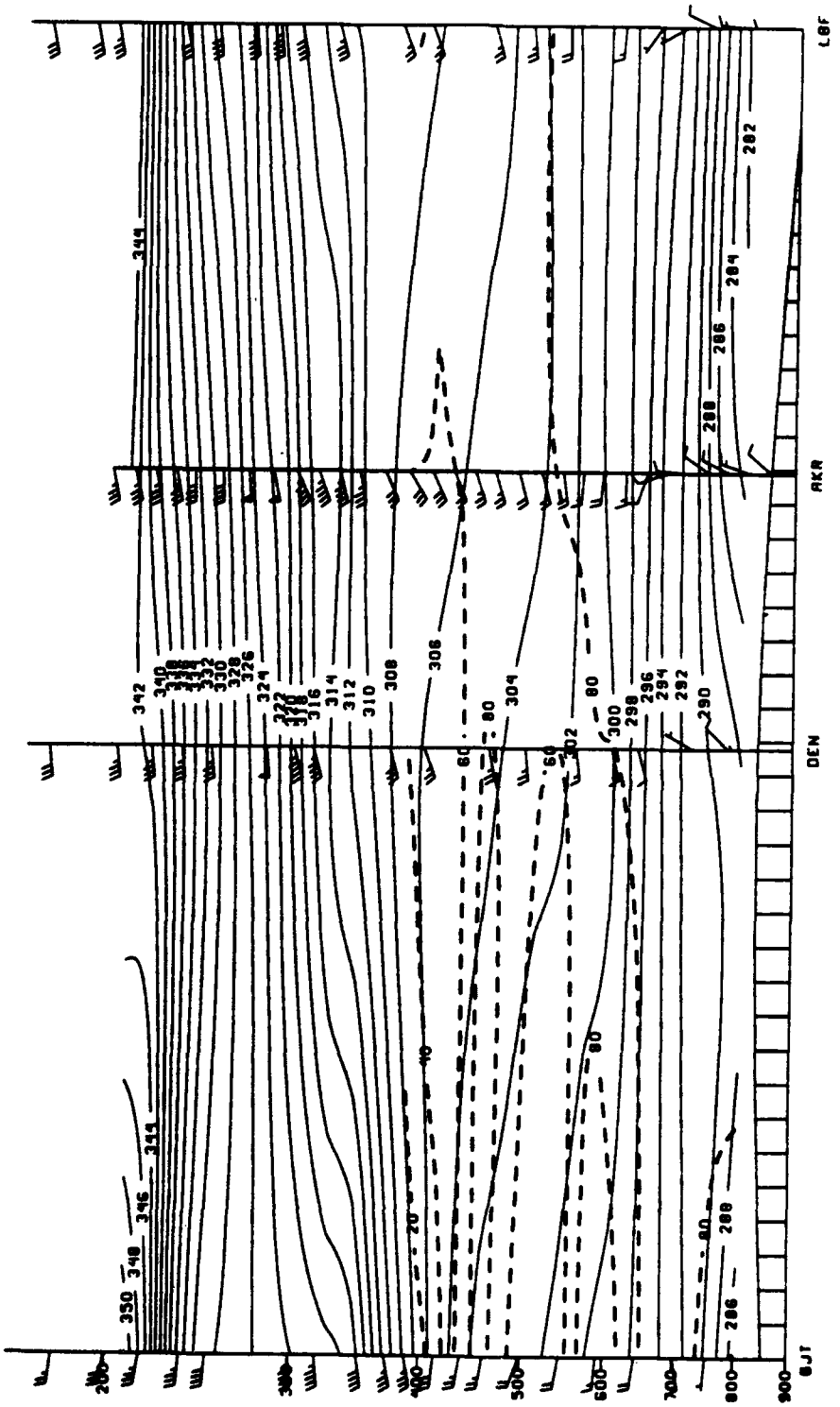

Figure 2.12: (b) Same as (a) except between Grand Junction, CO. and North Platte, NE.

Figure 2.13: 1800 UTC 19 January to 0300 UTC 20 January 1991 vertical cross section of equivalent potential temperature for a) Akron, b) Wiggins), c) Berthoud, and d) Flagler. Solid lines are pseudo isentropes (°K) and dashed lines are relative humidities (per cent). Pennants, long barbs, and short barbs on wind shafts represent 25 ms^{-1}, 5 ms^{-1}, and 2.5 ms^{-1} respectively.

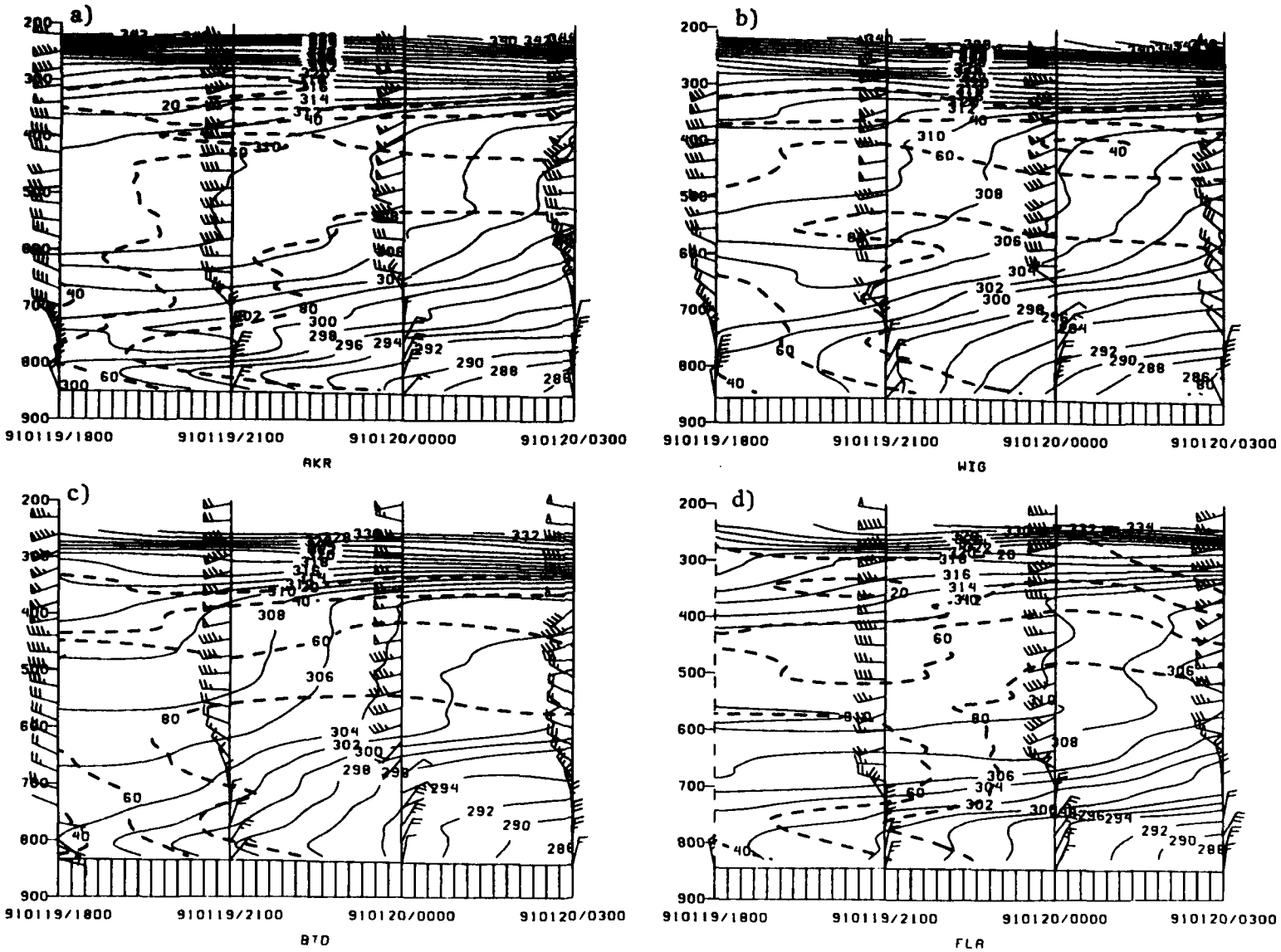
a)
b)
c)
d)
910119/1800
910119/2100
910120/0000
910120/0300
AKR
WIG
BTD
FLA

Figure 2.14: (a) NMC Surface analysis for 1200 UTC 19 January 1991. Solid lines are pressure in mb.

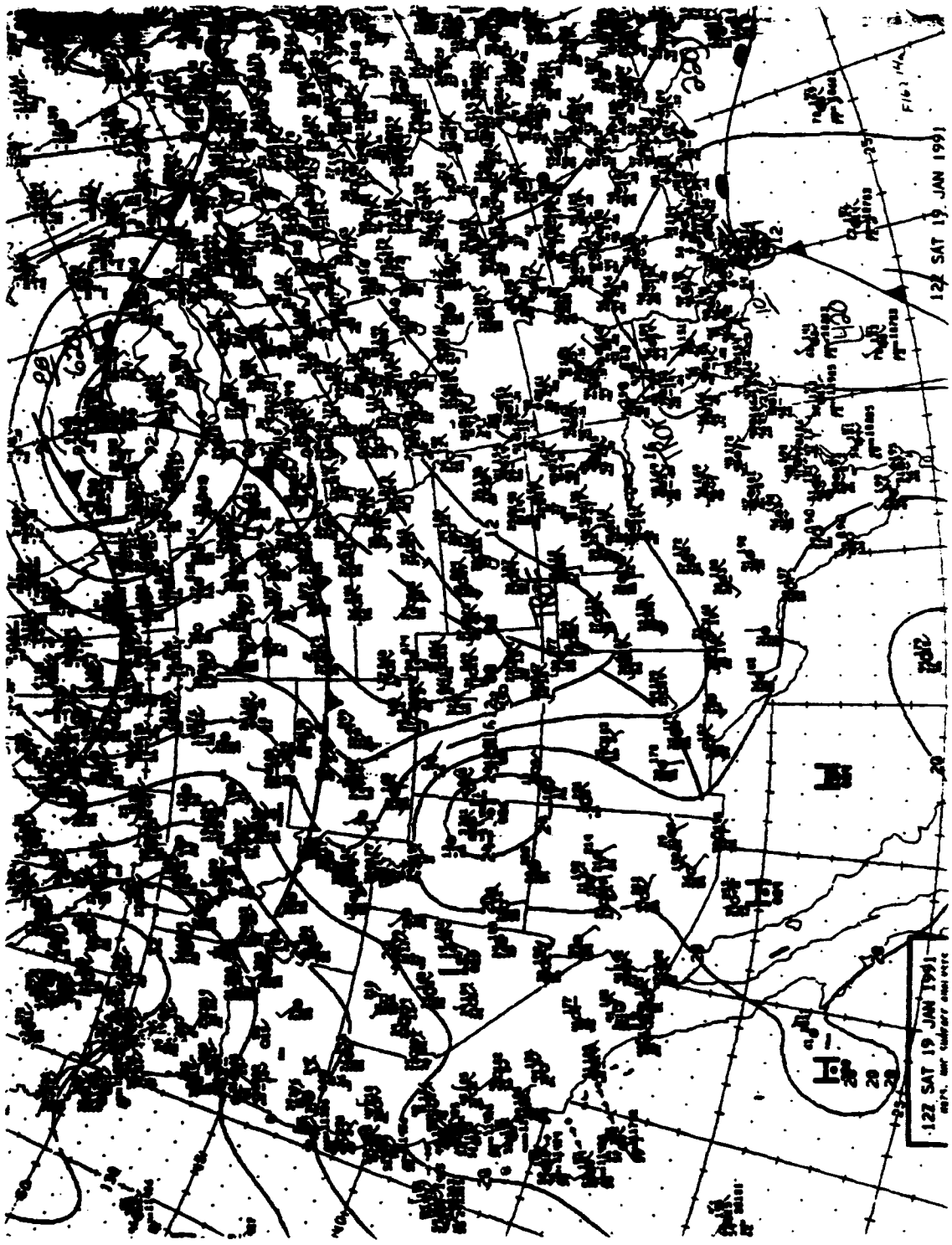
12Z SAT 19 JAN 1991
12Z SAT 19 JAN 1991

Figure 2.14: (b) Same as (a) except for 0000 UTC 20 January 1991.

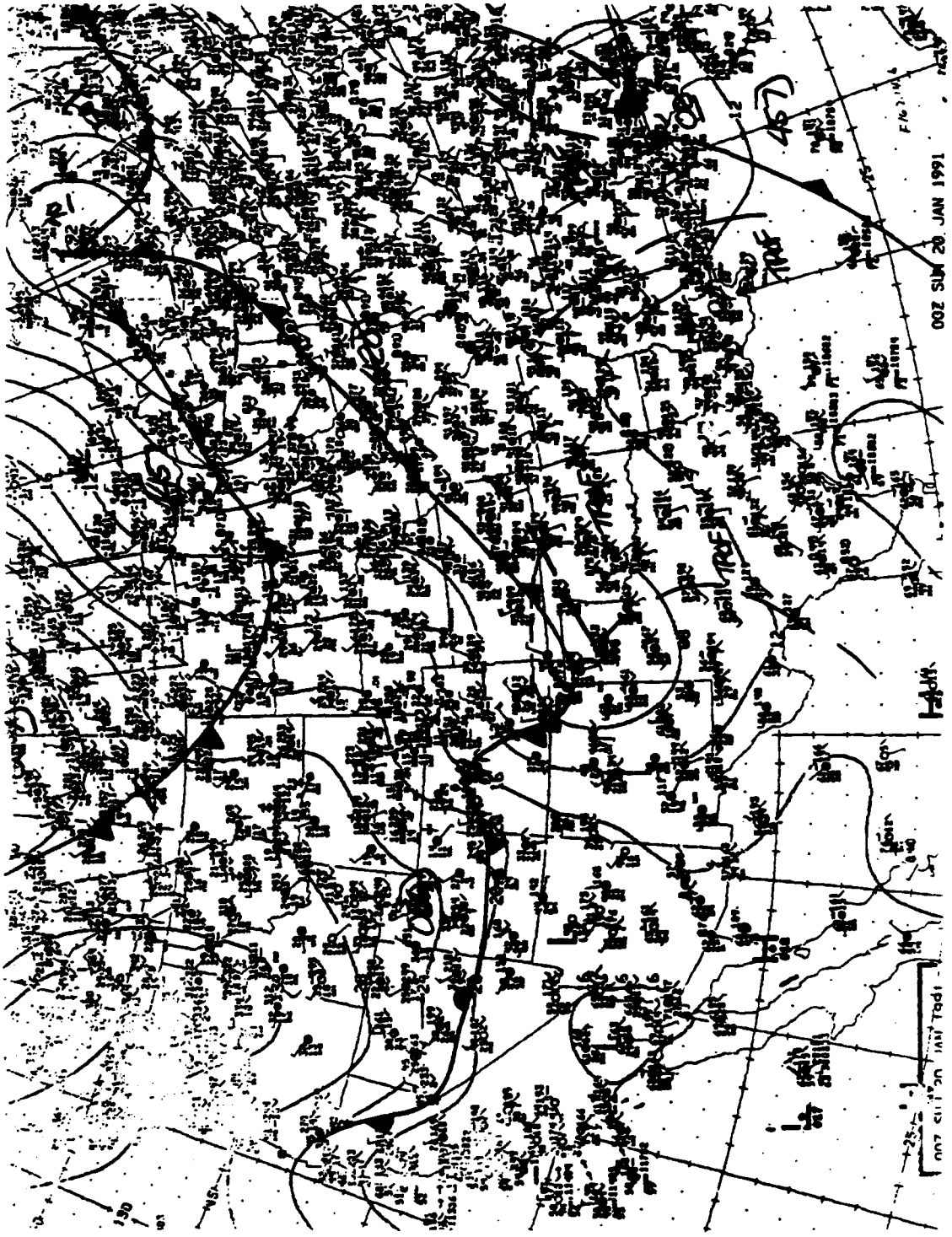
SUN 20 JAN 1991 00Z

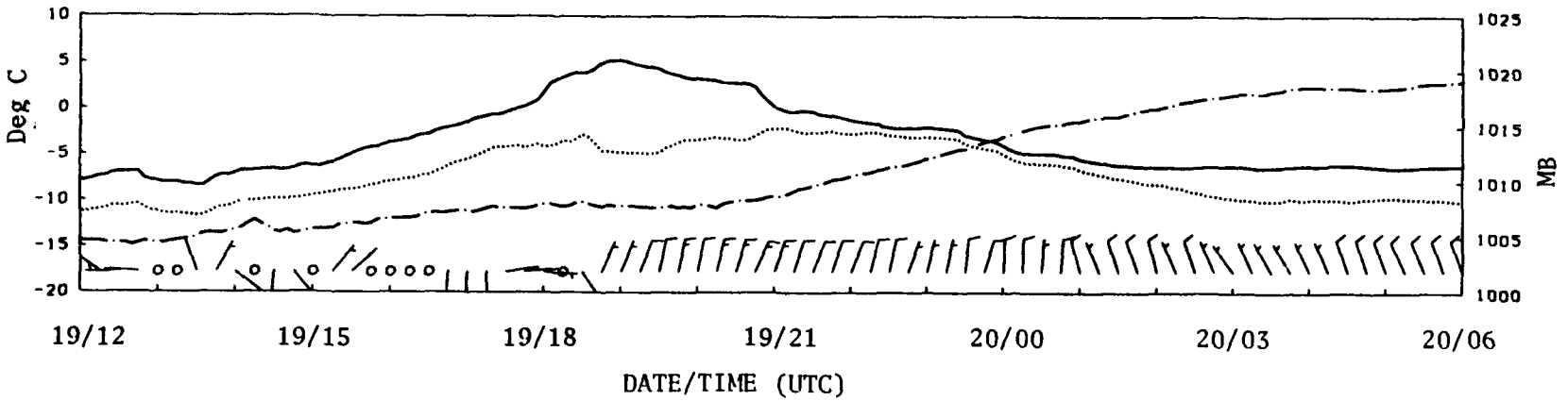

Figure 2.15: Time cross section of temperature, dewpoint, winds, and pressure at Greeley, CO. Solid, dotted, dash-dot lines are represent the temperature curve, dewpoint curve, and pressure curve respectively. Long barbs and short barbs on wind shafts represent 5 ms^{-1} and 2.5 ms^{-1} respectively.

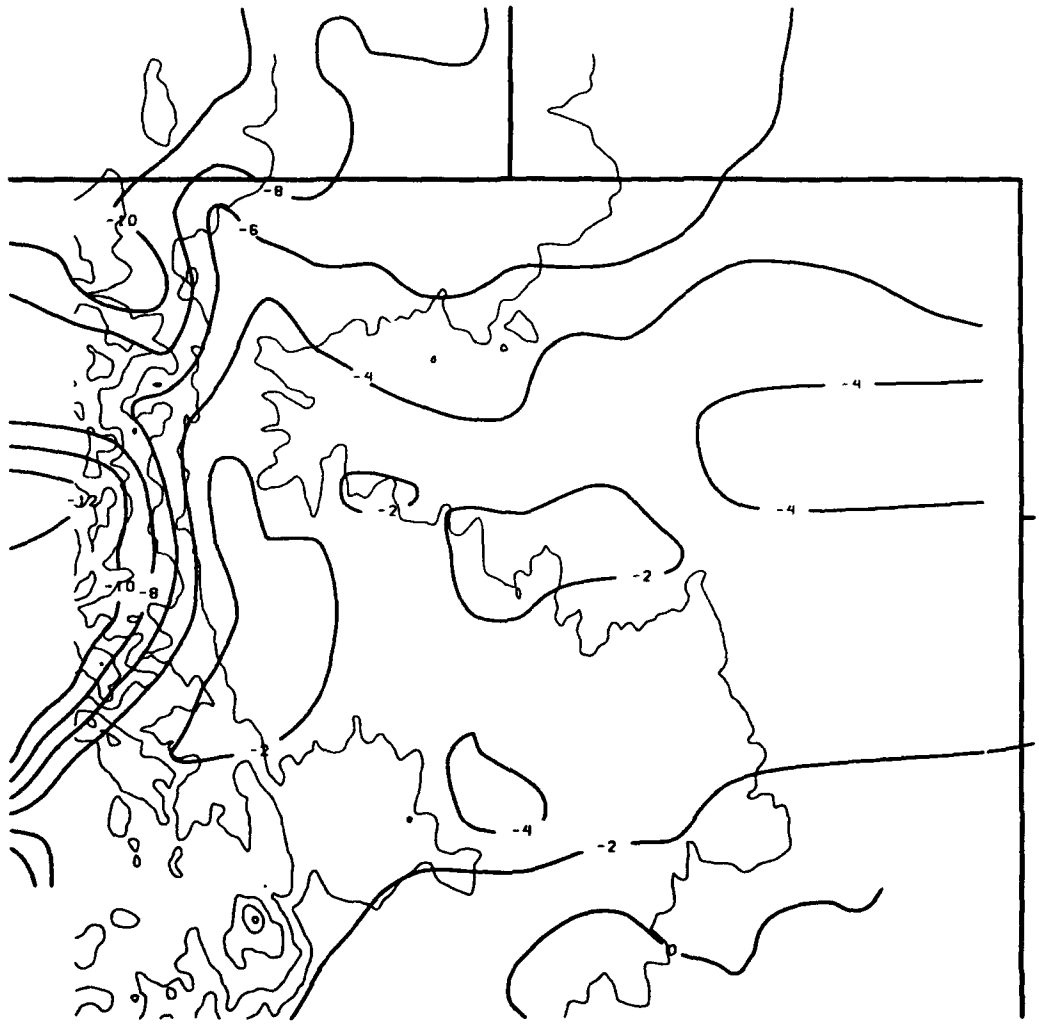

Figure 2.16: 0000 UTC 20 January surface isotherm analysis over Northeast Colorado. Heavy lines are isotherms (°C) and thin lines are 500 m terrain height contours.

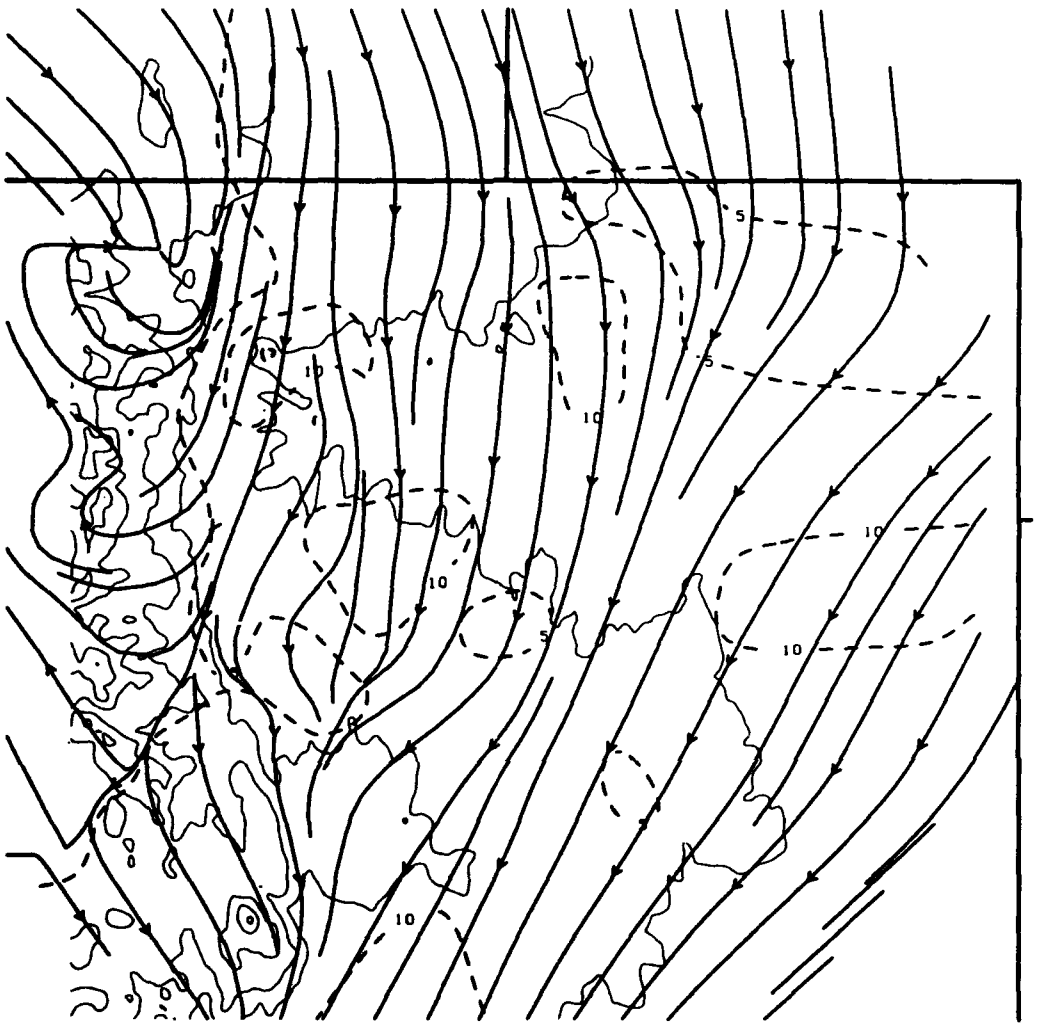

Figure 2.17: 0100 UTC 20 January surface streamline and isotach analysis over Northeast Colorado. Lines with arrows are streamlines, heavy dashed lines are speeds in ms^{-1}, and thin lines are 500 m terrain height contours.

Chapter 3

RADAR OBSERVATIONS AND ANALYSIS

In this chapter attention is given to description of observations and analysis of single- and dual-Doppler radar data. Previous studies on precipitation bands in winter storms cited in Chapter 1 made extensive use of radar data to locate, measure intensities, and evaluate kinematic properties of the bands. Similarly, use of WISP-91 radar data aided in the observation and analysis of snow bands occurring during the 19-20 January storm. Organized patterns in PPI displays of equivalent reflectivity (Z_e) were used to identify the bands, their orientation, and their structure. A brief description of data collection and processing techniques is given in section 3.1. Single-Doppler radar observations documenting bands of several scales, orientations both parallel and perpendicular to the upper level flow, and precipitation cores are presented in section 3.2. Estimates of mesoscale vertical motion (discussed in section 3.3) were made using the extended vertical-azimuth display (EVAD) technique (Srivastava *et al.* 1986, Matejka and Srivastava 1991). Finally, section 3.4 describes a dual-Doppler analysis performed at 2327 UTC 19 January to describe a particular snow band in greater detail. Appendix C lists the radar characteristics for the Colorado State University (CSU) CHILL and National Oceanic and Atmospheric Administration (NOAA)/NCAR Mile High (MHR) radars.

3.1 Data Collection and Processing

Data collection at the CSU-CHILL radar began at 1811 UTC 19 January and lasted until 0030 UTC (transmitter arcing forced an end to operations at this time). The MHR collected data between 1719 UTC 19 January and 1036 UTC 20 January. During operations, scientists at CSU-CHILL monitored the storm progress and communicated with the WISP operations center in Boulder, CO by radio. Decisions on scanning strategy were made on the basis of on-site scientist inputs, support for aircraft operations, and storm type. For this case the CSU-CHILL alternated between 360° volume scans consisting of 24 elevation angles, with the highest being 22.5°, and RHI scans. In an effort to keep the size of radar data sets more manageable, data were not collected for the portion of any beam that was above 6 km AGL (which was above observed echo tops for this event). The scanning strategy of the MHR consisted of 21 elevation angle scans, with the highest being 17 degrees. All CSU-CHILL volume scans began at the same time as MHR volume scans.

Field data from CSU-CHILL radar were recorded on nine track tapes for subsequent transfer to a universal format (NCAR 1991) Exabyte® tape for processing on Sun® workstations. MHR data were archived on the NCAR Mass Storage System (MSS) after completion of the experiment. Radar volumes of interest were retrieved from MSS for local processing by file transfer protocol (ftp) over the high speed INTERNET data network. Volume scans between 1900 and 2356 UTC 19 January and 2104 UTC 19 January to 0053 UTC 20 January were processed for CSU-CHILL and MHR radars respectively. Appendix B summarizes the major processing steps necessary to edit folded velocities and noisy data, convert spherical coordinate data to Cartesian coordinates, and display the results as constant altitude plan position indicator (CAPPI) displays or vertical cross sections, or use the Cartesian data to generate dual-Doppler syntheses. Data were used in radar polar coordinates for EVAD analysis. Regions of Doppler velocity folding were small due to low target velocities with respect

to the Nyquist velocities (28.67 ms^{-1} and 24.75 ms^{-1} for the CSU-CHILL radar and MHR respectively). Data contaminated by ground clutter near the radar or returns from the Rocky Mountains, approximately 40-60 km southwest to northwest of the radars (see Fig. 1.1) were deleted using the Research Data Support System (RDSS) (Mohr *et al.* 1986). Data points with radial velocities $\pm$ 2 ms^{-1} and reflectivities exceeding 35 dBZ (precipitation echoes were generally less than 35 dBZ) within 80 km of the radar, were deleted, though care was taken to avoid eliminating good data. After the first few volumes, regions that corresponded to ground clutter or mountain returns were known with sufficient accuracy that only the bad data were removed.

3.2 Single-Doppler Observations

Passage of the cold front between 1800 and 2100 UTC 19 January over northeast Colorado signaled the onset of north-northeast flow and upslope conditions over the region, particularly over the northern portion of the Palmer Divide. Echoes developed rapidly between 1900 and 2100 UTC. After 2100 UTC widespread precipitation generated nearly solid radar echoes, particularly below 3 km MSL (approximately 1600 m and 1400 m AGL at CSU-CHILL and MHR respectively) and over the northern portions of the radar coverage area. Above 3 km, echoes took on a distinct banded structure that paralleled the 800-400 mb thermal wind field. This organization to the echo pattern, with the exception of variations due to movement and intensity changes, persisted through at least 0100 UTC when radar data processing was discontinued. Figures 3.1a-d show a series of MHR 2249 UTC CAPPI reflectivity plots, which characterize the echo organization during the observation period, for the levels of 2.5, 3.5, 4.5, and 5.5 km (MSL). Snow was widespread over the northern portions of the region at the lower levels with no obvious echo structure. At higher levels and particularly to the south of the radar, echoes exhibit a highly-banded

structure. Bands were oriented south-southwest to north-northeast, and paralleled the upper level winds. This is similar to the cases described by Wolfsberg *et al.* (1986), Shields *et al.* (1991), Seltzer *et al.* (1985) and others.

The radial velocity field corresponding to Figs. 3.1a-d is shown in Figs 3.2a-d. The 2.5 km (MSL) CAPPI shows well defined north-northeast flow. Soundings and wind profiler data indicated the depth of this layer to be on the order of 1.5 to 2 km. There was little change in this depth over the radar observational period. Winds backed rapidly over a shallow shear layer near 4 km (MSL) and became west-southwesterly and increased in speed with height above 4 km (MSL). There was little change in wind direction above the shear layer.

After 2330 UTC 19 January low level reflectivities developed and increased in area over a region north of the western portions of the Palmer Divide. The growth and intensification of low level echoes is illustrated by the reflectivity field changes at 2.5 km observed between 2346 UTC 19 January and 0044 UTC 20 January (Figs. 3.3a-b). A video loop of the MHR 1.6 degree elevation scans for the period between 1900 UTC 19 January and 0300 UTC 20 January showed the region grew slowly in areal extent, and moved south-southwest coincident with the low level north-northeast winds. Periods of moderate snow at Jefferson County Airport (BJC), Centennial Airport (APA), and Denver (DEN) corresponded to passage of this low level enhanced reflectivity region. Centennial Airport (APA), the station closest to the northern slope of the Palmer Divide, reported moderate snow between 0145 and 0600 UTC 20 January while Jefferson County Airport (BJC) nearest station to the rapid terrain rise of the Front Range, reported moderate snow between 0055 and 0400 UTC. Farther out in the plains, Denver (DEN) had periods of moderate snow between 2219 - 2302 UTC 19 January, 0030 - 0138 UTC 20 January, and 0332-0452 UTC.

The period of moderate snow at Denver between 2219 and 2302 appears related to a phenomena other than low level upslope flow. Reflectivity CAPPIs at 5 km in Figs. 3.4a-b show an upper level band crossing over Denver during one of the periods of moderate snow. There was a corresponding region of higher reflectivities at lower levels as well. The band also had cores of higher reflectivities similar to cores described by Carbone and Bohne (1975) in their examination of cellular regions of snow generation. They found upper level reflectivity maxima were associated with vertical velocities of $\pm$ 1.5 ms^{-1} and deduced that a trail of falling ice crystals associated with the cores played a role in snow crystal growth at lower levels, similar to the "seeder-feeder" mechanism discussed by Rutledge and Hobbs (1983).

Bands with embedded reflectivity cores were a common feature in this case. The video loop of MHR 1.6 elevation angle scans showed well defined bands and cores in the upper levels. In Figs. 3.4a-d, a band and associated cores identified by the yellow and orange tints representing higher reflectivities illustrate this movement. The west-southwest to east-northeast movement of the cores at speeds of approximately 18 ms^{-1} mirrored the CLASS reported winds near 5 km which ranged between 17 and 21 ms^{-1} with the stronger winds reported by the southern stations. Examination of the video loop showed that bands propagated to the southeast and at a slower speed than the cores. It appeared that the band motion reflected the synoptic scale motion associated with the upper level trough of low pressure which was moving to the southeast about 14 ms^{-1}, as estimated by the movement of the 500 mb trough axis.

The 0044 UTC MHR 3.5 and 5 km (MSL) reflectivity CAPPI in Figs. 3.5a-b show the leading edge of another band south of the radar. Vertical cross sections of reflectivity and radial velocity are shown in Figs 3.6a-b. Note the region of almost zero velocity near 18 km in the horizontal and 5.5 km in the vertical. A case could be made for clockwise rotation (looking upwind towards the west or counterclockwise looking

downwind towards the east) around an axis near 20 km south of the radar. Hence upward vertical motion to the south of the axis and downward (or weaker upward) motion to the north would be expected. The reflectivity cross section supports this observation with stronger echoes to the south in the upward vertical motion region and weaker echoes in the north.

Another type of banded or wavelike feature is shown in Fig 3.7. Here a highly banded feature had a series of higher reflectivity cores spaced at regular intervals of approximately 12 km within the band. Figs. 3.8 a-b show cross sections of reflectivity and radial velocity taken through the axis indicated by the black line in Fig. 3.7. The periodic and wave-like appearance of the echoes suggest a different formation mechanism than that which caused the east-northeastward propagating cores in the bands described above. The periodic cores observed in this band showed little motion relative to the band. Satellite imagery (not shown) indicated the band extended to the Colorado-Utah border which is beyond the range of the radar, thus the band appears to end some 70 km west of Pike's Peak. This is fortuitous since it permits display of the terrain upwind of the band which is dominated by the abrupt rise of the Continental Divide, illustrated by the gray shaded region in Fig. 3.7 and west of the lower and flatter terrain of South Park. The 12 km spacing between reflectivity cores, lack of band parallel core motion to the east-northeast, and upwind terrain features are characteristics found with trapped lee waves (Durran 1986). The wave like structure in the band was a persistent feature and is seen in Figs 3.4a-d. Chapter 4 presents more discussion on the possibility of mountain waves and their role in precipitation bands.

3.3 Extended Velocity-Azimuth Display (EVAD) Analysis

Radar data can provide insight into the kinematic structure of mesoscale features beyond that obtained from simple examination of horizontal or vertical cross sections.

In general, dual-Doppler techniques provide an effective means of determining properties such as divergence, vorticity, and horizontal and vertical velocities on the order of a kilometer (Srivastava *et al.* 1986) and is limited by radar beamwidth (which increases with range), ambiguities associated with the intersection angle between the two radar beams, and gridpoint spacing (Davies-Jones 1979, Mohr *et al.* 1986). Estimates of the above properties, particularly the vertical velocity, over a larger scale represents another problem. Averages of the grid point values over the dual-Doppler domain could be generated as one way to look at larger scale vertical motions. However, this method is subject to errors introduced by the interpolation scheme as well as errors in the measurement of divergence. Divergence errors may introduce errors into the vertical motion calculation that are even larger than the actual vertical velocities under consideration for areas of widespread precipitation.

Early radar meteorology studies showed the potential capability of Doppler radar to evaluate the horizontal kinematic structure of widespread precipitation echoes. Lhermitte and Atlas (1961) laid the foundation for the method used here with the velocity-azimuth display (VAD) technique. Browning and Wexler (1968) refined their idea so that VAD gave reliable estimates of various horizontal kinematic properties over the radar volume depth. These properties included divergence, wind speed and direction, deformation and axis of dilation, and are the results of calculation using coefficients obtained from a Fourier series analysis of the radial wind field. Browning and Wexler (1968) discussed several limitations to their technique including inhomogeneities in precipitation fall speed and vertical wind shear effects. They suggest using elevation angles less than 27 (9) degrees in snow (rain) to avoid large errors in VAD divergence calculations introduced by the hydrometer terminal fallspeed, which gains computational significance with increasing elevation angles. The VAD technique has been used to evaluate horizontal divergence and vertical velocity with success by

several winter storm researchers including Lilly (1981), Shields *et al.* (1991), Hobbs *et al.* (1980), and Houze *et al.* (1981).

The extended velocity-azimuth display (EVAD) was designed by Srivastava *et al.* (1986) to minimize the sources of error identified by Browning and Wexler (1968). The VAD technique is *extended* by incorporating the hydrometeor terminal fall speeds, avoided in VAD, into the divergence calculation. Also, EVAD makes use of higher elevation angle sweeps than used in VAD to obtain better estimates of terminal fall speeds. The increased accuracy of EVAD divergence calculations permit more accurate estimates of the mean vertical velocity incorporating all the data in a user specified cylindrical volume around the radar. This technique was originally designed to study the stratiform regions associated with mesoscale convective systems (Srivastava *et al.* 1986). Matejka and Srivastava (1991) provide suggestions on data collection techniques in which they recommend at least 20 sweeps with a maximum elevation angle of at least 50 degrees. In this study the maximum elevation angles were 22.5 and 17 degrees and the number of scans in each volume were 24 and 21 for CSU-CHILL and MHR respectively. Since the depth of the storm was less than 6 km, and horizontal velocities were fairly uniform, it was felt that the data loss from lack of high elevation angles would not be too significant. Results from the EVAD technique appear reasonable and agree with values for similar types of storms over northeast Colorado using different methods (Reinking and Boatman 1986, Wesley 1991). However, the data provided by increasing the elevation angle might provide more accurate estimates of terminal fall speeds which would lead to better divergence results, primarily at high elevation angles where terminal fall speeds gain significance in the calculation. An experiment to compare true EVAD scans with the scanning strategy used during this case would help resolve ambiguities over the accuracy of the results presented below. EVAD analyses

were computed approximately every half hour and examined for continuity and agreement between both radars.

The EVAD program is a two step process, VAD analysis is run first to obtain coefficients used in the radial wind equation computed over a series of rings along a constant elevation angle scan from the radar to the maximum cylinder radius. The coefficients obtained from all sweeps constitute a data set in which values are identified by range and altitude above the ground. In EVAD, a finite depth is selected (usually the range gate spacing) over which coefficients having altitudes within the specified layer are used to calculate the divergence, and terminal fall speed. This process is repeated for each layer until the top (bottom, if using top down integration) is reached. Once the divergence profile was obtained, the vertical velocity was computed using the anelastic version of the continuity equation:

$$\nabla_h \cdot \mathbf{V} + \partial(\rho w)/\partial z = 0 \qquad (1)$$

Sensitivity tests were conducted to examine the results of varying the cylinder radius over which the EVAD was calculated. Within VAD and EVAD, calculations of wind coefficients and divergence/terminal fall speed can be performed over user defined radii. For the sensitivity tests conducted in this research, the largest radius used was 40 km in order to avoid interference from mountain returns, or deleted data gates associated with the mountains. After several iterations of various VAD and EVAD radii combinations, it was found that the EVAD results were fairly insensitive to changes in the VAD radius as long as the VAD radius remained larger than the EVAD radius and was greater than 20 km. Results were most sensitive to the choice of the EVAD radius particularly when it was less than 20 km. Increasing sensitivity with decreasing ring size was probably a result of using a maximum elevation angle of 22.5 degrees. The sensitivity study permitted optimization of the VAD portion of the program since more computer processing time was needed for larger VAD radii. A VAD cylinder diameter

of 25 km was chosen as the best compromise between processing time and results. A radius of 24 km was chosen for the EVAD portion of the program to take advantage of as many rings as possible.

Results of the temporal continuity comparison were encouraging, particularly with the CSU-CHILL data. Figs. 3.9a-d and Figs. 3.10a-d show EVAD vertical profiles at the same half hour intervals beginning 2202 UTC 19 January for CSU-CHILL and MHR respectively. The vertical velocity profiles for the CSU-CHILL EVADs were consistent over time and indicated a roughly parabolic shape to the profile with a maxima near 2800.m There is rather poor temporal agreement between MHR generated profiles at first glance. Upon closer inspection, several features persist through the series including peak upward motion near 3000 m. Profiles from MHR at later times showed better continuity between successive plots than those illustrated in 3.10a-d.

In both the CSU-CHILL and MHR profiles, the straight line at the top from 0 to the next data point down indicates a weakness in the procedure. It was assumed that the vertical velocity was zero at the radar cloud top. This is probably not the case given the insensitivity of 10 cm radar to small ice particles suspected at the cloud top. The actual cloud top probably extends beyond the radar cloud top by perhaps as much as 1km. Soundings indicate that the tropopause was near 7500 m (MSL) which represents a difference of at least 1 km to the highest echo tops. Matejka and Srivastava (1991) suggest that a value other than zero for the top boundary condition may give better results.

Inter-radar comparison shows agreement in the occurrence of a low level maxima between 2500 and 3000 m and an poorly defined minima near 4000 m. Beyond that there is not much agreement in magnitude or profile shape. Vertical velocities derived from the EVAD technique using CSU-CHILL appeared to have vertical

velocities approximately 8-10 cms^{-1} greater than results obtained from MHR data which may stem from two possibilities:

1. CSU-CHILL had more scans and a higher maximum elevation angle than MHR. This would lead to more data points for EVAD calculations.
2. CSU-CHILL and MHR experienced different meteorological conditions.

Despite the differences, EVAD analyses showed upward vertical motion through the entire depth of the cloud for nearly all profiles. The peak magnitudes (18 to 25 cms^{-1}) from this study compare favorably with observations and modeling studies of Front Range snow storm vertical velocities obtained by other researchers and are shown in Table 1.

Table 1: Summary of Vertical Velocities for Front Range Upslope Storms.

Author	O* or M*	Vertical Velocity (cms^{-1})	Remarks
Lilly (1980)	O	5	Derived from VAD analysis
Walsh (1977)	O	10	Eastern Wyoming Anticyclonic winter storm
Boatman and Reinking (1984)	O	1-2	Shallow anticyclonic system, terrain induced
Shapiro (1984)	O	600	Associated with strong frontal passage at BAO†
Auer and White (1982)	O	6.5	Cyclonic storm
Raddatz and Khandekar (1979)	M	15	Modeling study of upslope precip over western Canadian Plains
Abbs and Pielke (1986)	M	10	Model results at 1.35 km (AGL)
Wesley (1991)	M	40	Model study of cold air damming

* O = Observational study. M = Modeling study.
† BAO - Boulder Atmospheric Observatory; 300 m instrumented tower.

3.4 Dual-Doppler Observations

One of the earliest (and few) dual-Doppler studies of winter storms was that performed by Bohne (1979). He examined shallow snow bands (< 2.5 km in depth) that were associated with a deep, vertically stacked low pressure area over central Illinois. The bands did not have the well defined thermal wind orientation found in the bands studied here. However, as with this case, the bands propagated in a manner that suggested a connection to the synoptic flow, while precipitation cores moved in the band with the mean wind vector through the layer. Bohne (1979) also used dual-Doppler techniques to evaluate the vertical motion distribution and found a maximum magnitude of 1.25 ms^{-1}, though the mean magnitude was typically 20-40 cms^{-1}. VAD analysis was not performed on this case. Heymsfield (1979) conducted a dual-Doppler study of precipitation bands associated with a warm front over northern Illinois. Three major bands were spaced about 100 km apart and associated with organized vertical circulations in a layer 2.5 km deep just over the warm frontal boundary. Synoptically, both cases were different from each other as well as the case examined here. Finally, Kessinger and Lee (1991) describe the results of real-time operations of a dual-Doppler network during WISP-90 strictly from the standpoint of computer software evaluation.

Dual-Doppler analysis in this study was accomplished by using three programs to edit, transform data from spherical to Cartesian coordinates, and synthesize data from two radars into a single data set. As described in section 3.1, data were edited with RDSS. For the Cartesian transformation, the Sorted Position Radar INTerpolation (SPRINT) (Mohr *et al.* 1986) program was used. The program requires specification of the x, y, and z ranges of the Cartesian coordinate axis system as part of the program input file. The coordinate ranges were selected on the basis of data availability, crossing angle of the radar beams, and the spatial resolution. The last two criteria are geometrical factors that determine the accuracy of the dual-Doppler derived horizontal wind field (Davies-Jones 1979). For this case a 30 degree crossing angle and 1.25 km spatial

resolution were used to define the prime coverage area having acceptable horizontal velocity errors. Usually, there are two dual-Doppler lobes, one on each side of the base line (see Fig 1.1). Missing data from MHR created large data gaps in the northeast sector of the volume precluding use of the eastern dual-Doppler lobe. The box shown in Fig. 1.1 shows the region selected for the horizontal transform. Grid spacing was 1 km in both the x and y directions. Vertical spacing was 500 meters from 2 to 7 km MSL (0.5 to 5.5 km AGL). Figure 3.13 shows a close-up of the dual-Doppler region, radar locations, the geometric discriminators, and terrain contours.

Once the Cartesian transform of the radial velocity and reflectivity fields from both radars was complete, a synthesis was performed using the Custom Editing and Display of Reduced Information in Cartesian Space (CEDRIC) program (Mohr *et al.* 1986) to obtain u (east-west) and v (north-south) winds, convergence fields, and vertical velocity. Vertical velocities were obtained by integration of the anelastic form of the continuity equation, assuming $w = 0$ at the top of each echo column. The two radar solution obtained in CEDRIC necessitated computing hydrometer fallspeeds from a reflectivity-fallspeed relationship derived by Atlas *et al.* (1973).

Unfortunately, the first attempt at a dual-Doppler analysis indicated there was a problem in the chain of programs leading to the dual-Doppler synthesis. There were unacceptable gaps in the vertical velocity field across a horizontal plane, furthermore, gaps increased with height. After many sensitivity tests in which input and output parameters for RDSS, SPRINT, and CEDRIC were altered in a variety of ways for both radars to find maximum coverage, the conclusion was reached that a problem existed with the SPRINT interpolation scheme. The problem was particularly noticeable with CSU-CHILL data and may be a result of fewer data points from running the radar at slightly reduced power due to transmitter arcing. An independent test run of CSU-CHILL data by CSU-CHILL personnel using other transformation software developed

at the University of Chicago, verified SPRINT was not interpolating all the RDSS universal format spherical coordinate data to Cartesian coordinates. It is unclear where the problem with SPRINT lies and time constraints prohibited an examination of the software or seeking an alternative program.

Despite the problems encountered in generating vertical velocities from synthesized fields, enough data was extracted to prepare horizontal wind vector fields at most levels for the 2328 UTC 19 January volume scan. Figs 3.14a-f show the MHR CAPPI reflectivity patterns and horizontal winds obtained from the dual-Doppler analysis. An arrow with the length of one gridpoint spacing represents a speed of 15 ms^{-1}. Comparison between dual-Doppler derived winds and the Denver wind profiler (Fig. 2.7b) shows good agreement. Low-level flow was north-northeasterly backing with height, then increasing in speed with little change in direction above 4 km. Note the weak winds at 3 km (Fig. 3.14c), this corresponds to the layer of maximum shear between the northeasterly surface winds associated with the arctic airmass and the west-southwesterly winds aloft. Tables 2 and 3 list the mean, standard deviation, minimum, and maximum of the u and v wind components computed for each level between 2 and 5 km MSL.

Finally, a bulk Richardson number profile was computed using the mean wind values for the dual-Doppler region and thermodynamic data from the 0000 UTC 20 January Berthoud sounding. The bulk Richardson number was calculated using Stull's (1988) equation:

$$R_B = \frac{g\,\Delta\theta_v\,\Delta z}{\theta_v[(\Delta U)^2 + (\Delta V)^2]} \qquad (2)$$

where :

g = gravity

$\Delta\theta_v$ = the change in the virtual potential temperature over a layer

Δz = Layer depth

θ_v = Mean virtual potential temperature in the layer

ΔU = Change in the u (east-west) wind component over the layer

ΔV = Change in the v (north-south) wind component over the layer

The results of the calculation are summarized in Table 4. There appears to be good agreement between the dual-Doppler derived Richardson number and the sounding derived values which are discussed in Chapter 4.

Table 2: Dual-Doppler u Wind Component Statistics.

Height (km)	Mean u (ms^{-1})	u Std Dev (ms^{-1})	u Min (ms^{-1})	u Max (ms^{-1})
2.0	-4.83	1.85	-14.9	4.7
2.5	-5.18	1.32	-13.0	6.5
3.0	-2.10	1.66	-10.9	17.3
3.5	3.52	2.43	-9.3	19.0
4.0	8.27	3.15	-8.3	24.3
4.5	13.01	3.09	-4.8	25.0
5.0	13.98	3.50	-5.3	22.7
5.5	13.69	3.92	-6.1	28.4
6.0	13.56	3.91	3.2	25.0
6.5	13.91	2.77	4.7	20.0

Table 3: Dual-Doppler v Wind Component Statistics.

Height (km)	Mean v (ms^{-1})	v Std Dev (ms^{-1})	v Min (ms^{-1})	v Max (ms^{-1})
2.0	-7.20	1.38	-11.5	-0.9
2.5	-6.10	2.04	-11.2	10.1
3.0	-4.89	1.92	-17.7	20.7
3.5	-1.49	2.53	-18.7	9.1
4.0	1.53	2.03	-7.7	18.0
4.5	1.25	2.82	-11.0	17.0
5.0	1.01	3.35	-14.2	9.3
5.5	1.21	3.60	-13.9	12.3
6.0	1.83	3.80	-13.2	10.2
6.5	3.32	4.30	-13.2	7.7

Table 4: Dual-Doppler Richardson Number Calculation

Center of Layer	Richardson Number
2.25	12.26
2.75	3.26
3.25	1.05
3.75	1.57
4.25	0.84
4.75	26.01
5.25	9.44
5.75	41.83
6.25	12.81

3.5 Summary

Radar data collection and processing techniques were discussed in this chapter as well as single- and dual-Doppler analyses. Results of EVAD calculations of vertical velocity were also presented. Single-Doppler analysis showed the banded nature of

echoes associated with this storm including some wave-like bands over the southern portions of the radar coverage area. Higher reflectivity cores were embedded within the bands. The cores propagated with the upper level winds. Vertical velocity profiles derived from the EVAD technique compared favorably with values obtained by other researchers. Problems with the interpolation program precluded calculations of the vertical velocity distribution using dual-Doppler analysis. However, good agreement was found between horizontal winds computed from dual-Doppler analysis and the DEN profiler. The next chapter will address possible mechanisms for snow band formation.

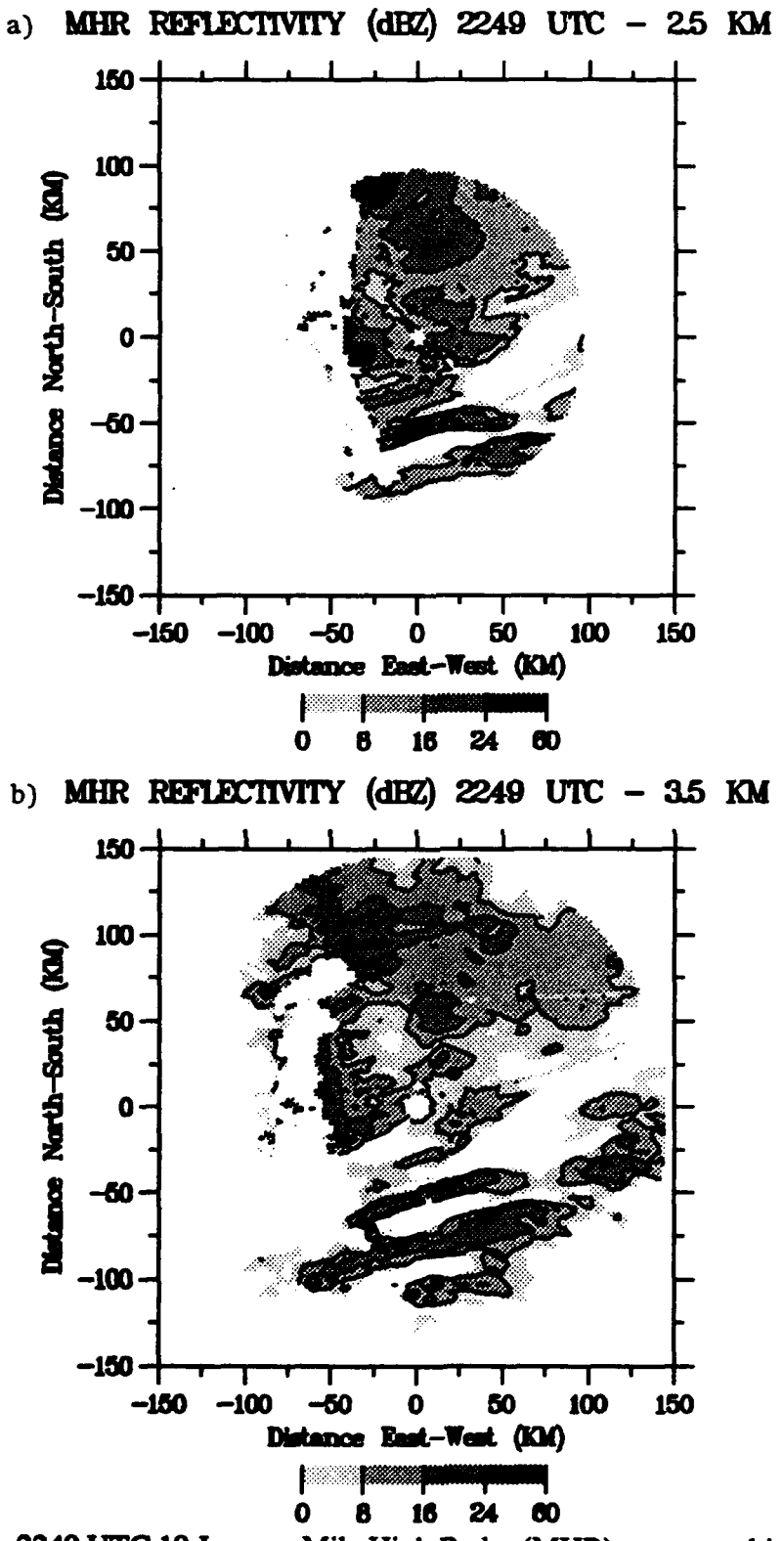

Figure 3.1: 2249 UTC 19 January Mile High Radar (MHR) constant altitude plan position indicator (CAPPI) display for a) 2.5 km MSL and b) 3.5 km MSL. Color bar at bottom indicates ranges of reflectivity in dBZ for each shading, east-west and north-south distances are in km. Gaps in coverage from the southwest to northwest are due to deletion of mountain returns.

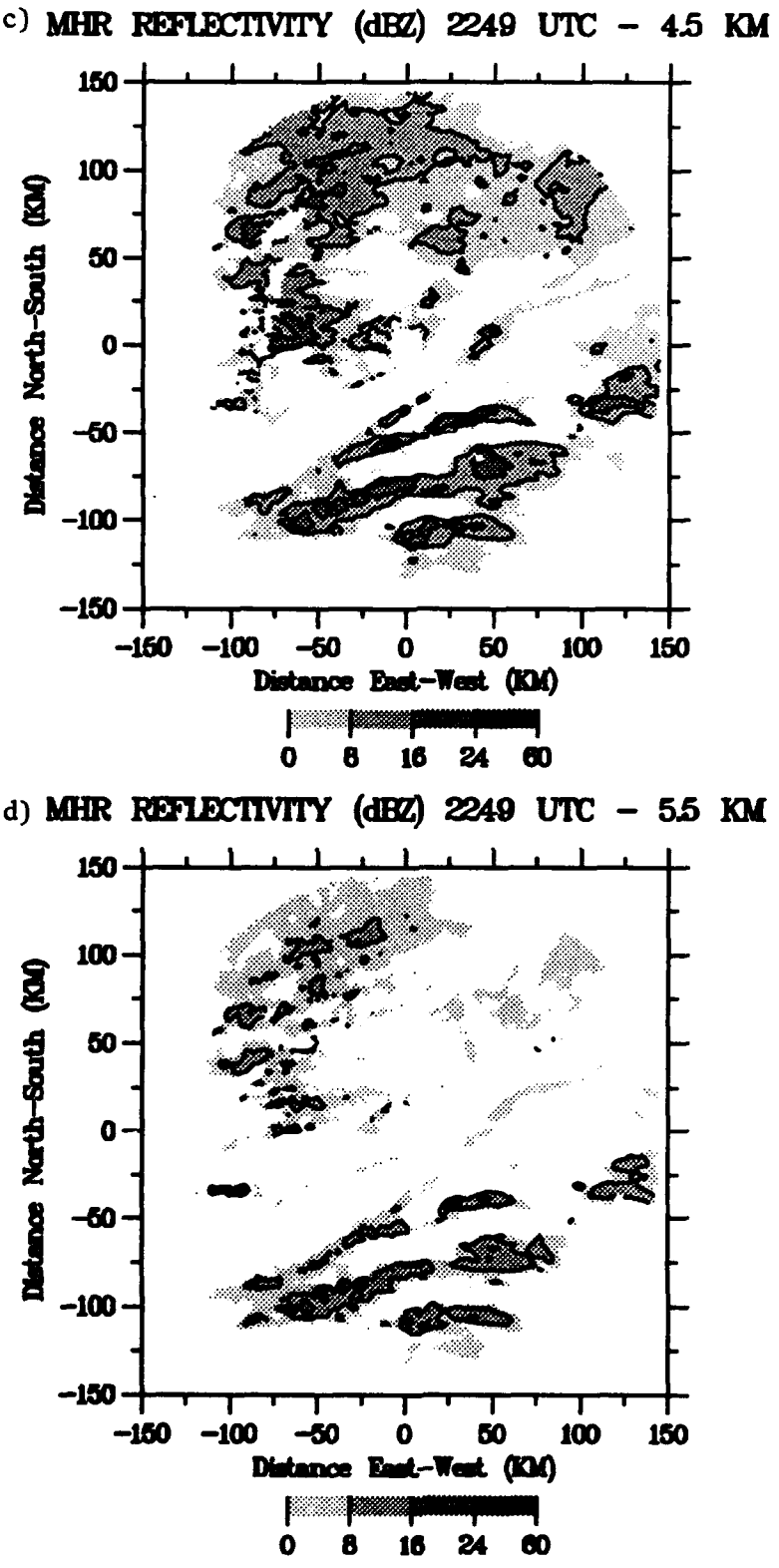

Figure 3.1c-d: Same as (a) except for c) 4.5 km MSL and d) 5.5 km MSL.

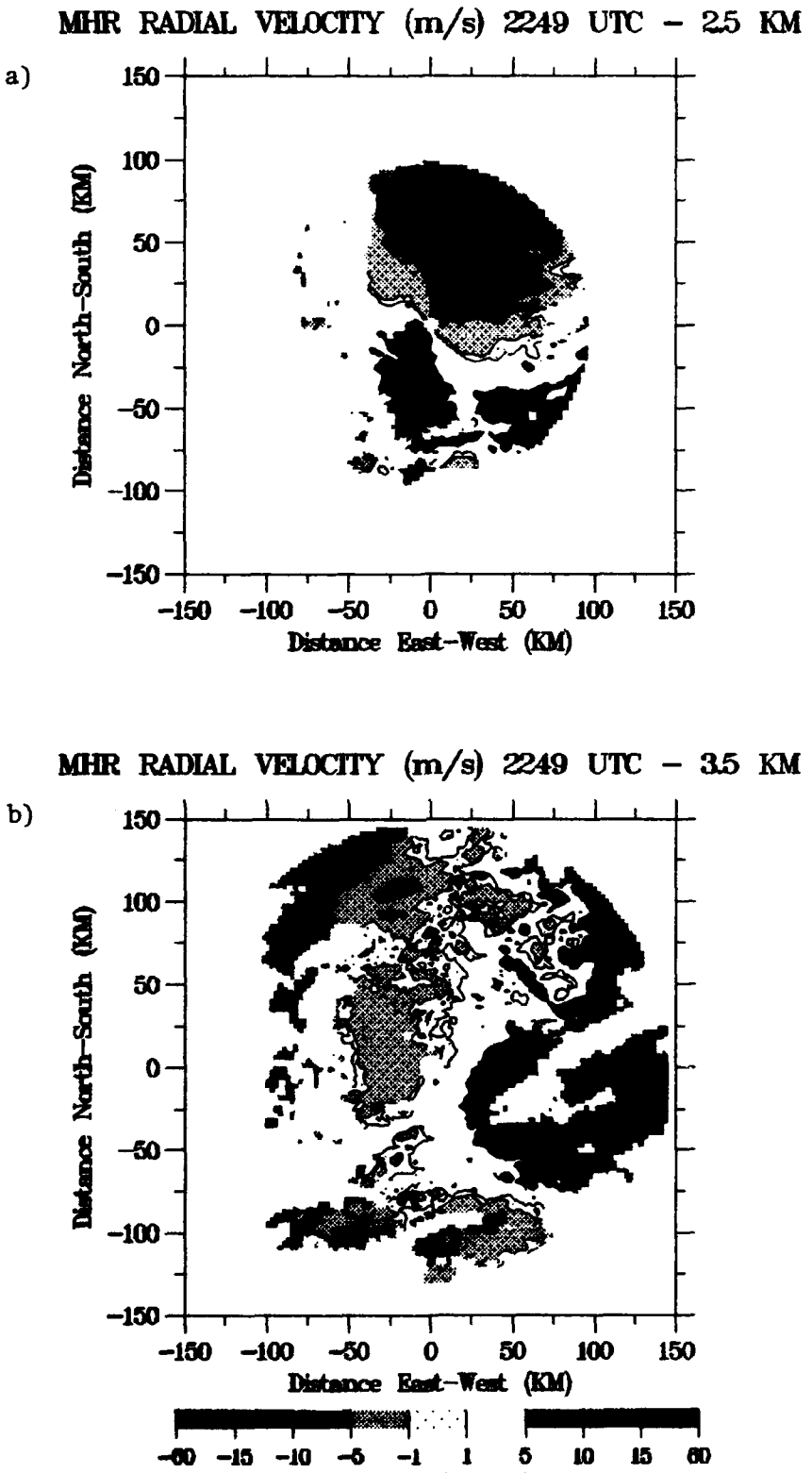

Figure 3.2: 2249 UTC 19 January Mile High Radar CAPPI display of radial velocity for a) 2.5 km MSL and b) 3.5 km MSL. Color bar at bottom indicates ranges of radial velocity in ms^{-1} for each shading, east-west and north-south distances are in km. Dashed contours indicate negative velocities (towards the radar), solid contours represent positive velocities (away from the radar). Coverage gaps to west are due to mountains.

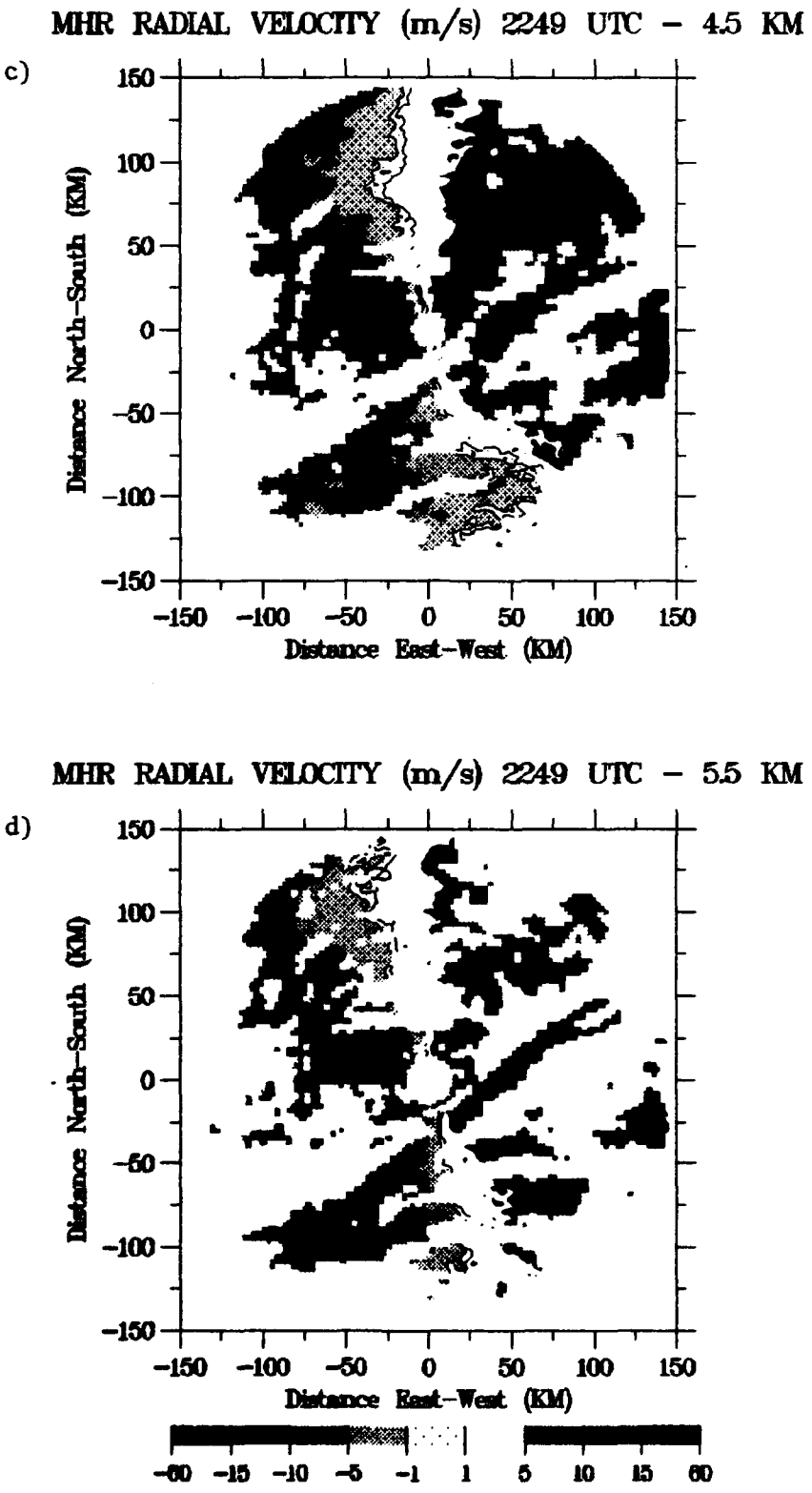

Figure 3.2c-d: Same as (a) except for c) 4.5 km MSL and d) 5.5 km MSL.

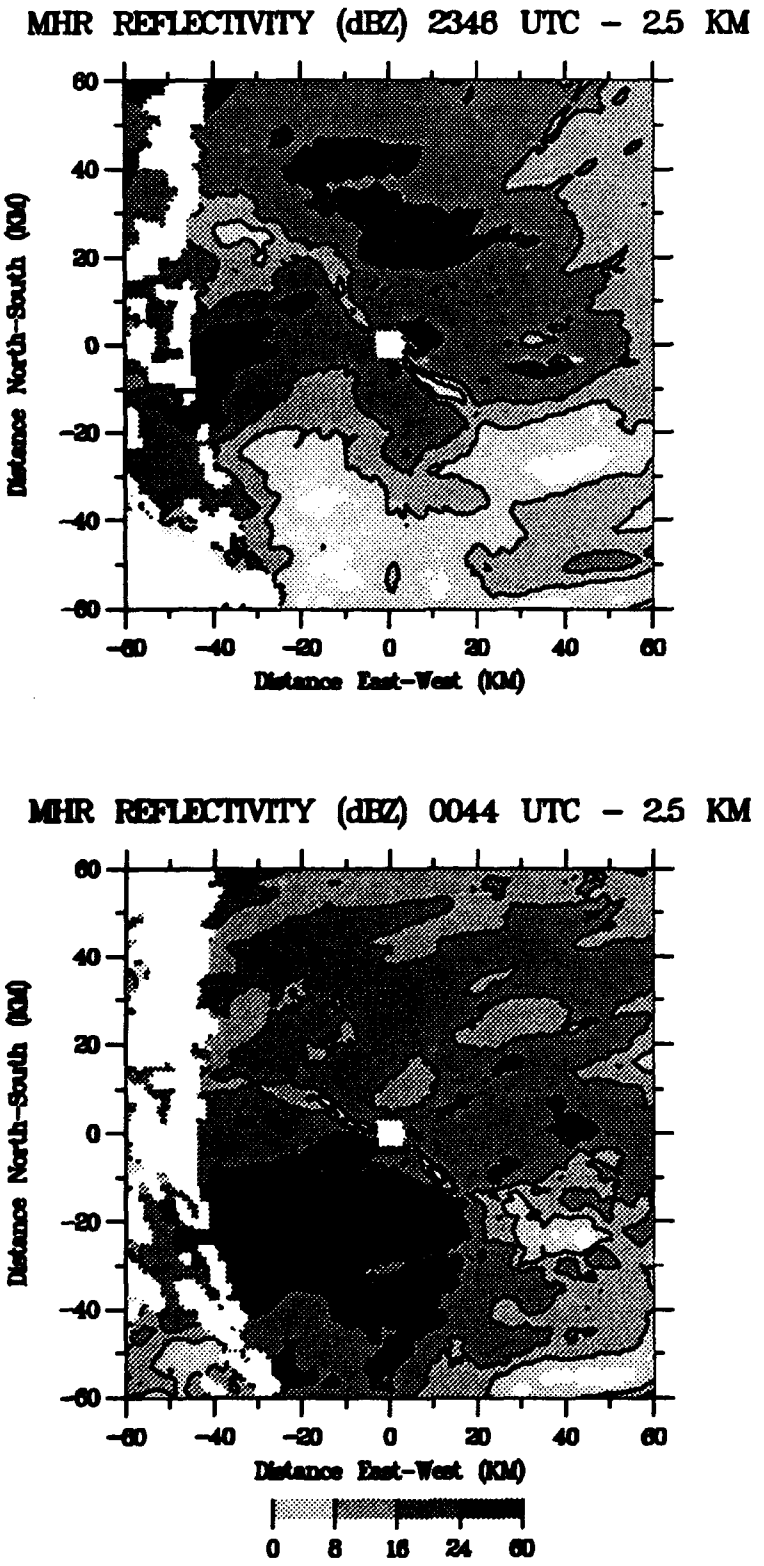

Figure 3.3: 2.5 km MSL Mile High Radar CAPPI reflectivity display of reflectivity for a) 2346 UTC 19 January and b) 0044 UTC 20 January. Color bar at bottom indicates ranges of reflectivity in dBZ, east-west and north-south distances are in km. Gaps in coverage from the southwest to northwest are due to deletion of mountain returns.

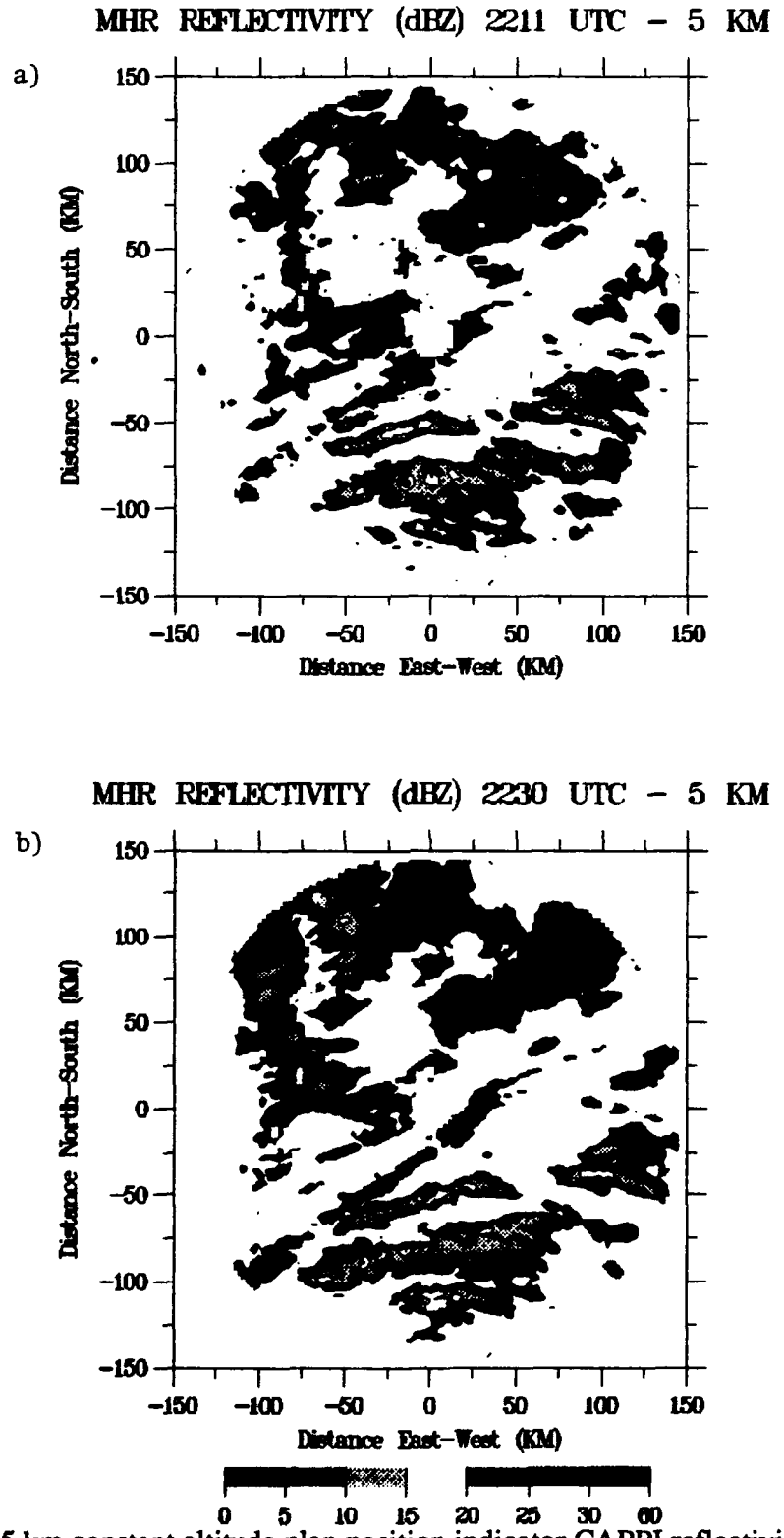

Figure 3.4: 5 km constant altitude plan position indicator CAPPI reflectivity display for a) 2211 UTC and b) 2230 UTC 19 January. Color bar at bottom indicates ranges of reflectivity in dBZ, east-west and north-south distances are in km. Gaps in coverage from the southwest to northwest are due to deletion of mountain returns.

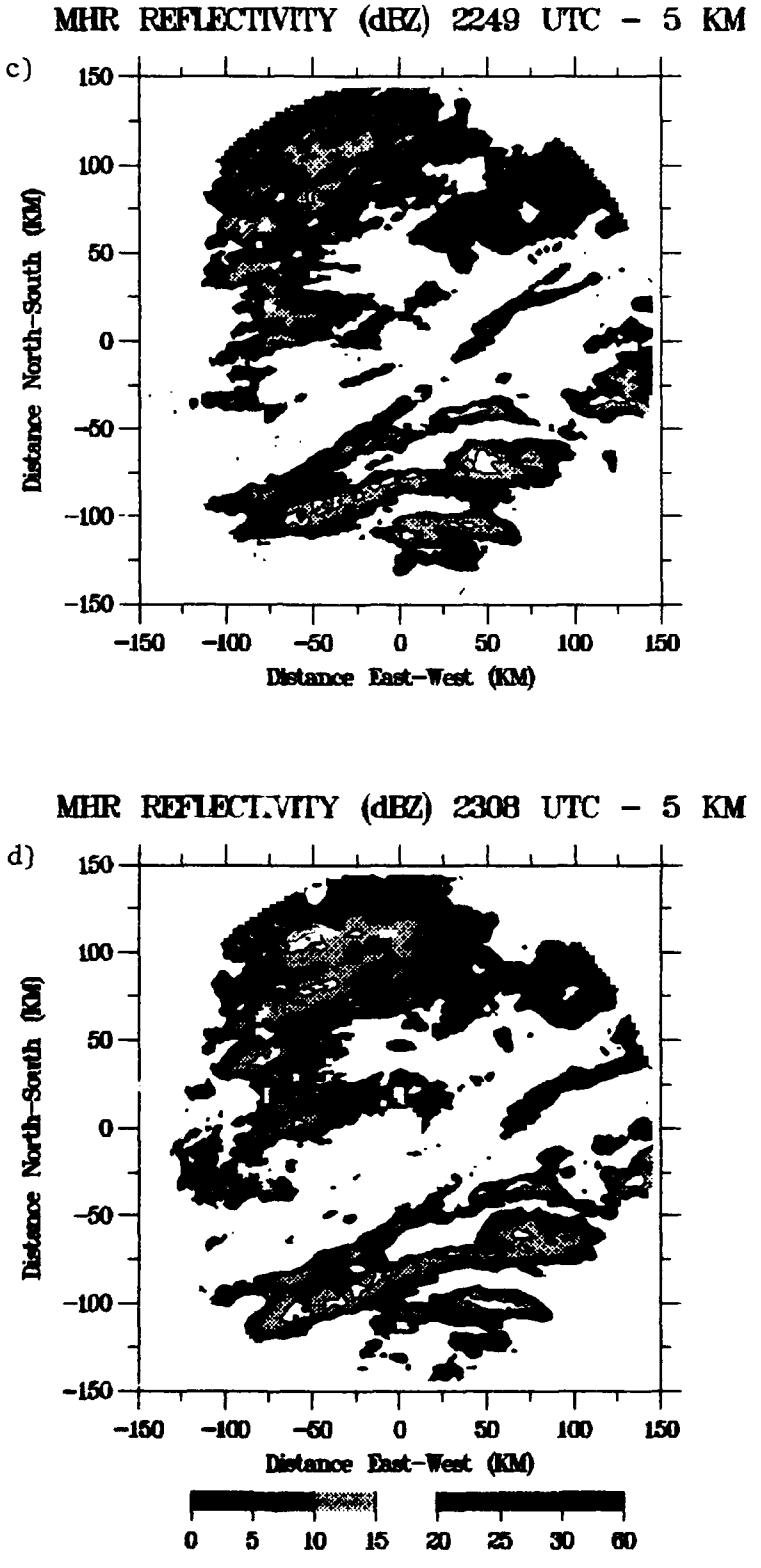

Figure 3.4c-d: Same as (a) except for c) 2249 UTC and d) 2308 UTC 19 January

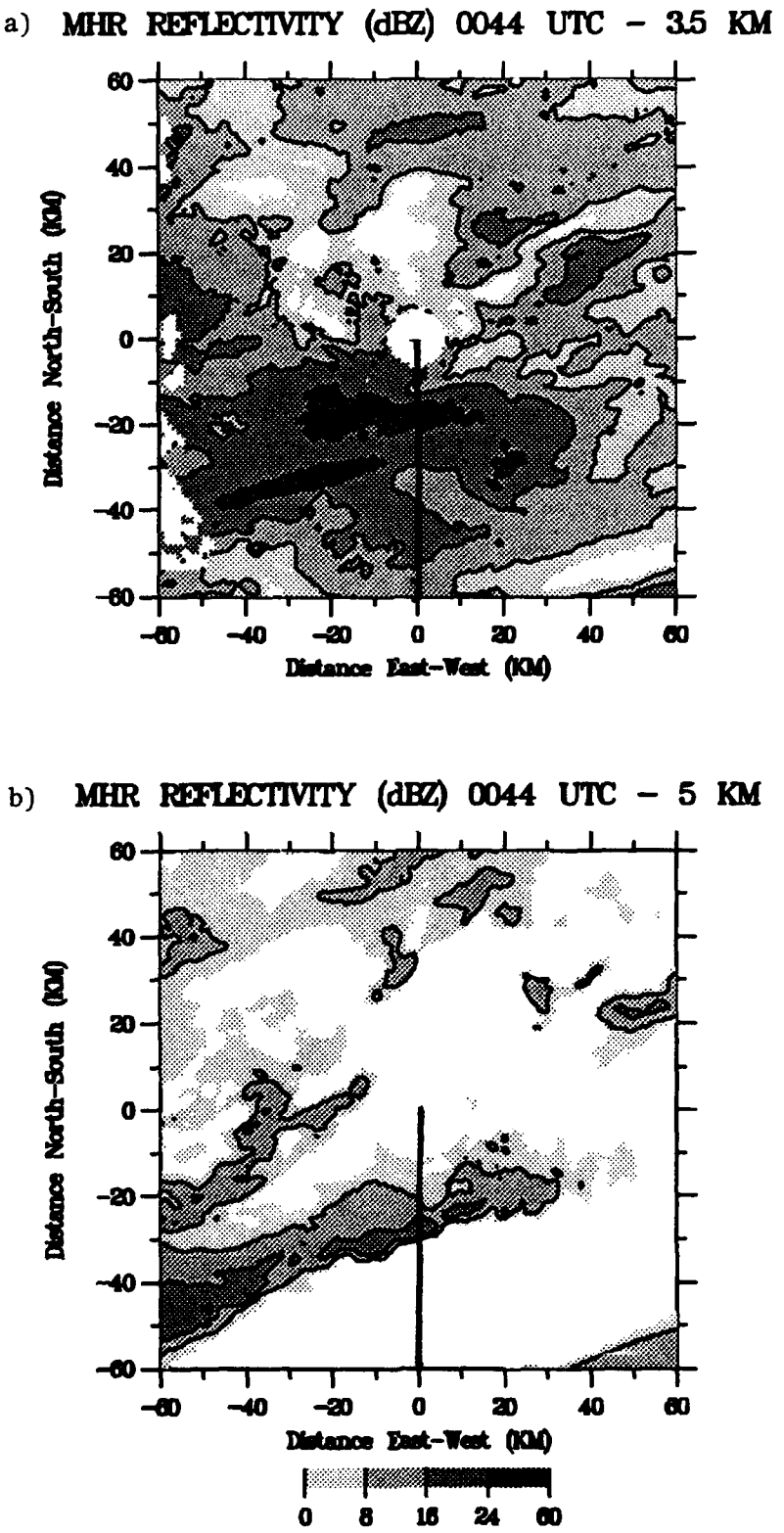

Figure 3.5: 0044 UTC 20 January CAPPI reflectivity display for a) 3.5 km MSL and b) 5.0 km MSL. Color bar at bottom indicates ranges of reflectivity in dBZ, east-west and north-south distances are in km. Gaps in coverage to west are due to deletion of mountain returns. North-south line shows cross section transect used for Figs. 3.6a-b.

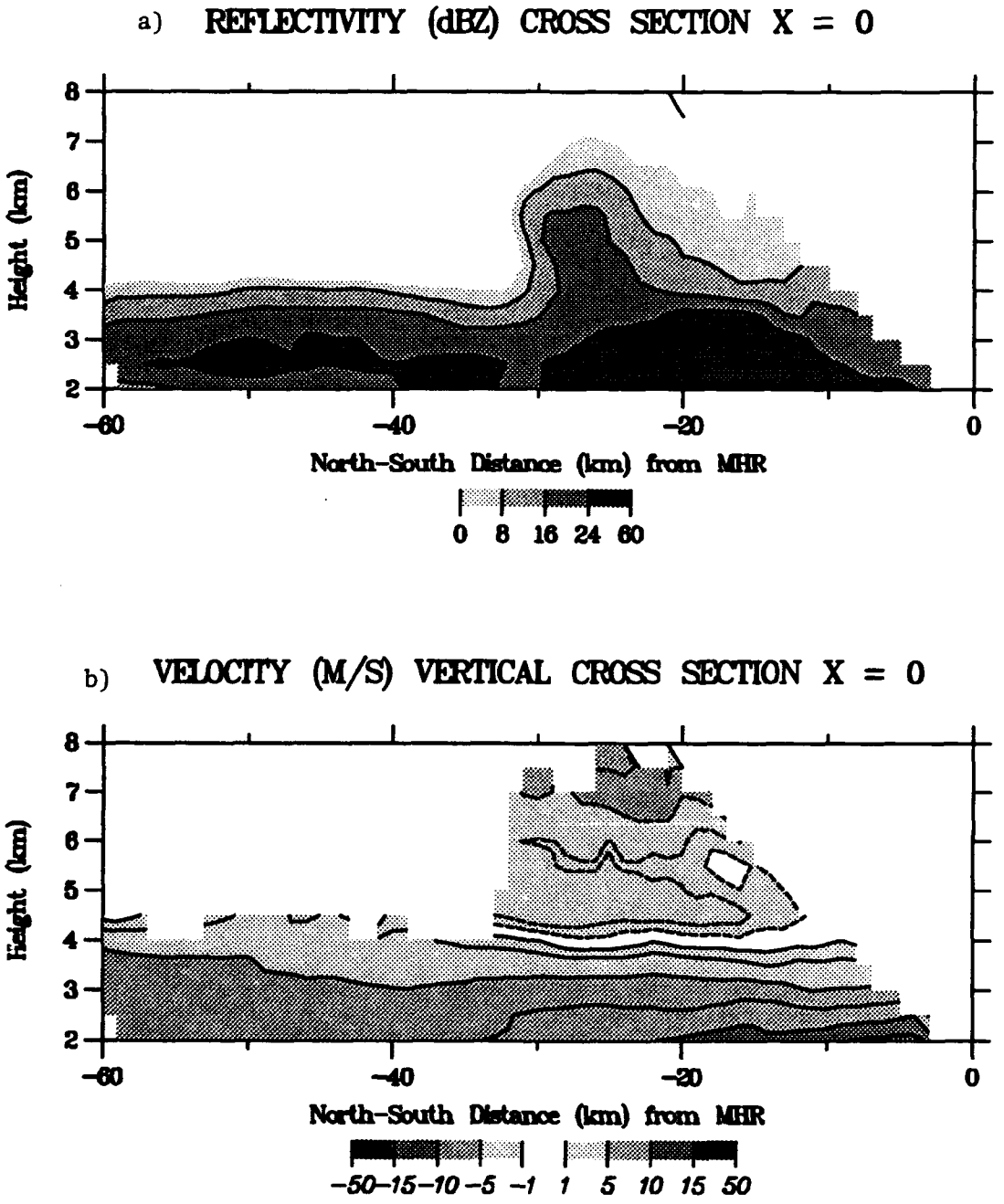

Figure 3.6: 0044 UTC 20 January Mile High Radar vertical cross section of a) reflectivity and b) radial velocity. Color bar at bottom indicates ranges of reflectivity in dBZ. South is to the left, West is looking into the figure. Dashed lines in Fig 3.6b indicate regions of negative (towards the radar) velocity.

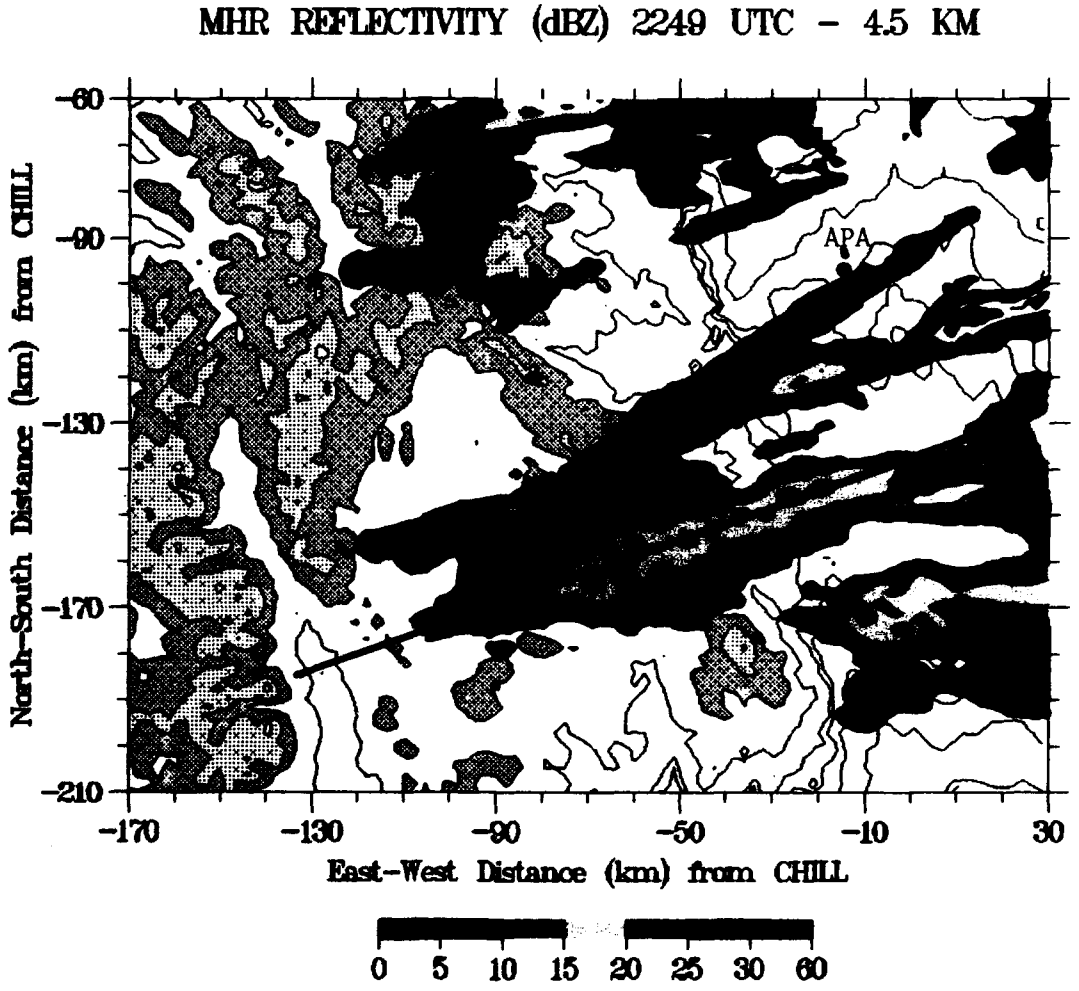

Figure 3.7: 2249 UTC 19 January Mile High Radar CAPPI display of reflectivity for 4.5 km MSL. Red lines are terrain contours in intervals of 200 m to 2000 meters then every 500 m. Dark gray shading indicates terrain between 3000 and 3500 m. Light gray shading represents terrain above 3500 m. APA indicates location of Centennial airport. Color bar at bottom indicates ranges of reflectivity in dBZ for each shading. Black line represents axis used in Figs. 3.8a-b.

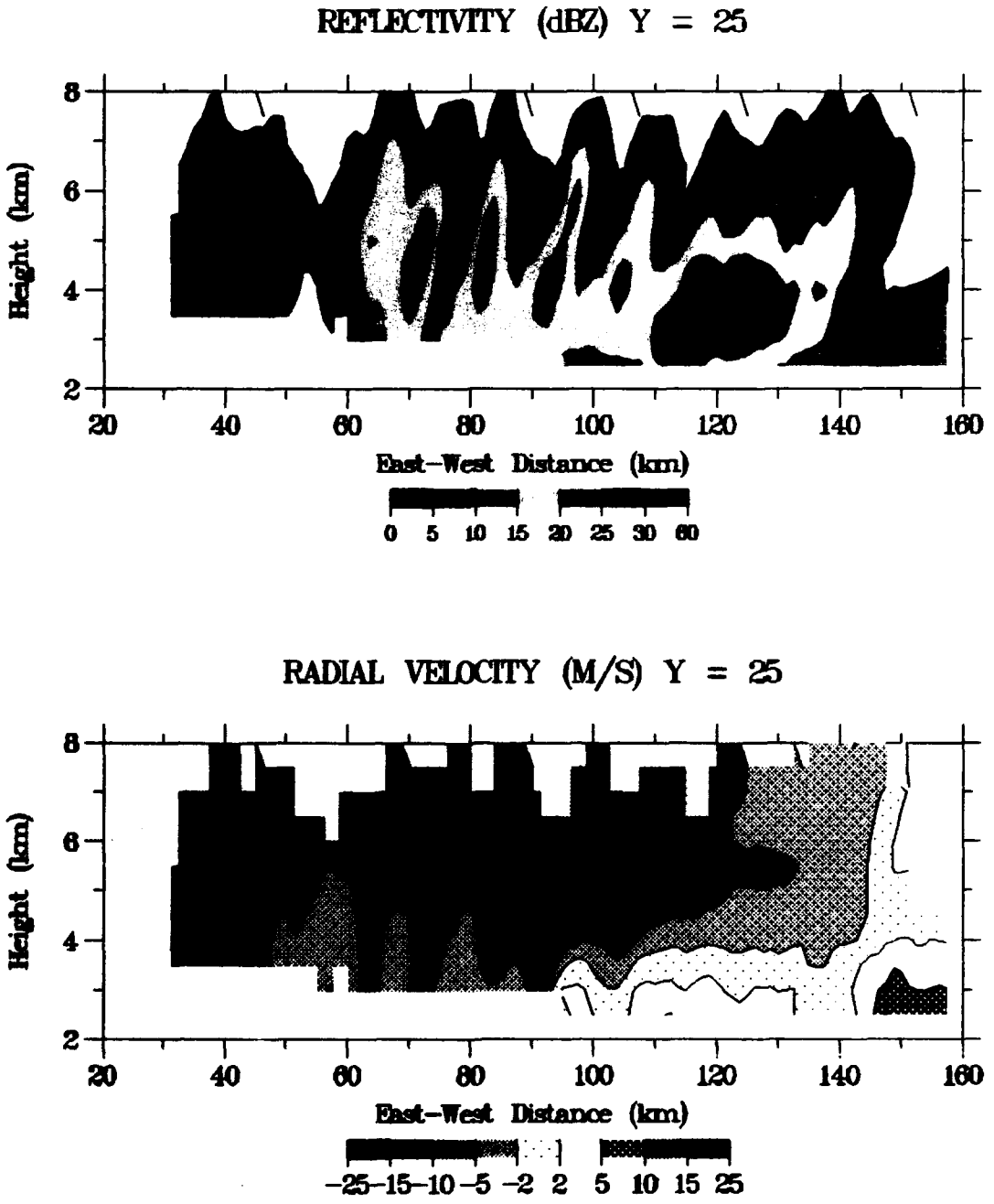

Figure 3.8: 2249 UTC 19 January Mile High Radar vertical cross section of a) reflectivity and b) radial velocity. Color bar at bottom indicates ranges of reflectivity in dBZ for each shading. Horizontal distance is measured from the left end of the black line in Fig. 3.7.

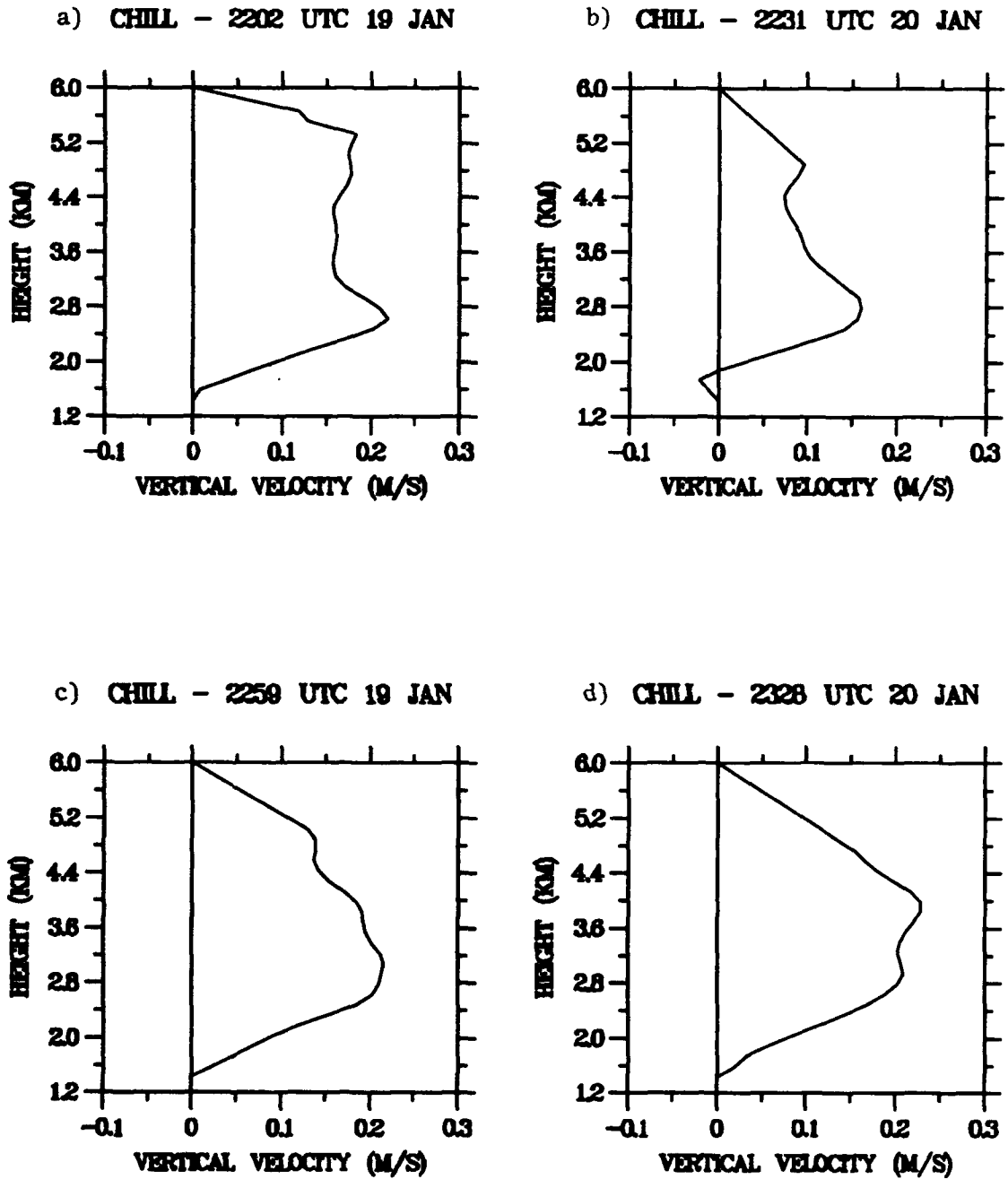

Figure 3.9: CSU-CHILL EVAD vertical velocity profile for a) 2202 UTC, b) 2231 UTC, c) 2259 UTC, and d) 2328 UTC 19 January.

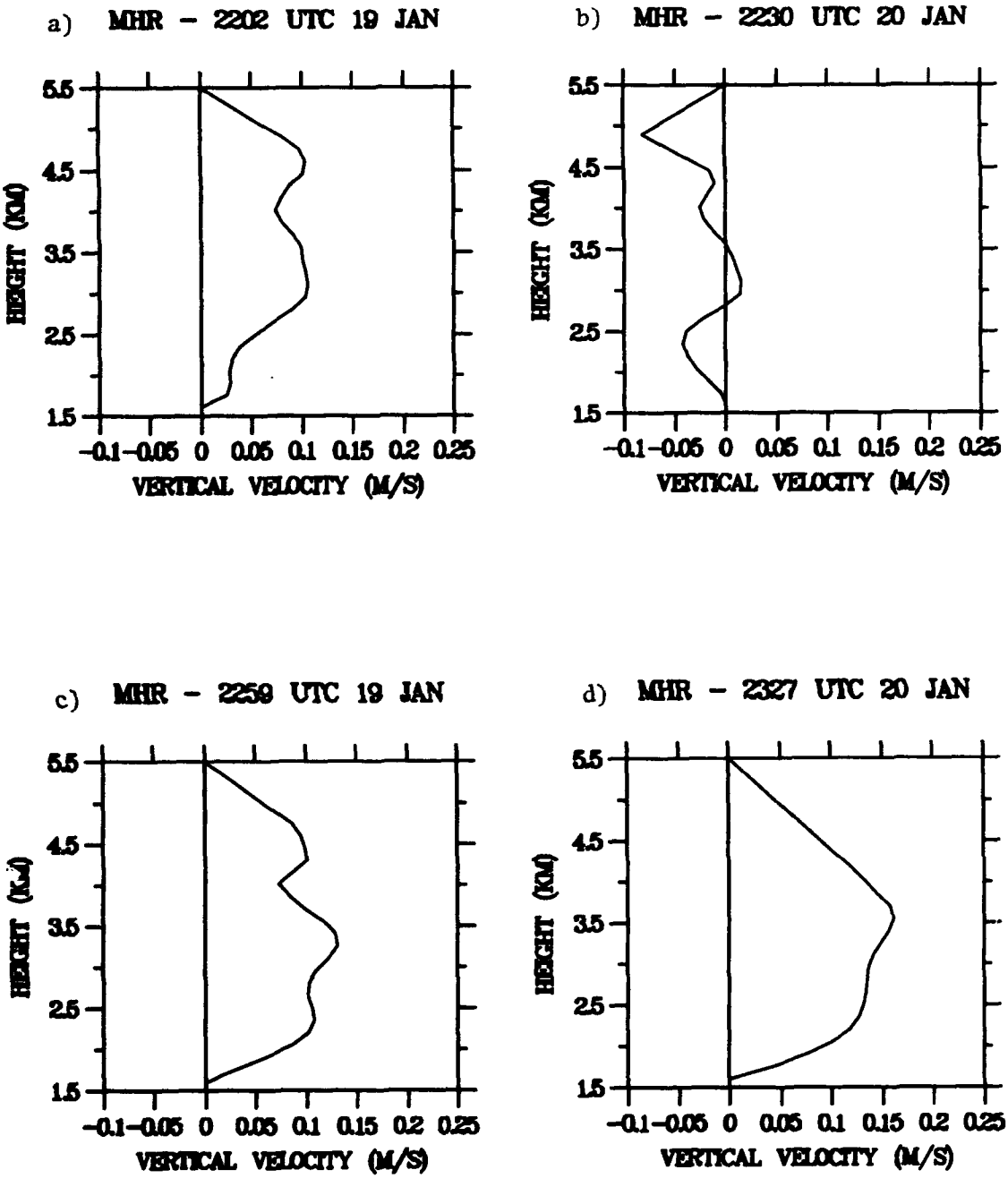

Figure 3.10: MHR EVAD vertical velocity profile for a) 2202 UTC, b) 2230 UTC, c) 2259 UTC, and d) 2327 UTC 19 January.

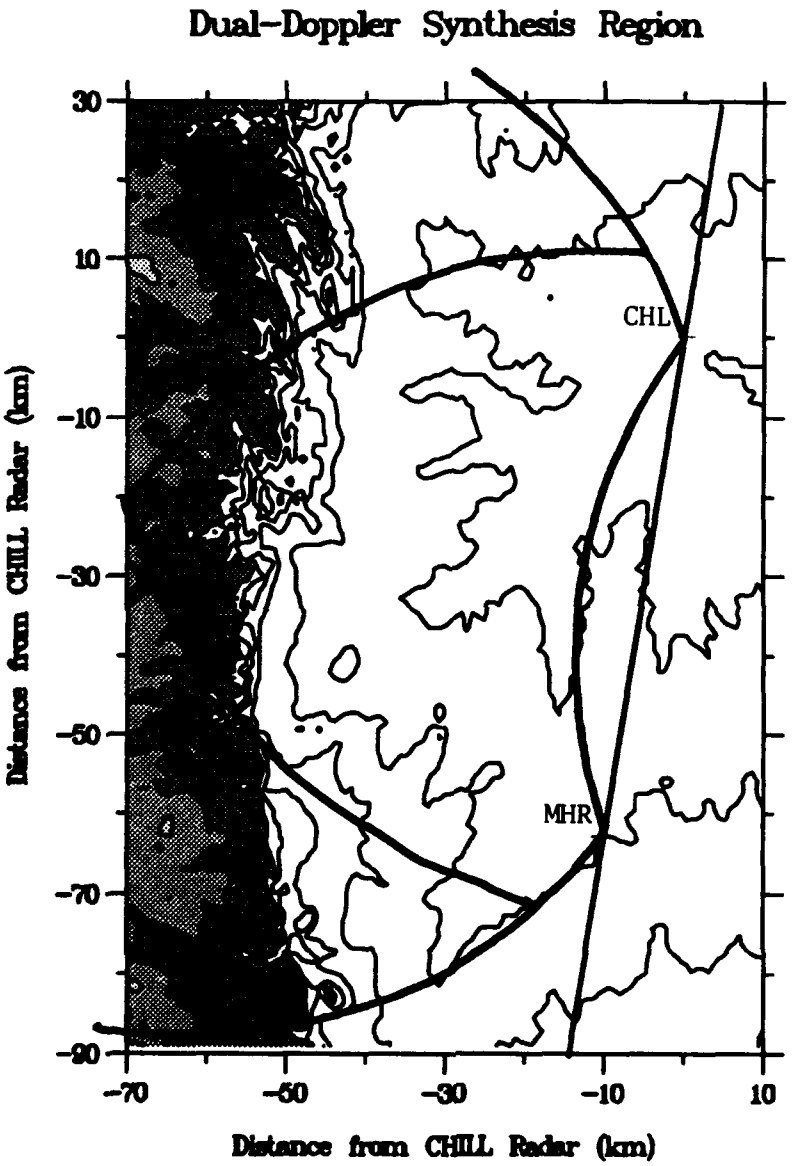

Figure 3.11: Dual-Doppler synthesis region. CSU-CHILL and MHR are indicated by CHL and MHR. Large area within arc represents regions where crossing angle is greater than 30 degrees. Area within curved triangle represents region where the spatial resolution is less than 1.25 km. Terrain contours are shown for every 200 m to 2000 m and dark and light gray shading highlight terrain between 2000-3000 and 3000-4000m respectively.

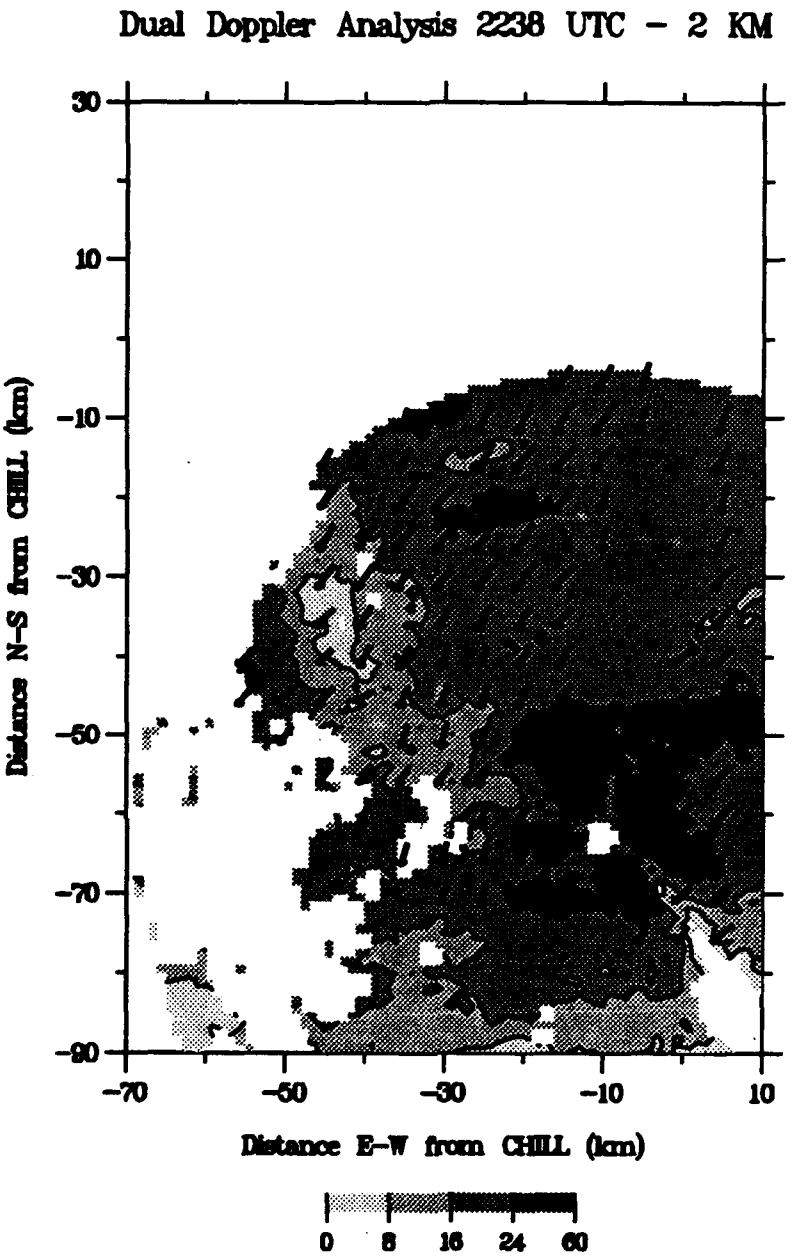

Figure 3.12 (a): 2.0 km (MSL) 2328 UTC 19 January Dual-Doppler derived wind vectors and MHR reflectivity field. Vector length of one gridpoint spacing represents 15 ms^{-1}.

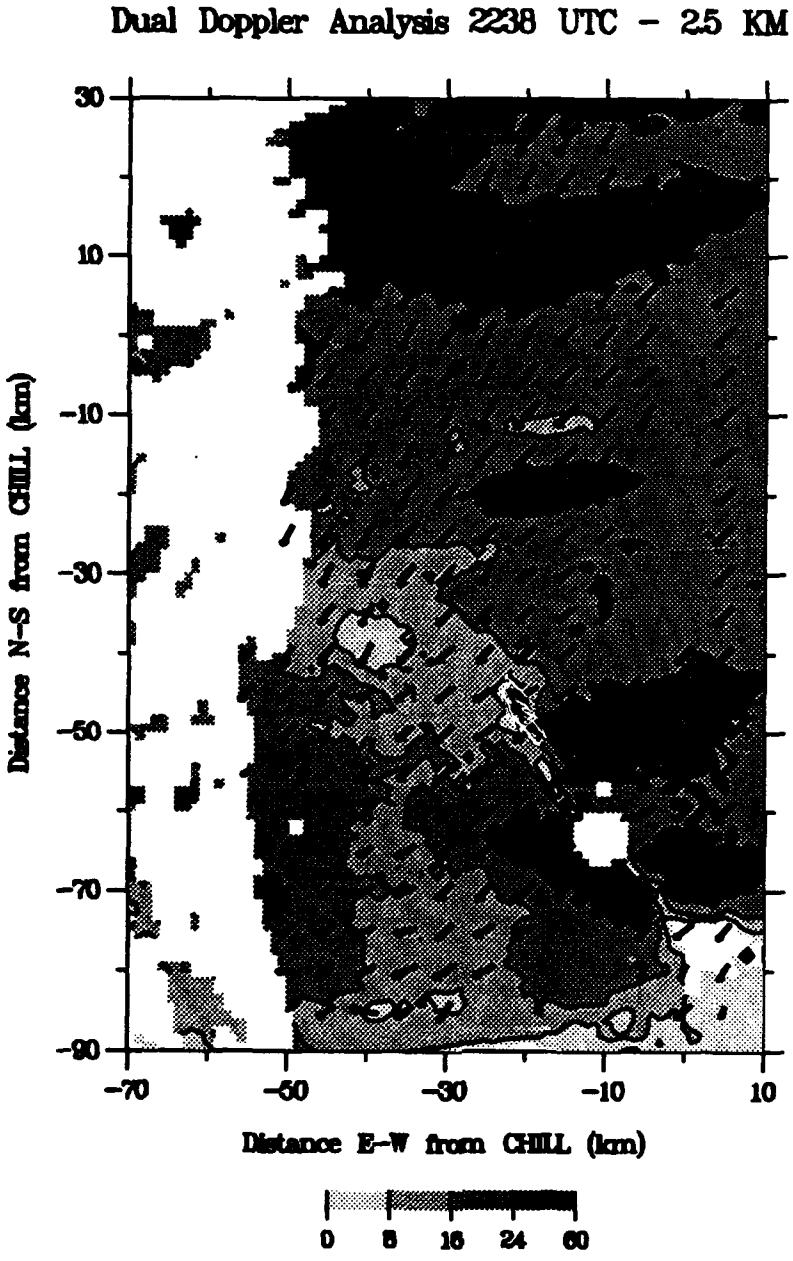

Figure 3.12 (b): Same as (a) except for 2.5 km.

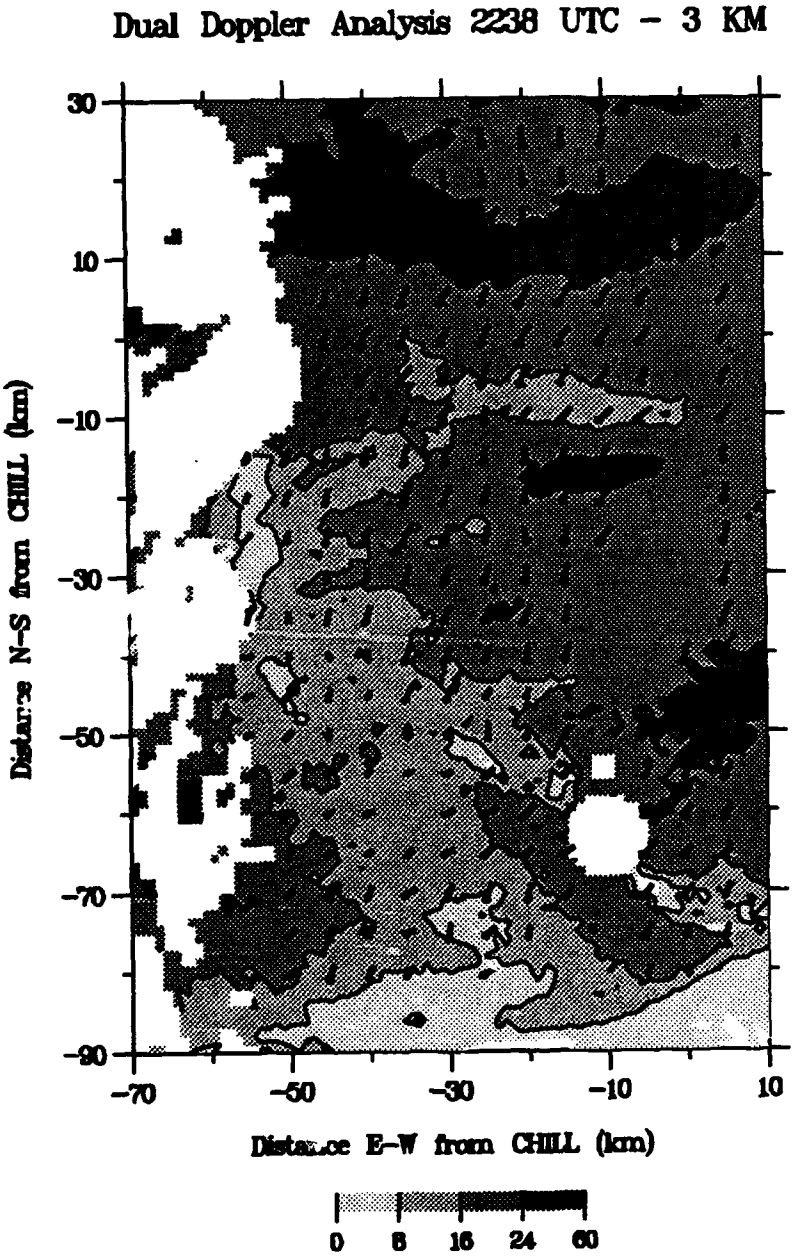

Figure 3.12 (c): Same as (a) except for 3.0 km.

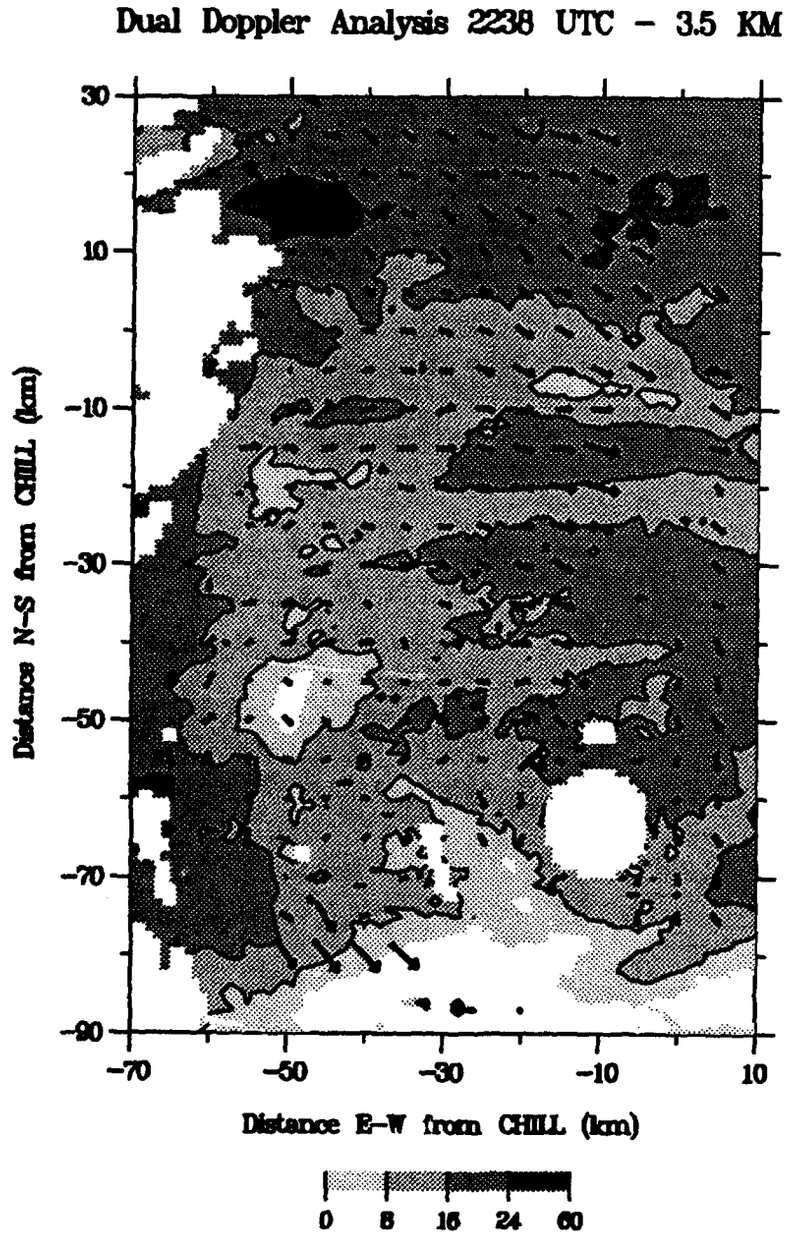

Figure 3.12 (d): Same as (a) except for 3.5 km.

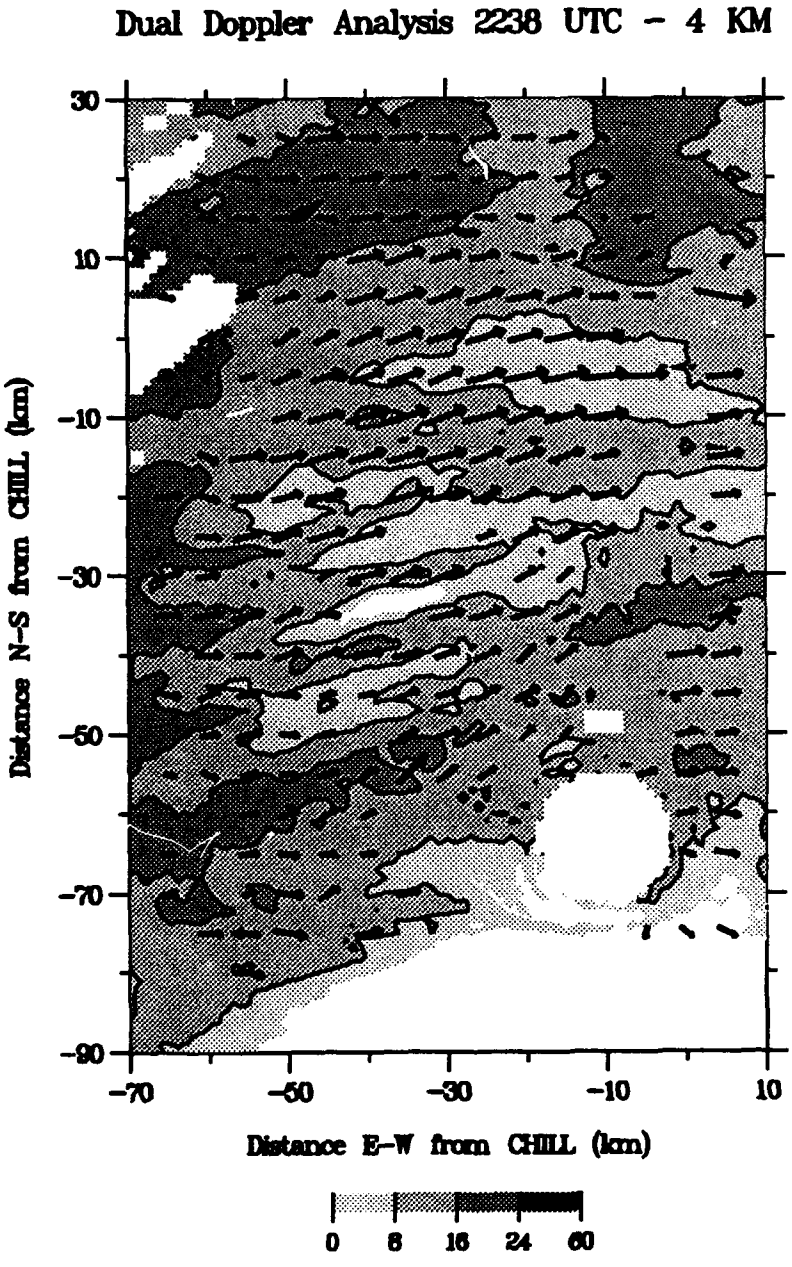

Figure 3.12 (e): Same as (a) except for 4.0 km.

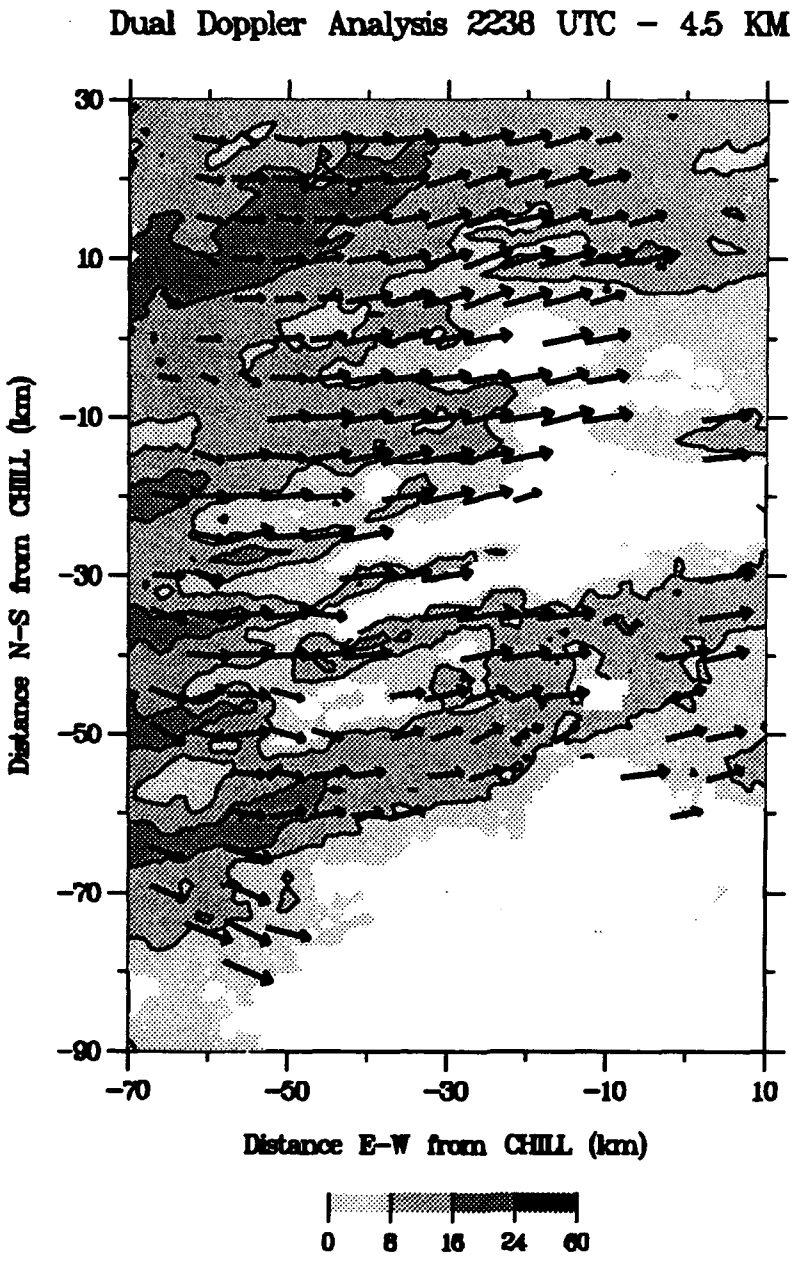

Figure 3.12 (f): Same as (a) except for 4.5 km.

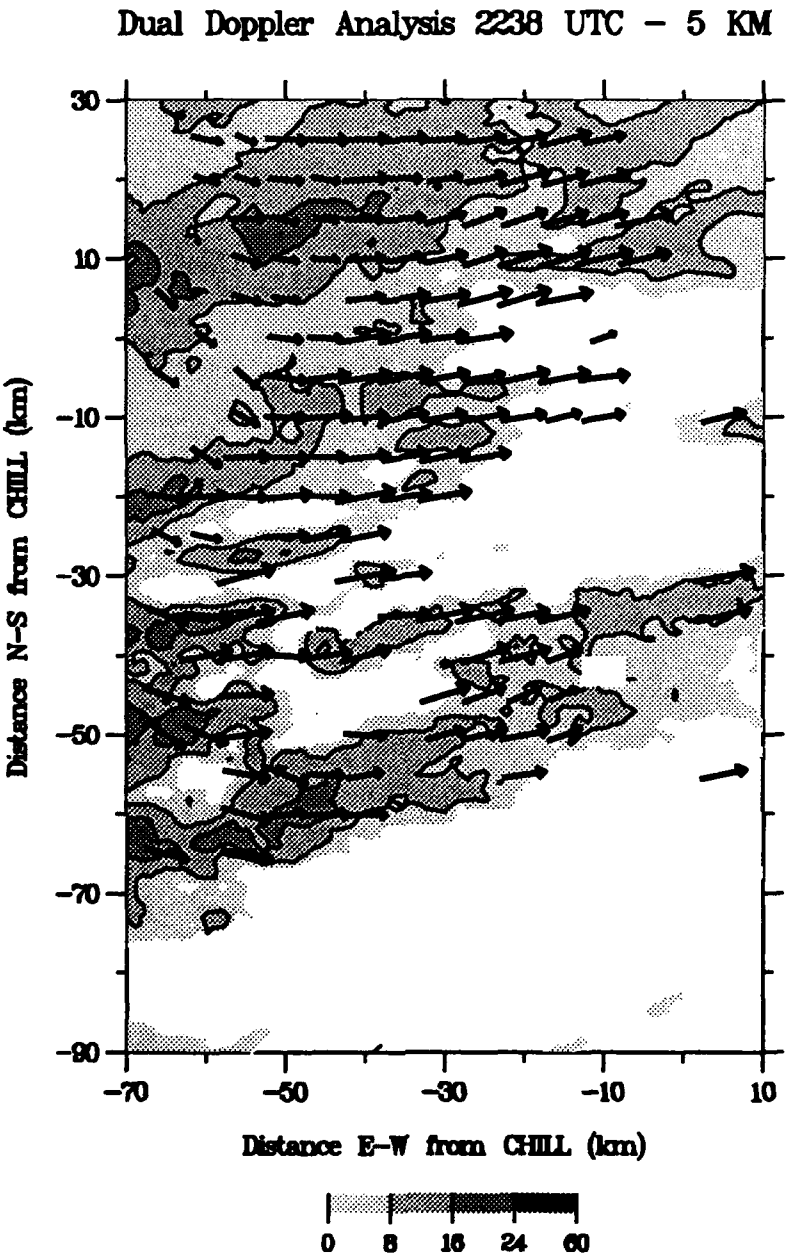

Figure 3.12 (g): Same as (a) except for 5.0 km.

Chapter 4

POSSIBLE SNOW BAND FORMATION MECHANISMS

As discussed in Chapter 1, mesoscale precipitation bands have been observed in diverse geographical locations and under a wide range of synoptic situations. Various dynamic mechanisms have been proposed to explain the formation of these bands including: conditional and convective instabilities, conditional symmetric instability (CSI), internal and ducted gravity waves, Kelvin-Helmholtz waves, gravity currents, and upper level jet streaks. However, terrain influences caused by the Rocky Mountains add mechanisms not sufficiently addressed in other major winter storm studies. Wesley (1991) discusses the role of a barrier jet in causing heavy snow along the Front Range in cases of strong cold air damming. Precipitation bands over eastern Colorado may also be the result of mountain wave activity (Wesley and Pielke 1990). In this chapter, various mechanisms are examined for their potential in forming the snow bands observed during this study.

4.1 Conditional Instability

Instability as a result of con· ·ve processes in the vicinity of frontal zones can cause precipitation bands (Snook 1992), similar to mechanisms responsible for squall line activity (Hane, 1986). Emanuel (1983b) mentions that the susceptibility of the atmosphere to moist adiabatic vertical motions from conditional instability governs the structure of bands associated with CSI. Conditional instability was assessed using Stull's (1988) method to evaluate its role in creating bands or influencing CSI

circulations. Stull (1988) states that air can be considered conditionally unstable when the dry static stability gradient is positive ($\partial s/\partial z > 0$) and the saturation static stability is negative ($\partial s_{es}/\partial z < 0$). Where:

$s = C_pT + gz$; Dry static energy or Montgomery stream function

$s_{es} = s + L_v r_{sat}$; Saturation static energy

$C_p = 1004.67\ m^2\ s^{-2}\ K^{-1}$; Specific heat of dry air at constant pressure

$L_v = 2.5 \times 10^6\ J\ kg^{-1}$; Latent heat of vaporization

r_{sat} = Saturation mixing ration for water

Vertical profiles of s and s_{es} change were prepared for 0000 UTC 20 January soundings and examined for regions of conditional instability. Figs. 4.1a-b show vertical profiles dry and saturated static energy change ($\partial s/\partial z$ and $\partial s_{es}/\partial z$ respectively) at Akron and Elbert, CO. Conditional instability criteria were met where the dashed line (saturation static energy change) is negative and the solid line (dry static stability change) is positive. The Akron data shows conditional instability was limited to a layer between 5000 and 6500 MSL while the Elbert profile indicates a more unstable environment with lower over all values compared to Akron. Akron was located in a region of diminished snow band activity compared to the pronounced bands in the vicinity of Elbert. The Elbert profile also shows shallow, low level layers of conditional instability within 1000 m of the surface (below 2500 m MSL) and a distinct inclination towards conditional instability above 4000 m MSL where well defined bands were observed in the radar data. Low level convergence (and upward vertical motion) in the upslope flow over the northern portions of the Palmer Divide may have played a role in the release of conditional instability and subsequent CSI snow band formation (Emanuel 1983a, b). It is unlikely that the shallow layers of conditional instability near the surface alone are responsible for snow band development.

4.2 Conditional Symmetric Instability

Conditional symmetric instability (CSI) and its role in the formation of precipitation bands has been studied by many of the winter storm researchers cited in this thesis. Bennetts and Hoskins (1979) proposed precipitation bands formed as a result of CSI in a layer. Emanuel (1983a, b) simplified the process by introduction of a Lagrangian parcel method of CSI evaluation which has since been embraced by most researchers. Briefly, CSI theory states that slantwise convection is the result of combining convective and inertial instabilities that arise from an unstable distribution of body forces acting on parcels within a fluid. Convective instabilities cause vertical motion since the body force is gravity, whereas inertial instability causes radial motion on a horizontal plane where centrifugal body forces dominate (Emanuel 1983a). Symmetric instability, the sum of these two instabilities, produces slanted motion with respect to the horizontal and vertical directions.

In the case of "purely meridional, steady, moist baroclinic shear flow in thermal wind balance", Emanuel (1983 a,b) defines a quantity M_g, the geostrophic pseudo-angular momentum by:

$$M_g \equiv v_g + fx, \tag{3}$$

where v_g is the geostrophic flow normal to an x-z cross section of M_g surfaces, f is the Coriolis parameter, x is the distance along the x axis of the plane, increasing from left to right. If the pressure gradient in the y direction is zero, then the y component of the momentum equation can be written as:

$$\frac{dv_g}{dt} + fu = 0 = \frac{dM_g}{dt}, \tag{4}$$

indicating that M_g is conserved following an air parcel. From Emanuel (1983b), the horizontal (x) and vertical (z) components of the momentum equation are:

$$\frac{du}{dt} = f(v - v_g) = f(M_p - M_g), \tag{5}$$

$$\frac{dw}{dt} = \frac{g}{\theta_{vo}}(\theta_{vp} - \theta_{vg}), \tag{6}$$

where θ_v is the virtual potential temperature, subscript p refers to the parcel M or θ_v, similarly g refers to geostrophically balanced M or θ_v, of the free atmosphere, o refers to a reference θ_v. Acceleration of an air parcel in the positive (negative) x direction takes place if $(M_p - M_g)$ in Eq. 3 is positive (negative), implying the parcel momentum is greater (less) than the environmental momentum. Vertical acceleration of an air parcel up (down) will occur if $(\theta_{vp} - \theta_{vg})$ is positive (negative) indicating a parcel virtual potential temperature greater (less) than the environment. Snook (1992) points out the requirement for slantwise convection is met when $(M_p < M_g)$ and $(\theta_{vp} > \theta_{vg})$. From the practical standpoint of evaluating CSI on vertical cross sections, this implies M_g must decrease in the positive x direction along a constant θ_e line (Sanders and Bosart 1985a, Wolfsberg *et al.* 1986). There are several quick qualitative assessments that will help in evaluating the potential for CSI. From Snook (1992) and Seltzer *et al.* (1986):

1) Winds increase with height indicating a baroclinic atmosphere.

2) A unidirectional wind profile (though not always necessary).

3) A nearly saturated, well-mixed vertical thermodynamic profile with neutral to near moist adiabatic lapse rate.

4) Observations of multiple bands. Frontogenetic forcing can explain single bands, but not multiple bands.

5) Bands oriented parallel to the thermal wind.

6) A region in the atmosphere where the Richardson number is less than one.

Using the qualitative indicators above, data were checked for CSI potential before preparation of a CSI cross section. Examination of wind profiles (see for example Figs. 2.7a-b and 2.10a-c) showed that winds had an almost unidirectional profile, and increased with height (above the arctic airmass), which can be taken as evidence of the required atmospheric baroclinicity. A nearly saturated atmosphere with lapse rates approaching moist adiabatic was indicated by the 0000 UTC 20 January soundings. Multiple bands were observed by radar, particularly over the southern portions of the project area. Precipitation bands visible in the radar data nearly paralleled the thermal wind (compare Figs. 3.4a-d with Fig. 2.4).

The requirement for a Richardson number less than one occurred at several levels (Figs. 4.2a-b). The Richardson numbers obtained from the dual-Doppler synthesis (Table 4) compare favorably with numbers obtained from soundings. The radar derived values have the advantage of being calculated with an average horizontal wind. The disadvantage of this technique comes from the use of relatively thick shear layers. Stull (1988) cautions that Richardson number calculations from soundings (even more so when using the coarse vertical resolution in the radar data analysis technique) are prone to inaccuracies due in part to approximation of the vertical partial derivatives by finite differences. It is possible that actual Richardson numbers were lower than those calculated, particularly if there were large gradients over a shallow depth. If this hypothesis is true, then the dual-Doppler derived values might have been lower than those in Table 4. In summary however, both sounding and dual-Doppler Richardson number calculations met CSI criteria.

Once it was established that the qualitative criteria for CSI were met, a cross section of M_g and θ_e contours was prepared. The vertical cross section was taken along the line shown on Fig. 2.4. This is approximately orthogonal to the geostrophic wind at

most levels. M_g was calculated using Eq. 3, then plotted and analyzed. The analysis was combined with the equivalent potential temperature analysis and is shown in Fig. 4.3. Solid lines represent θ_e in °K and dashed lines represent M_g in ms^{-1}. Following CSI convention, regions of possible CSI are indicated by the hatched region where M_g decreases along a constant θ_e line. Two regions of possible CSI are apparent, one near the surface and the other in the middle troposphere. The region near the surface should be ignored as the θ_e analysis is suspect at this level and is probably an artifact of the analysis routine, since surface pressures are close to 850 mb along the cross section. However, at upper levels, CSI could have played a role in forming bands. There is good agreement with radar observations since they show most bands were well defined above 4 km (~615 mb). However, despite the favorable indications of CSI, other mechanisms still must be considered for their role in snow band development.

4.3 Ducted Gravity Waves, Internal Gravity Waves, and Kelvin-Helmholtz Instabilities

Lindzen and Tung (1976) proposed ducted gravity waves as another cause of precipitation bands. Originally directed towards explaining bands associated with convective activity, others have applied the theory to winter storms (Parsons and Hobbs 1983, Wolfsberg *et al.* 1986). Parsons and Hobbs (1983) examined internal gravity waves and ducts as a system in relation to generating and maintaining warm sector and wide cold-frontal rain bands. In the case of warm sector rainbands, they found some agreement between theory and observation, however low level potential instability and lack of a stable duct forced them to conclude that this rainband type was associated with other mechanisms. They assessed gravity wave potential as being even lower for the wide cold-frontal rain band due to a critical level in the duct, and slow phase speed of the band compared to predicted propagation speeds of waves in a low Richardson

number regime. Wolfsberg *et al.* (1986) noted the vertical atmospheric profile in the case they studied was favorable for a gravity wave duct but they could find no evidence of a surface pressure perturbation and thus concluded bands were the result of other mechanisms.

In the case studied here, the possibility of internal and ducted gravity waves was considered and rejected (except internal waves associated with mountain waves discussed in section 4.4) as a cause of major snow bands for the following reasons:

1. Bands were not orthogonal to the mean flow as required by ducted gravity wave theory, but instead were parallel to the mean flow.

2. Examination of surface pressure traces showed no evidence of perturbations which Lindzen and Tung (1976) use as a measure of "response" to ducted waves.

3. Location of the bands with respect to synoptic fronts did not favor propagation of waves from frontal disturbances. Bands occurred well behind the surface cold front, unlike the cases examined by Parsons and Hobbs (1983).

The presence of Kelvin-Helmholtz (K-H) instabilities as a cause for major band formation was discounted since again, the orthogonal flow requirement (bands were parallel to the flow) was not met (Stull 1988). However, within the bands, flow conditions could be favorable for K-H waves transverse to the major bands. Richardson number profiles at Elbert and Denver (Figs. 4.2a-b) show shallow, well defined regions of low Richardson numbers (less than one) just above 5000 m in both profiles which were similar to profiles from other soundings (not shown). Stull (1988) states that in the presence of laminar flow the onset of K-H instability waves requires a Richardson number < 0.25. However, if the atmosphere is already turbulent, Richardson numbers < 1 indicate turbulent conditions will persist and K-H instabilities can occur until the Richardson number increases to greater than one. Stull (1988)

remarks that K-H waves can have horizontal scales up to hundreds of kilometers but are limited in vertical extent to tens to hundred of meters. Richardson number profiles indicate favorable conditions for K-H wave formation in this storm, however there was no means to confirm or deny their existence.

4.4 Gravity Currents

Hobbs and Persson (1982) used the concept of gravity currents as a possible explanation for narrow cold-frontal bands observed during the CYCLES program. Convective instabilities arise from bulges and clefts associated with a denser fluid advancing into a region of lower densities. Bulges at the top of the denser fluid come from internal circulations in the fluid. Clefts are the result of frictional effects on the denser fluid by the lower boundary. A nose of denser fluid protrudes over a shallow layer of less dense fluid near the lower boundary. This causes convective instabilities and bands near the frontal boundary (Parsons and Hobbs 1983). The cold front in the case examined here had passed though the region several hours before well organized banded features were observed, consequently a gravity current mechanism for snow band formation is not considered likely since this phenomena is expected in the vicinity of the front.

4.5 Upper Level Jet Streaks

Dunn (1988) showed the importance of considering upward vertical motions associated with jet streaks when evaluating the potential for snow band formation over northeast Colorado. Uccellini and Kocin (1987) examined the role of jet streaks in producing heavy snow over the Eastern Seaboard. Upward vertical motions associated with jet streaks under no temperature advection conditions typically occur in favored quadrants which are the left exit and right entrance regions when viewed looking down

wind (Keyser and Shapiro 1986). Fig. 4.4a illustrates the no temperature advection example of a jet streak where isotherms parallel the axis of the jet streak. Mid-tropospheric vertical motion maxima (illustrated by + and –, in pressure coordinates) are located symmetrically about the jet streak axis. One would expect to find regions of enhanced precipitation in those areas under the negative sign (i.e. left exit and right entrance). Keyser and Shapiro (1986) also examined the effects of temperature advection on the location of vertical motion centers with respect to the jet streak. Fig. 4.4b is their example of a warm air advection case and is similar to conditions observed over northeast Colorado (compare with Fig. 2.5c). Note the northward shift of the upward vertical motion maximum in the entry region as a result of warm air advection.

Examination of the NMC 300 mb analysis (Fig. 2.5c), Platteville wind profiler data (Fig. 7.a), and time cross sections (Figs 2.13a-d) shows jet stream level winds decreased (i.e. the core of the jet streak has moved east) and warm air advection at jet stream level. Furthermore, closer inspection of cross sections (Figs 2.12a and 2.13a-d) and 300 mb CLASS station plots (Figs. 2.6a-d) show the axis of the jet was near the southern stations. If the region of vertical velocity was shifted northward from temperature advection, the southern portions of the project area would experience greater upward motion and precipitation. Radar data supports this conclusion since, in general, bands with higher radar tops were observed to the south. Also, there was a region of higher snowfall over the Palmer Divide (see Fig. 2.1) that corresponded with radar observed reflectivity bands. Finally, satellite imagery (not shown) showed the major band over the Palmer Divide extended west beyond the radar coverage area to the axis of the 300 mb trough near the Utah-Colorado border.

4.6 Terrain-Induced Mechanisms

During arctic outbreaks the rising terrain of the Front Range acts as a barrier to the cold air and effectively *blocks* the flow from further westward movement (Wesley 1991). Furthermore, in some cases the forced lifting of warmer, moist air over the cold stable air below can result in *damming*. Wesley and Pielke (1990) showed examples of blocking and damming and discussed how these phenomena can enhance precipitation over the eastern plains of Colorado adjacent to the Front Range. In the case of damming, snow bands form along low level convergence lines that develop near the Front Range in response to cyclonic turning of the easterly flow due to its inability to ascend higher terrain. Snow bands that develop during blocking conditions are often parallel to the thermal wind. There is little correlation between bands and surface convergence zones except in extreme cases of blocking when development of a low level barrier jet forms parallel to the Front Range. This can lead to a band of heavier snow just east of the Front Range (Wesley 1991). The existence of damming and location of convergence zones can easily be determined by checking isotherm and streamline analyses. Surface temperatures will decrease from east to west and the streamline analysis should indicate rapid cyclonic turning in the easterly flow near the Front Range. Isotherm analyses (Fig. 2.16 for example) for the case under study here showed no well defined cold pool near the mountains, nor did stream line analyses (Fig. 2.17 for example) show any easterly flow, let alone any well defined convergence zones associated with cyclonic turning. Therefore, we conclude that cold air damming was not present in this case. While blocking conditions were present as illustrated by the inability of the cold air to ascend over the mountains and west southwesterly flow aloft, there was no evidence of a low level barrier jet in CLASS or wind profiler data. Snow bands aligned themselves with the thermal wind, which was similar to the blocking case discussed by Wesley and Pielke (1990).

One of the most striking features in Figs. 3.1a-d and 3.4a-d is the band south of the radar having rather evenly spaced reflectivity cores with an approximate interval of 12 km. Fig. 3.7 and Figs. 3.8a-b provide a more detailed look at the horizontal and vertical structure of the band. Observations showed there was little movement of the cores within the band, unlike the single precipitation cores discussed in Chapter 3. The cores in this band appeared to develop and dissipate with little down wind movement, in a band relative sense. The periodic nature of the reflectivity pattern suggests wave features were embedded in the the larger scale band. Durran (1986) states trapped mountain waves can form in the lee of a mountain barrier if certain conditions are met. Fig. 4.5 shows a model of the air flow associated with trapped mountain waves. These waves are the result of upward propagating waves, initiated by the barrier, being reflected downward by an upper boundary (a stable layer) which in turn become upward propagating waves again on striking the ground. In the ideal case there will be no loss in wave amplitude since there is no energy exchanged during the reflections, thus the process will (theoretically) create an infinite number of waves. The visible downstream waves, called trapped waves, are the superposition of the upward and downward propagating waves and typically have wavelengths between 5 and 25 km (Durran 1986).

Calculation of the Scorer parameter (Scorer 1949) represents a relatively simple means of evaluating the potential for trapped mountain waves. The Scorer parameter, L^2 can be calculated from:

$$L^2 = \frac{N^2}{U^2} - \frac{1}{U}\frac{d^2U}{dz^2} \tag{7}$$

where N^2 is the Brunt-Väisälä frequency, and U is the wind speed at the center of the layer under evaluation. In practice, Durran (1986) recommends excluding the second term from the equation, as it is difficult to evaluate from the coarse vertical resolution of rawinsonde observations and its contribution to the result is small compared to the first term. If the Scorer parameter decreases significantly with height, then the potential for

trapped waves exists. Queney *et al.* (1960) identified other qualitative requirements for strong lee wave development:

1. The mountain barrier must have a steep lee slope. The strongest waves occur when there is a gradual windward slope and steep lee slope.

2. The wind must have a direction within 30° of normal to the ridge line through a deep layer. Ridge top wind speed must be at least 7-15 ms^{-1} (depending on the character of the ridge), and wind speeds must increase with height above the ridge.

3. An inversion or stable layer must be present at the ridge top level and upstream of the barrier with weaker stability aloft.

Examination of Grand Junction, CO sounding (Fig. 4.6) shows the top of the low level inversion at 672 mb or 3310 m with decreasing stability aloft. The sounding also shows winds were within the 30° of perpendicular to mountain tops if the axis of the Continental Divide is assumed to be oriented north-south over central Colorado. Furthermore, winds were greater than 13 ms^{-1} at mountain top level and increased with height. Scorer parameter calculations were performed for all CLASS stations, Denver, and Grand Junction. Grand Junction, Denver, Elbert, and Berthoud (Figs. 4.7a-d) Scorer parameter profiles had many similarities including a maximum near 3.5 km (MSL) (except Grand Junction), and a rapid decrease to a minimum near 6 km (MSL). Figure 3.7 shows the waves were organized downstream of the Continental Divide, which has a steeper lee slope compared to its windward slope.

Scorer (1949) developed an equation to calculate the wave number of trapped waves in a two layer atmosphere. According to Durran (1986) use of his equation can provide useful estimates of the wavelength. From Scorer, the wave number, k, of the trapped wave can be obtained from the following expression:

$$(L_1^2 - k^2)^{1/2} \cot[(L_1^2 - k^2)^{1/2} H] + (k^2 - L_2^2)^{1/2} = 0 \qquad (8)$$

Where:

L_1 = Scorer parameter in the lower layer

L_2 = Scorer parameter in the upper layer

H = Depth of the lower layer

k = Wave number of the trapped wave.

Values for L_1^2 and L_2^2 were obtained from the lowest two layers in the Elbert Scorer parameter profile (Fig. 4.7c) where there was the smallest change with height. Thus the mean values of L_1^2 and L_2^2 were 3.162×10^{-6} and 3.162×10^{-7} m^{-2} respectively corresponding approximately to +0.5 and -0.5 on the x-axis of figure 4.7c. H was estimated to be 1000 m. By numerical methods, k was found to be 5.845×10^{-4} m^{-1} which equates to a wavelength (λ) of approximately 10.7 km since $\lambda = 2\pi/k$. This numerically derived value of the wavelength compares favorably with the 12 km value obtained from direct observation which lends support to the conclusion that trapped waves were present.

Determination of trapped wave amplitudes is a complex problem with no simple solution as it depends on the interaction of several factors: the scale and shape of the upwind barrier, vertical wind stratification, and vertical stability (mainly temperature) stratification. Corby and Wallington (1956) developed a relationship that attempts to explain the vertical displacement of a streamline that incorporates the factors listed above from which one might infer characteristics about the wave amplitude. Their equation is:

$$\zeta_z = -2\pi(hbe^{-kb})\ (U_o/U_z)\ [\psi_{z,k}(\partial\psi_{o,k}/\partial k)^{-1}]\ \sin kx \qquad (9)$$

$$\text{A} \qquad \text{B} \qquad \text{C}$$

Where:

ζ_z = Vertical displacement of a streamline

h = Height of barrier

b = Half width parameter of the barrier

k = Wave number of the trapped wave

U = Horizontal wind

ψ = Stability parameter. ψ satisfies the condition:

$$\partial^2\psi/\partial z^2 + (L^2 + k^2)\psi = 0 \qquad (10)$$

L = Scorer parameter

x = Horizontal distance

Subscripts o, z, and k represent with respect to the surface, some height z, and wave number respectively.

A, B, and C represent the terms associated with modifications of the streamline displacement as a result of barrier characteristics, wind stratification, and stability stratification respectively.

Despite the difficulties encountered in computing the amplitude of the waves, Corby and Wallington offer some qualitative observations and comments. From (9), the wave amplitude depends in a complex manner on the topography and the vertical distribution of atmospheric properties. However, in examining the elements of the equation, two statements can be made about the amplitude:

1. The maximum amplitude will occur when the barrier width is approximately equal to the airstream wavelength (i.e. $-kb = 0$).

2. Large amplitude waves occur when a shallow layer of great stability rather than a deep layer of slight stability is present (i.e. term C is large).

Non linearities make solution of (9) extremely difficult so that at best only general statements can be made about the wave amplitude. Unfortunately, no means of

determining the amplitude of the waves from observations (hence inferences of wave induced vertical velocities) was available during the experiment.

The enhanced reflectivity cores in the waves (see Figs. 3.7 and 3.8a) probably represent regions where upward ascent in the flow modified the ice crystal number density and/or radar back scatter cross section. Similarly, weaker reflectivities between the cores probably correspond to regions of descent. Radar theory (see Battan, 1973) states that the reflectivity factor Z (or equivalent reflectivity factor Z_e in this case) for a given volume is directly proportional to the summation of scatterer number density, n, of diameter, D, times the diameter raised to the sixth power or:

$$Z = \sum_i n_i D_i^6 \text{ mm}^6 \text{ m}^{-3} \tag{11}$$

Also,

$$dBZ = 10 \log Z \tag{12}$$

Examination of Fig 4.8a shows that the maximum difference between cores and weak echo regions was approximately 25 dbZ. Thus ΔZ would be $10^{2.5}$ or 316 $\text{mm}^6 \text{ m}^{-3}$. Since temperatures were below freezing through the atmosphere, assume that nearly all the radar energy was scattered by ice crystals. If the ice crystal diameters were all the same, the number concentration would have to increase (decrease) on the order of 300 to account for the increase (decrease) in returned power associated with the cores (weak echo regions).

A more likely cause for the observed structure in the radar echo is a change in the ice crystal diameter. If the number concentration stayed constant and all ice crystals were of the same initial diameter, then an increase (decrease) in the diameter by a factor of 2.6 would explain the increase (decrease) in returned power. If the level of maximum ascent rate occurred in a region where the temperature regime was between -12 and

-16°C ice crystals would experience maximum growth rates according to Auer and White (1982). Consider an ice crystal in water saturated air at a temperature between -5 and -20 °C traveling along the rising half of a sinusoidal wave that is 9 km long at a speed of 25 ms^{-1}. Under these conditions the ice crystal will grow by deposition during an ascent that would last for 360 seconds (6 minutes), neglecting the increase in its terminal velocity as its mass increases. The ice crystal should increase in diameter by at least a factor of 2.6 during the time of ascent. As the air descends during the other half of the cycle, adiabatic warming and lower ice saturation may cause the crystal to sublimate, thus reducing the amount of radar energy scattered back to the receiver. Growth and decay of ice crystals, rather than large change in number density, seems a much more reasonable explanation for the observed echo pattern.

Since it is unlikely that a uniform size distribution existed, the actual cause for the periodic structure in the radar echoes was probably due to a complex interaction between deposition and sublimation, aggregation, riming as crystals travel through regions of high liquid water content, precipitation of ice crystals, and changes in the number density. Detailed in-situ measurements of microphysical and kinematic properties throughout the volume of the wave clouds would have provided much greater insight into the processes involved in creating the observed periodic structure. Unfortunately, profiler data from the Palmer Divide region were not available. Aircraft data was limited, however, a pass over the Palmer Divide by the University of Wyoming King Air after 0040 UTC at 3500 m MSL showed the temperature to be between -10 and -12 °C. Crystal habits included a mixture of graupel and dendrites, including aggregates and rimed crystals. Dendrites seemed to predominate indicating vapor deposition was the primary cause of crystal growth, at least in the upper levels. Riming probably aided in growth, particularly in the lower levels where higher liquid water contents were likely. Radiometer data from Elbert indicated periodic depletions of

the vertical integrated liquid water content between 2200 UTC 19 January and 0000 20 January. Values ranged between 0 and 0.44 mm, while the integrated water vapor varied between 0.50 and 0.67 cm. Greater snowfall (or at least higher liquid water equivalent) was likely during periods of high liquid water content since rimed crystals with greater terminal velocities and aggregates would have been present. These periodic fluctuations in the radiometer data were probably associated with the movement of other features in the bands and not the periodic reflectivity cores since they showed little movement with respect to the band.

The question of how non-trapped wave precipitation cores were formed still remains largely unanswered. Wesley and Pielke (1990) suggested that droplets forming in nucleation zones upwind of mountain peaks first reported by Rauber *et al.* (1986), might undergo freezing and sufficient lifting to clear the barrier in regions of mountain wave vertical ascent. Alternatively, ice nucleation from deposition or freezing may take place in the wave above the mountain barrier. Rogers and Vali (1987) found that clouds in contact with a snow surface experienced an increase in ice nucleation perhaps due to ice crystals carried aloft by the airflow. Regardless of the primary mechanism, secondary ice formation processes such as splintering, fragmentation of crystals, and contact freezing as discussed by Hobbs and Rangno (1985) would multiply the number of ice nuclei.

The shallow convective cell theory proposed by Carbone and Bohne (1975) and a similar seeder-feeder model developed by Rutledge and Hobbs (1983, 1984) represents another approach where seeder cells deposit ice crystals into feeder clouds of relatively higher liquid water content. The low integrated liquid water contents associated with heavier snow may represent those locations in a snow band where liquid water in the feeder cloud has been converted to ice crystals by seeding from upper level clouds.

Mulvey (1977) reported the results of a modeling study on the survival time and transport distance for ice crystals as functions of ice saturation, wind velocity, temperature, and ice crystal size. For example, an ice crystal of diameter 1.7 mm initially formed at -25 °C and ice saturation of 0.9, and experiencing a wind speed regime of 20 ms^{-1}, had a maximum range of 347 km. A more realistic example was a maximum distance of 124 km experienced by an ice crystal of 2.5 mm diameter initially formed in an ice saturation of 0.9 at -15 °C and transported by 20 ms^{-1} winds. Transport distance of ice crystals in a subsaturated environment is limited by sublimation thus large crystals will have the greatest range. In a super saturated environment, transport distance is limited by the fall speed of the crystal, therefore small crystals will have the greatest range. Incorporating the results of Mulvey's study with the findings of Rogers and Vali (1987), under the right saturation and temperature regime, strong winds at mountain top level could cause considerable downwind transport of ice crystals picked up from the surface. These ice crystals could serve as nuclei, or have a role in a seeder-feeder mechanism.

4.7 Discussion and Conceptual Model

Analysis of the total snowfall (Fig. 2.1) showed three distinct maxima. What were the mechanisms responsible for the observed snowfall distribution? There is no question that orographic lifting in conjunction with cooling after frontal passage over northeast Colorado helped create a nearly saturated environment at the surface and saturated conditions aloft. Strong upslope ascent appears to have occurred near Fort Collins and offers a partial explanation for the maximum west of the city. However, radar data showed that an upper level band crossed over the region during the storm which leads to speculation that upslope induced snowfall was enhanced by a seeder-

feeder mechanism. Ice crystals falling from the band probably seeded the relatively high liquid water content in lower level clouds.

The same orographic lifting and seeder-feeder enhancement couplet appears to have occurred over the region northeast of Denver, though orographic effects were probably less important than in the Fort Collins region. The seeder-feeder mechanism played a more important role. Radar data showed two distinct flow regimes and enhanced reflectivity regions. Within the low level arctic airmass a well defined region moved from the north northeast with the low level flow. The region increased in areal coverage and intensified somewhat as it approached the western edge of the Palmer Divide. Above the arctic airmass were well defined bands with embedded enhanced reflectivity cores. The cores moved from south southwest to north northeast. Seeding of the low level clouds by ice crystals may have played a more important role here than over the region west of Fort Collins. As discussed in section 2.3 terrain induced vertical motions were on the order of 5 cm s^{-1}, thus a seeder-feeder mechanism might might provide an explanation for the heavier snowfall northeast of Denver.

The region of higher snowfall over the eastern portions of the Palmer Divide appears related to a different mechanism. Radar data and satellite imagery showed a well defined continuous band crossing the region. The band was oriented parallel to the upper level winds and was near the northern edge of the jet axis. This situation may have been similar to that examined by Dunn (1988). In Dunn's case, jet streak induced vertical motions in a region of conditional symmetric instability were argued to trigger slantwise convection and heavier precipitation. Radar data did not show any well defined low level reflectivity enhancements (except the band) as with the other two regions described above.

Analysis of CSI showed there was potential for slantwise convection and thus formation of bands. Two mechanisms seemed to have played a role in triggering the

convection, release of conditional instability, possibly from a seeder-feeder couplet, and jet streak induced vertical motions. It would seem likely that the conditional instability release mechanism might involve a positive feedback circuit, in which ice crystals falling from a band into the feeder zone release instability that in turn leads to slantwise convection which results in more ice crystal precipitation and so on.

The process of band formation is complex and involves the interaction of several phenomena. However, a conceptual model of the kinematic structure is presented in Fig. 4.8a-b. Figure 4.8a shows a plan view of a band with an embedded transient core. For the sake of clarity low level clouds are not shown. The thin solid arrow parallel to the band axis shows the band relative motion of the core. The long arrows parallel to the band show the upper level stream lines. Short arrows pointing to the lower right represent motion of the band. Note that the core moves parallel to the streamline and bands move in an off axis direction that seems to correspond to the movement of synoptic scale features. Dashed arrows represent low level wind flow. The shear region between the low level northeasterlies in the arctic air mass and the upper level west southwesterlies is shallow, on the order of 500 to 1000 m.

Figure 4.8b shows a cross section of the band. Scalloped regions represent clouds. The Rocky Mountains are the higher terrain to the left. The shear zone is the hatched region mid way up into the cloud. Winds are from the north to northeast below the shear zone, winds are from the southwest to west above. Cores and ice crystals falling into the lower clouds (the feeder zone) are shown. Ice crystals in the cores probably form by contact nucleation as described in Hobbs and Rangno (1985) then fall into the feeder zone where they can grow by deposition, aggregation, and riming, or play a role in ice multiplication. The larger ice particles can then fall out as snow (or graupel if heavily rimed).

4.8 Summary

In this chapter various mechanisms were examined for the role, if any, they might have played in producing the upper level snow bands and precipitation cores described in the radar observations. Evaluation of the data suggests that conditional instability, jet streaks, and mountain waves played a role in band formation and that CSI analysis showed the atmosphere was susceptible to slantwise convection. Conditional instability probably played a role in triggering bands over the northern portions of the project area, while jet streak induced vertical motions were more important to the south. The most striking examples of banding occurred over the southern portions of the project area where it appears mountain wave activity, in conjunction with jet streak induced vertical motions, may have enhanced bands.

a) AKR DELTA ENERGY - 0000 UTC 20 JAN

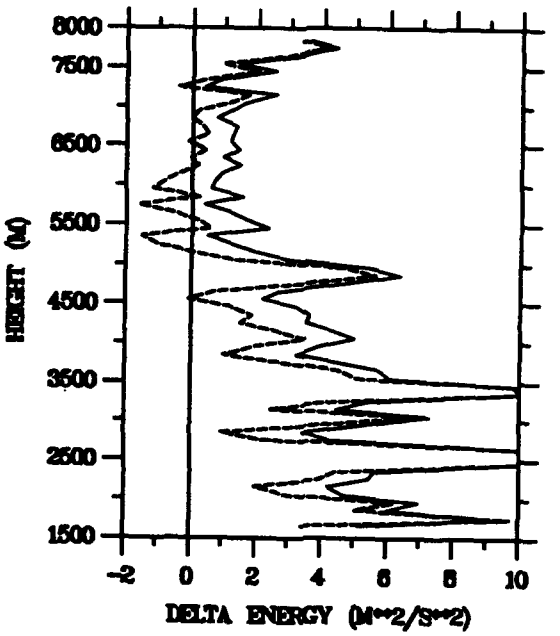

b) ELB DELTA ENERGY - 0000 UTC 20 JAN

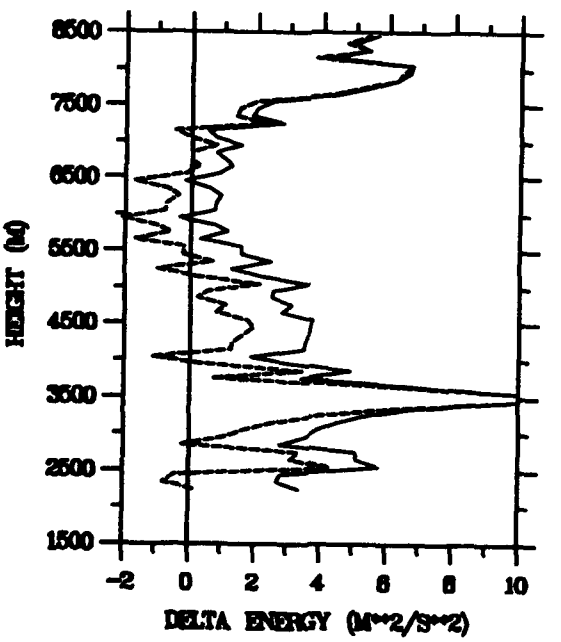

4.1 0000 UTC 20 January dry and saturation static energy change for a) Akron and b) Berthoud. Solid line is dry static energy change, dashed line is saturation energy change.

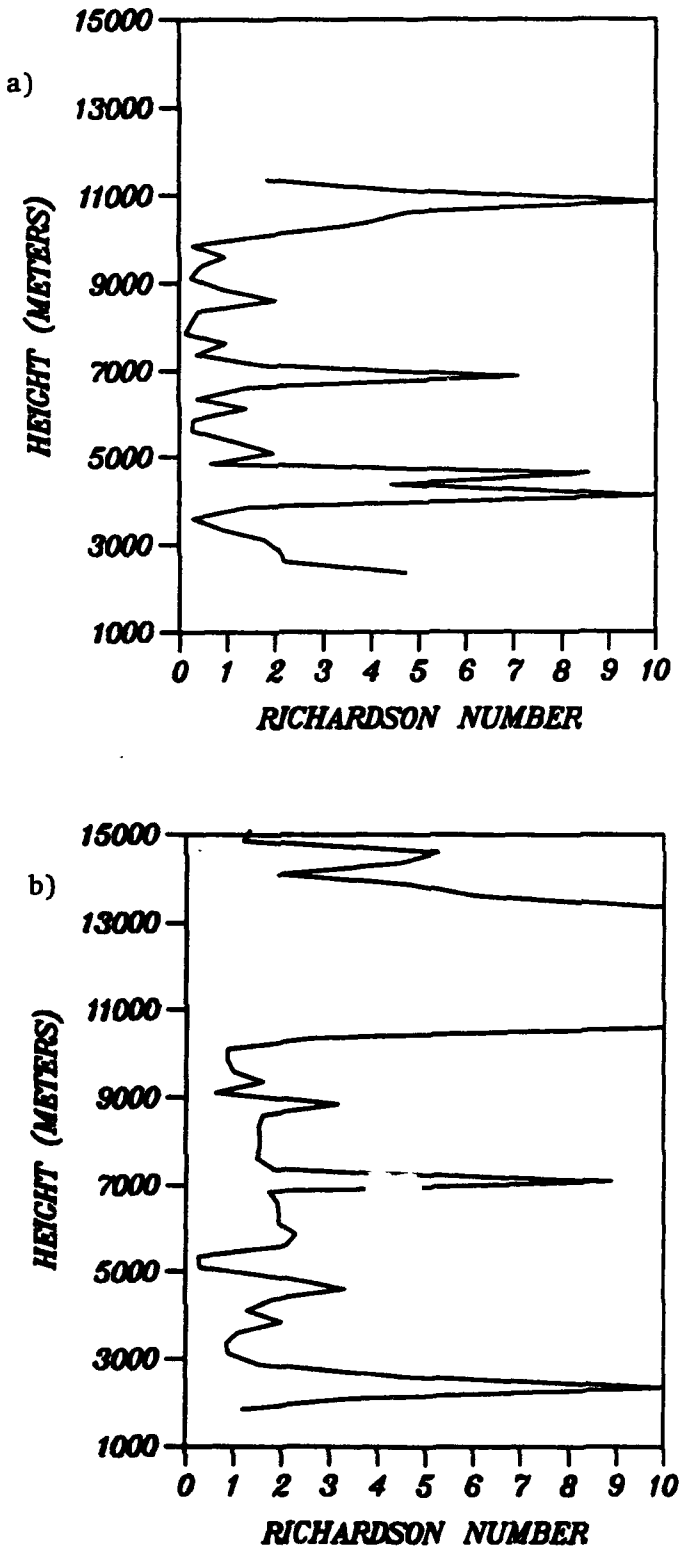

4.2 0000 UTC 20 January Richardson number profile for a) Elbert and b) Denver

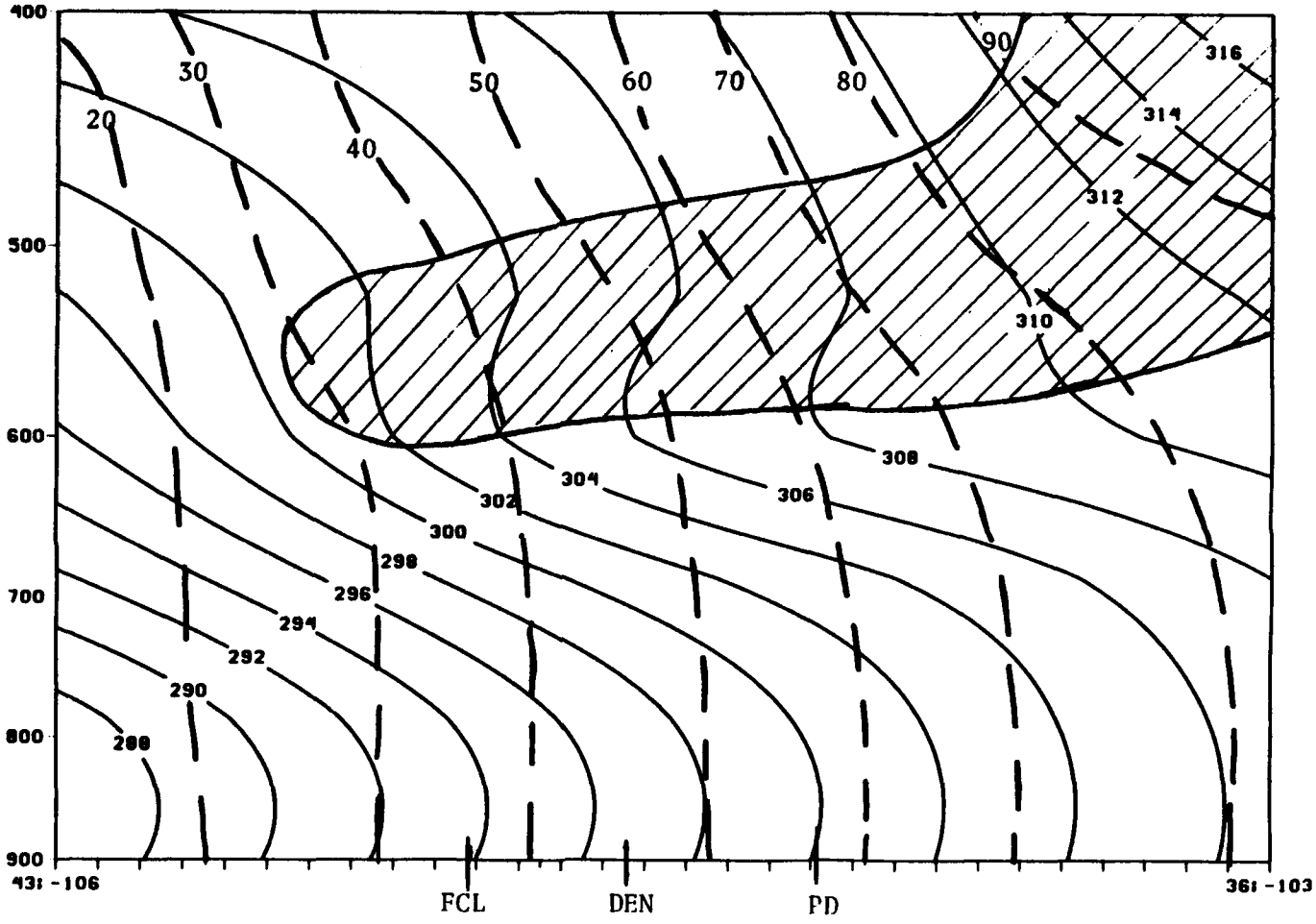

4.3 Vertical cross section of θ_e and M_g. Solid lines are θ_e contours in °K, dashed lines are M_g contours in ms^{-1}. FCL, DEN, PD represent approximate positions of Fort Collins, Denver, and the Palmer Divide respectively.

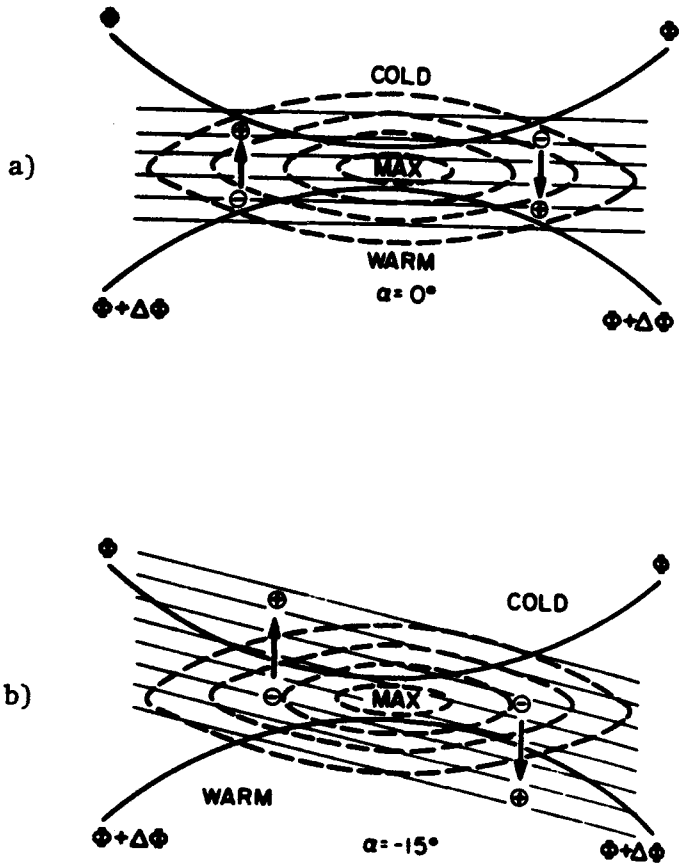

4.4 Schematic illustration of a jet streak, a) no temperature advection case and b) warm air advection case. Thick solid lines, thick dashed lines, thin solid lines, thick solid arrows, and plus and minus signs represent geopotential height contours, isotachs, isotherms, sense of cross-flow ageostrophic wind component at level of maximum wind, and sense of midtropospheric pressure-coordinate vertical velocity, ω respectively (after Keyser and Shapiro 1986)

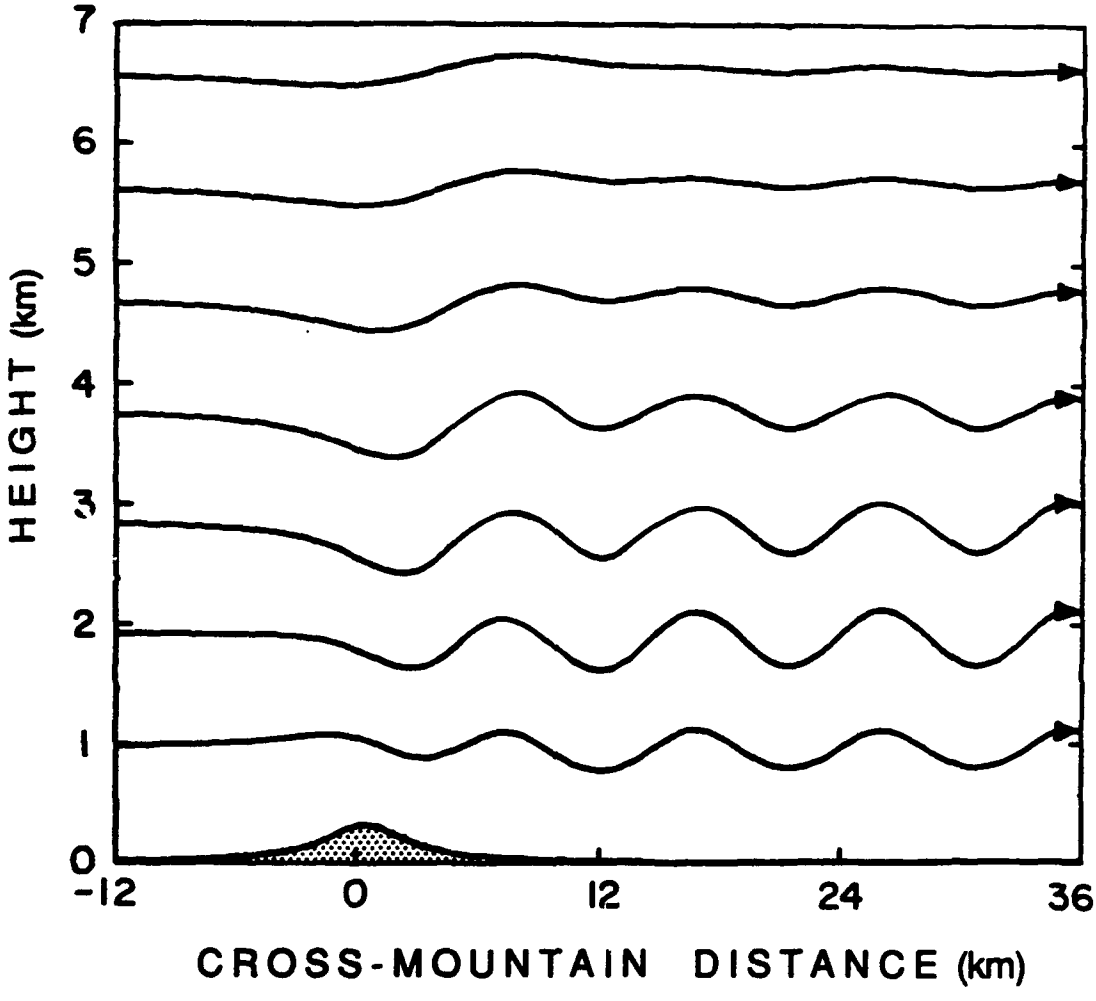

4.5 Model of trapped mountain waves in the x-z plane. Thin lines are streamlines (after Durran 1986).

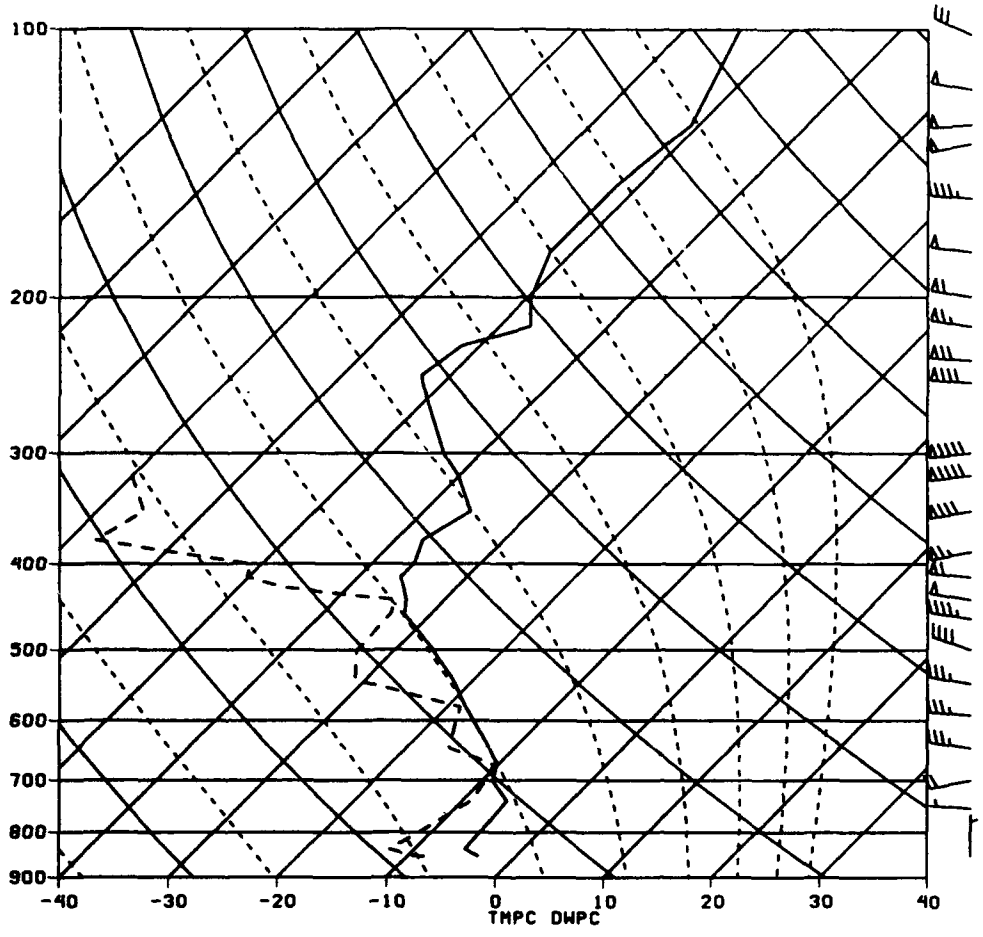

4.6 Grand Junction, CO 0000 UTC 20 January rawinsonde sounding. Heavy solid line is the temperature curve, heavy dashed line the dewpoint curve. Horizontal solid lines are isobars (mb), solid diagonal lines sloping from lower left to upper right are isotherms (°C), dry adiabats are the solid curved lines sloping from the lower right to upper left, and the moist adiabats are the dashed lines sloping from lower right to upper left. Pennants on wind shafts represent 25 ms^{-1}, long barbs 5 ms^{-1}, and short barbs 2.5 ms^{-1}.

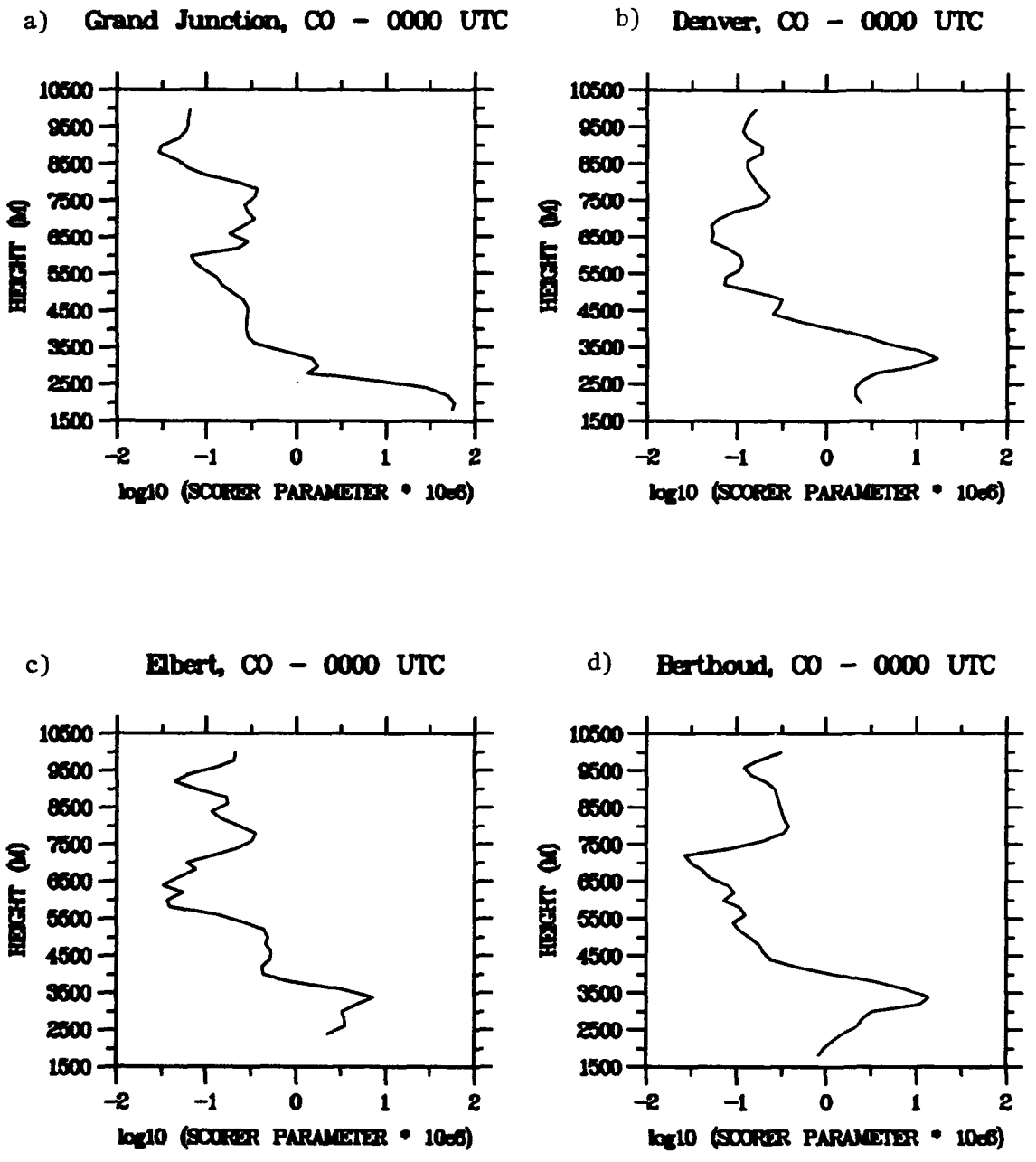

4.7 (a) 0000 UTC 20 January Scorer parameter profiles for a) Grand Junction, b) Denver, c) Elbert, and d) Berthoud.

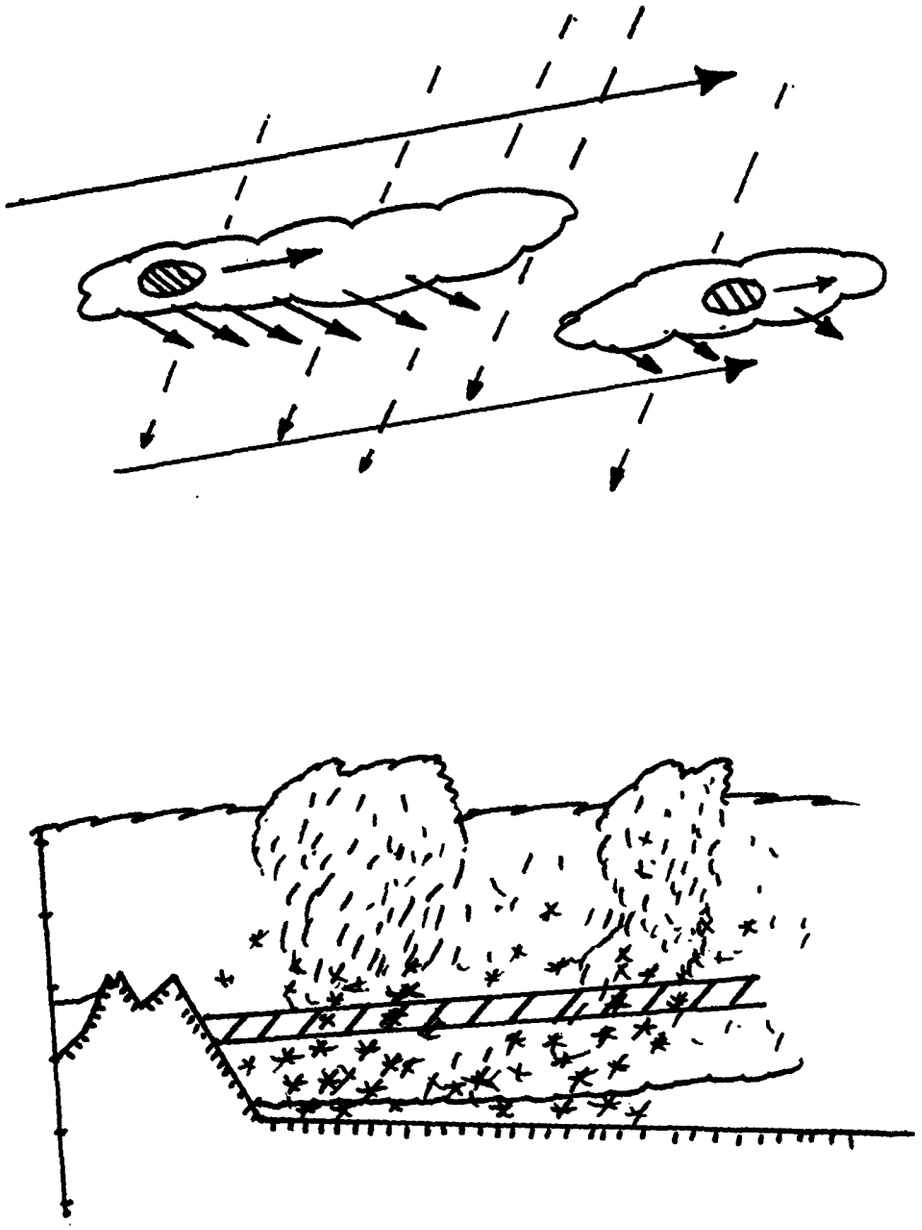

4.8 Conceptual model of snow band structure in a) plan view and b) vertical profile. See text for explanation.

Chapter 5

DISCUSSION AND CONCLUSIONS

This research used the WISP-91 data set to examine a winter storm that occurred over northeast Colorado on 19-20 January 1991 with the objectives of detailing observations of snow bands and gaining insight into possible band formation mechanisms. Radar data were used to identify and study the organization and structure of the bands as well as provide quantitative insight into their kinematic structure. Terrain features had a significant impact on snow fall amounts over the region, particularly when considering the low level flow and its orientation to topographic barriers. However, above the arctic air mass well defined bands of higher radar reflectivity had similarities to precipitation bands studied by other researchers with the exception of mountain wave induced bands and associated trapped wave phenomena. Various causes for precipitation band formation published in the literature were evaluated for their potential in causing the snow bands observed in this case.

The WISP-91 data set permitted mesoscale analysis of surface and upper air data obtained from 59 automated weather stations over northeast Colorado, Wyoming and Nebraska, in addition to the standard surface airway observation reporting stations. The data set also included radar data from CSU CHILL and MHR radars, 3 hourly CLASS rawinsonde soundings from five to six sites over northeast Colorado, two wind profilers, microwave radiometers, and a special snow spotter network. Software was written to give existing meteorological analysis and display packages the capability of

processing the volume of data collected during the experiment. Also, terrain data was incorporated into analyses, including overlaying radar data on terrain maps.

On the synoptic scale, an upper level trough of low pressure and associated arctic cold front moved over northeast Colorado. Post-frontal northeast surface flow brought upslope conditions to the region with up to 15 cm (6 in) of snow over an 18 hour period. The heaviest snow fall was organized into three distinct regions (see Fig. 2.1). Isotherm and streamline analysis showed that cold air damming as defined by Wesley (1991) was not present in this case. Blocking of the arctic air by the mountains did occur but not with sufficient intensity to cause formation of a low level barrier jet. Strong west-southwesterly flow (over 50 ms^{-1}) aloft associated with a jet streak, and a favorable thermodynamic profile, caused trapped mountain waves down wind of the Continental Divide. The vertical thermodynamic profile also showed the temperature was between -12 and -15 °C near 600 mb which is a favorable condition for heavy snows.

Radar data showed mesoscale snow bands were a common feature of this storm. There was a preference for more intense band formation over the southern portions of the project area. A video loop of radar data that included terrain contours helped identify two distinct flow features, a low level regime that was influenced by terrain, and an upper level regime where bands moved in response to free atmosphere motions. Within the bands, higher reflectivity cores, (typically 5-10 dBZ greater than the surrounding band echo) were present. The cores transited the band following the upper level winds, while the band itself drifted slowly to the south-southeast. Radar observations of trapped mountain waves illustrated the importance of considering mountain induced flow modifications in snowstorms and snow band formation over eastern Colorado.

Analysis of EVAD derived vertical motion profiles from both CSU-CHILL and MHR radar data, indicated similar values to vertical motion results for northeast

Colorado winter storms obtained by other researchers. The results of the experiment indicated that peak mesoscale vertical motions were on the order of 0.2 ms^{-1} between 2500 and 3000 m (MSL) and were associated with an ill-defined snow band and associated region of higher reflectivities near the surface.

Dual-Doppler analysis at one particular time provided insight into the horizontal flow structure. Low level northeasterly winds backed with height to a shallow shear zone between 3000 and 3500 m (MSL). Richardson number calculations, using mean winds derived from the dual-Doppler synthesis region and the Berthoud Class sounding thermodynamic data, agreed reasonably well with values obtained from soundings alone.

Of the band formation mechanisms examined, conditional instability and jet streak induced vertical velocities could have triggered slantwise convection and thus bands since the atmosphere showed potential for CSI. Mountain waves also played a role in explaining the radar echo structure. Midtropospheric vertical motions associated with the entrance region of a jet streak were shifted northward by warm air advection along the jet and helped explain the well defined band over the Palmer Divide. Satellite imagery showed this band extended west beyond the radar coverage area to the axis of the 300 mb trough near the Utah-Colorado border. Other bands farther north did not appear to have as strong a link to jet streak vertical motions, but instead seem related to conditional instability and CSI induced circulations. Scorer parameter calculations indicated nearly stationary trapped mountain waves, with wavelengths of about 12 km, occurred in the band over the Palmer Divide. Regions of vertical ascent associated with the waves, secondary ice production methods, and transport of surface based ice crystals, may have been responsible for creating small ice particles which in turn could have been important in a seeder-feeder process (where clouds associated with low level flow may provide the feeder portion of the couplet). Reflectivity cores within other

bands appeared to be weak convective regions, especially at higher levels, that probably provided seed ice crystals in a seeder-feeder process involving lower level clouds.

5.1 Suggestions for Future Research

Several questions could not be completely answered in this study and may form the basis for further research. These questions are:

1. What is the formation mechanism for the reflectivity cores? Are they truly associated with shallow convection, the result of mountain induced flows, or a combination of both?

2. Are well defined bands necessarily associated with jet streaks or was this case unique in that respect?

3. Are bands induced by mountain waves a common feature and if so are there any favored geographical regions for their formation?

4. What are the detailed microphysical processes associated with the trapped wave phenomena?

A radar based climatological study of snow bands might help resolve the issue of band location with respect to jet streaks and mountain barriers, while aircraft studies would provide more insight into the microphysics of bands associated with trapped waves. The EVAD technique looks promising as a means of determining mesoscale vertical motions. A sensitivity study comparing true EVAD volume scans with the scanning strategy employed during this experiment would help remove ambiguities surrounding results obtained from low elevation angles used during shallow (compared to thunderstorms) winter storms.

REFERENCES

Agee, E. M. and S. R. Gilbert, 1989: An aircraft investigation of mesoscale convection over Lake Michigan during the 10 January 1984 cold air outbreak. *J. Atmos. Sci.*, **46**, 1877-1897.

Atlas, D., R. C. Srivastava, and R. S. Sekhon, 1973: Doppler characteristics of precipitation at vertical incidence. *Rev. of Geophys. and Space Phys.* **2**, 1-35.

Auer, A. H. Jr. and J.M White, 1982: The combined role of kinematics, thermodynamics, and cloud physics associated with heavy snowfall episodes. *J. Meteor. Soc. Japan*, **60**, 500-507.

Battan, L. J., 1973: Radar observations of the atmosphere. Univ. Of Chicago Press, Chicago, Ill.

Bennetts, D. A. and B. J. Hoskins 1979: Conditional symmetric instability - a possible explanation for frontal rainbands. *Quart. J. Roy. Meteor. Soc.*, **105**, 945-962.

Boatman, J. F. and R. F. Reinking, 1984: Synoptic and mesoscale circulations and precipitation mechanisms in shallow upslope storms over the western high plains. *Mon. Wea. Rev.*, **112**, 1725-1744.

Bohne, A., 1979: A dual-Doppler radar study of mesoscale winter snow bands. Tech Report 40, 196 pp. Available from the Laboratory for Atmospheric Probing. Dept .of the Geophysical Sciences, Univ. of Chicago, Chicago, Ill.

Browning, K. A. and R. Wexler, 1968: The determination of kinematic properties of a wind field using Doppler radar. *J. Appl. Meteor.*, 7, 105-113.

Byrd, G. P., 1989: A composite analysis of winter season overruning precipitation bands over the southern plains of the United States. *J. Atmos. Sci.*, **46**, 1119-1132.

Carbone, R. E. and A. Bohne, 1975: Cellular snow generation - A Doppler radar study. *J. Atmos. Sci.*, **39**, 1384-1394.

Corby, G. A. and C. E. Wallington, 1956: Airflow over mountains: The lee wave amplitude. *Quart. J. Roy. Meteor. Soc.*, **82**, 266-274.

Davies-Jones, R. P., 1979: Dual-Doppler radar coverage area as a function of measurement accuracy and spatial resolution, *J. Appl. Meteor.*, **18**, 1229-1233.

desJardins, M. L., R. F. Brill, and S.S. Schotz, 1991: GEMPAK5 User's guide. NASA Tech Memo 4260.

desJardins, M. L., and R. L. Peterson, 1985: GEMPAK: A meteorological system for research and education. *Preprints, Int'l Conf on Interactive Information and Processing Systems for Meteorology, Oceanography, and Hydrology, Los Angeles, American Meteorological Society*, 313-319.

Dirks, R. A., J. P. Kuettner, and J. A. Moore, 1988: Genesis of Atlantic Lows Experiment (GALE): An overview. *Bull. Amer. Meteor. Soc.*, **69**, 148-172.

Doviak, R. J. and D. S. Zrnic, 1984: Doppler radar and weather observations. Academic Press Inc., New York, 458 pp.

Dunn, L., 1987: Cold-air damming by the Front Range of the Colorado Rockies and its relationship to locally heavy snows. *Wea. Forecasting*, **2**, 177-189.

Dunn, L. 1988: Vertical motion evaluation of a Colorado snowstorm from a synoptician's perspective. *Wea. Forecasting*, **3**, 261-272.

Durran, D. R., 1986: Mountain Waves. Chapter 20 in *Mesoscale Meteorology and Forecasting* . P. S. Ray, Ed. American Meteorological Society, Boston, MA 472-492.

Emanuel, K. A., 1983a: On assessing local conditional symmetric instability from atmospheric soundings. *Mon. Wea. Rev.*, **111**, 2016-2033.

Emanuel, K. A., 1983b: The Lagrangian parcel dynamics of moist symmetric instability. *J. Atmos. Sci.*, **40**, 2368-2376.

Emanuel, K. A., 1988: Observational evidence of slantwise convective adjustment. *Mon. Wea. Rev.*, **116**, 1805-1816.

Hane, C. E., 1986: Extratropical squall lines and rainbands. Chapter 16 of *Mesoscale Meteorology and Forecasting*, P. S. Ray, Ed. American Meteorological Society, Boston, MA 359-389.

Heckman, B. E. and T. Dulong 1989: Doppler radar reflectivity bands: Comparison with 500 mb patterns and implications for winter nowcasting. *Preprints 3rd Conf. on the Aviation Weather System*, Anaheim, CA. 233-237.

Herzegh, P. H. and P. V. Hobbs, 1980: The mesoscale and microscale structure and organization of clouds and precipitation in midlatitude cyclones. Part II: Warm-frontal clouds. *J. Atmos. Sci.*, **37**, 597-611.

Heymsfield, G. M., 1979: Doppler radar study of a warm frontal region. *J. Atmos. Sci.*, **36**, 2093-2107.

Hobbs, P. V., T. J. Matejka, P. H. Herzegh, J. D. Locatelli, and R. A. Houze, Jr., 1980: The mesoscale and microscale structure and organization of clouds and precipitation in midlatitude cyclones. Part I: A case study of a cold front. *J. Atmos. Sci.*, **37**, 568-596.

Hobbs, P. V.and P. O. G. Persson, 1982: The mesoscale and microscale structure and organization of clouds and precipitation in midlatitude cyclones. Part V: The substructure of narrow cold-frontal rain bands, *J. Atmos. Sci.*, **39**, 280-295.

Hobbs P. V. and A. L. Rangno, 1985: Ice particle concentrations in clouds. *J. Atmos. Sci.*, **42**, 2523-2549.

Houze, R. A., S.A. Rutledge, T. J. Matejka, and P. V. Hobbs, 1981: The mesoscale and microscale structure and organization of clouds and precipitation in midlatitude cyclones. Part III: Air motions and precipitation growth in a warm-frontal rainband. *J. Atmos. Sci.*, **38**, 639-649.

Kessinger, C. J. and W. C. Lee, 1991: Evaluation of real-time dual Doppler analysis for use during field operations. *Preprints 25th Int'l. Conf. on Radar Meteorology*, Paris, France 756-759.

Keyser, D. and M. A. Shapiro, 1986: A review of the structure and dynamics of upper-level frontal zones. *Mon. Wea. Rev.*, **114**, 452-499.

Koch, S.E., M. desJardin, and P. J. Kocin, 1983: An interactive Barnes objective map analysis scheme for use with satellite and conventional data. *J. Climate Appl. Meteor.*, **22**, 1487-1503.

Lhermitte, R. M. and D. Atlas, 1961: Precipitation motion by pulse Doppler radar. *Proc. Ninth Weather Radar Conf.*, Boston, MA. Amer. Meteor. Soc., 218-223.

Lilly, D. K., 1986: Instabilities. Chapter 11 of *Mesoscale Meteorology and Forecasting*, P. S. Ray, Ed. American Meteorological Society, Boston, MA 259-271.

Lilly, D. K., 1981: Doppler radar observations of upslope snowstorms. *Preprints, 2nd Conf. on Mountain Meteorology*, AMS, Steamboat Springs, CO. Nov 1981, 346-353.

Lindzen, R. S. and K. K. Tung, 1976: Banded convective activity and ducted gravity waves. *Mon. Wea. Rev.*, **104**, 1602-1617.

Long, A. B., B. A. Campistron, and A. W. Huggins, 1990: Investigations of a winter mountain storm in Utah. Part I: Synoptic analyses, mesoscale kinematics and water release rates. *J. Atmos. Sci.*, **47**, 1302-1322.

Marwitz, J., 1980: Winter Storms over the San Juan Mountains. Part I: Dynamical processes. *J. Appl Meteor.*, **19** 913-926.

Marwitz, J. and D. Day, 1991: The effect of melting in a Denver snow dump. *Preprints, First Int'l Winter Storms Symposium*, New Orleans, 14 - 18 Jan 1991, 241-244.

Matejka, T. J., R. A. Houze, and P. V. Hobbs, 1980: Microphysics and dynamics of clouds associated with mesoscale rainbands in extratropical cyclones. *Quart. J. Roy. Meteor. Soc.*, **106**, 29-56.

Matejka, T. J., and R. C. Srivastava, 1991: An improved version of the extended velocity-azimuth display analysis of single-Doppler radar data. *J. Atmos. Ocean. Tech.*, **8**, 453-466.

Mohr, C., L.J. Miller, R. Vaughan, and H. Frank, 1986: The merger of mesoscale datasets into a common Cartesian format for efficient and systematic analysis. *J. Atmos. Oceanic. Technol.*, **3**, 143-161.

Moore, J. T., and P. D. Blakely, 1988: The role of frontogenetical forcing and conditional symmetric instability in the midwest snowstorm of 30-31 January 1982. *Mon. Wea. Rev.*, **116**, 2155-2171.

Mulvey, G. J., 1977: Physical mechanisms of extra area effects from weather modification. Phd Dissertation, Dept.of Atmospheric Science, Colorado State University, Fort Collins, CO, 138 pp.

NCAR, 1991: 1991 Winter icing and storms project (WISP) data catalog, 15 January - 5 April 1991, Available from National Center for Atmospheric Research, Research Applications Program Office, Boulder, CO.

Parsons, D.B and P. V. Hobbs, 1983: The mesoscale and microscale structure and organization of clouds and precipitation in midlatitude cyclones. XI: Comparisons between observational and theoretical aspects of rainbands. *J. Atmos. Sci.*, **40**, 2377-2397.

Queney, P., G. Corby, N. Gerbier, H. Koschmieder, and J. Zierep, 1960: The airflow over mountains. WMO Tech. Note **34**, 135 pp.

Raddatz, R. L. and M. L. Khandekar, 1979: Upslope enhanced extreme rainfall events over the Canadian western plain: A mesoscale numerical simulation. *Mon. Wea. Rev.*, **107**, 650-661.

Ramamurthy, M. K., R. M. Rauber, B. P. Collins, M. T. Shields, P. C. Kennedy, and W.C. Clark, 1991: UNIWIPP: A University of Illinois field experiment to investigate the structure of mesoscale precipitation in winter storms. *Bull. Amer. Meteor. Soc.*, **72**, 764-776.

Raman, S. and A. J. Riordan, 1988: The Genesis of Atlantic Lows Experiment: The planetary-boundary-layer subprogram of GALE. *Bull. Amer. Meteor. Soc.*, **69**, 161-172.

Rasmussen, R. M. and M. K. Politovich, 1990: WISP Scientific Overview. NCAR publication available from authors, P. O. Box 3000, Boulder, Co 80307

Rasmussen, R., M Politovich, J. Marwitz, W. Sand, J. McGinley, J. Snook, R. Pielke, S. Rutledge, D. Wesley, G. Stossmeister, B. Bernstein, K. Elmore, N. Powell, E. Westwater, B. Stankov, D. Burrows, 1992: Winter Icing and Storms Project. Accepted for publication in *Bull. Amer. Meteor. Soc.*

Rauber, R. M., L. O. Grant, D. Feng, and J. B Snider, 1986: The characteristics and distributions of cloud water over the mountains of northern Colorado during wintertime storms. Part I: Temporal variations. *J. Clim Appl. Meteor.*, **25**, 468-488.

Reinking, R. F. and J. F. Boatman, 1986: Upslope precipitation events. Chapter 19 of *Mesoscale Meteorology and Forecasting*, P. S. Ray, Ed. American Meteorological Society, Boston, MA 437-471.

Reuter, G. W. and M. K. Yau, 1990: Observations of slantwise convective instability in winter cyclones. *Mon. Wea. Rev.*, **118**, 447-458.

Reynolds, D. W. and A. S. Dennis, 1986: A review of the Sierra Cooperative Pilot Project, Bull. *Amer. Met. Soc.*, **67**, 513-523.

Riordan, A. J., 1990: Examination of the mesoscale features of the GALE coastal front of 24-25 January 1986. *Mon. Wea. Rev.*, **118**, 258-282.

Rogers, D. C. and G. Vali, 1987: Ice crystal production by mountain surfaces. *J. Clim. Appl. Meteor.*, **26**, 1152-1168.

Rutledge, S. A. and P. V. Hobbs, 1983: The mesoscale and microscale structure and organization of clouds and precipitation in midlatitude cyclones. Part VIII: A model for the "seeder-feeder" process in warm-frontal rainbands, *J. Atmos. Sci.*, **40**, 1185-1206.

Rutledge, S. A. and P. V. Hobbs, 1984: The mesoscale and microscale structure and organization of clouds and precipitation in midlatitude cyclones. Part XII: A diagnostic modeling study of precipitation development in narrow cold-frontal rainbands. *J. Atmos. Sci.*, **41**, 2949-2972.

Sanders, F., 1986: Frontogenesis and symmetric stability in a major New England snowstorm. *Mon. Wea. Rev.*, **114**, 1847-1862.

Sanders, F. and L. F. Bosart 1985a : Mesoscale structure in the mega-lopolitan snowstorm of 11-12 February 1983. Part I: Frontogenetical forcing and symmetric instability. *J. Atmos. Sci.*, **42**, 1050-1061.

Sanders, F. and L. F. Bosart 1985b : Mesoscale structure in the mega-lopolitan snowstorm of 11-12 February 1983. Part II: Doppler radar study of the New England snowband *J. Atmos. Sci.*, **42**, 1398-1407.

Sassen, K., A. W. Huggens, A. B. Long, J. B. Snider, and R. J. Meitin, 1990: Investigations of a winter mountain storm in Utah. Part II. Mesoscale structure,

supercooled liquid water development and precipitation processes. *J. Atmos. Sci.*, **47**, 1323-1350.

Schlatter, T. W., D. V. Baker, and J. F. Henz, 1983: Profiling Colorado's Christmas Eve blizzard. *Weatherwise*, **36**, 60-66.

Scorer, R., 1949: Theory of waves in the lee of mountains. *Quart. J. Roy. Meteor. Soc.*, **75**, 41-56.

Shapiro, M. A., 1984: Meteorological tower measurements of a surface cold front. *Mon. Wea. Rev.*, **112**, 1634-1639.

Shields, M.T., R. M. Rauber, and M. K. Ramamurthy, 1991: Dynamical forcing and mesoscale organization of precipitation bands in a midwest winter cyclonic storm. *Mon. Wea. Rev.*, **119**, 936-964.

Snook, J. S., 1992: Current techniques for real-time evaluation of conditional symmetric instability. Accepted for publication in Weather *and Forecasting*.

Srivastava, R. C., T. J. Matejka, T. J. Lorello, 1986: Doppler radar study of the trailing anvil region associated with a squall line. *J. Atmos. Sci*, **43**, 356-377.

Stull, R. B., 1988: An introduction to boundary layer meteorology. Kluwer Academic Publishers, London.

Szoke, E. J., 1991: The use of Doppler radar in the short-range forecasting of snowfall in northeastern Colorado. *Preprints 25th Int'l. Conf. on Radar Meteorology,* Paris, France 71-74.

Toth, J. J., 1991: Surface horizontal pressure gradients in upslope winter storms.*Preprints First Int'l Winter Storms Symposium*, New Orleans, 14-18 Jan., 101-102.

Toth, J. J., 1987: Interaction of shallow cold surges with topography on scales of 100-1000 kilometers. CIRA Publication, Colorado State University, Fort Collins, ISSN No. 07373-5352-8, 135 pp.

Uccellini, L. W. and P. J. Kocin, 1987: The interaction of jetstreak circulations during heavy snow events along the East Coast of the United States. *Wea. Forecasting*, **2**, 289-308.

Walsh, P. A., 1977: Cloud measurements in wintertime clouds. M. S. thesis, Dept. of Atmospheric Science, Univ. of Wyoming, Laramie, 170 pp.

Wesley, D. A., 1991: An investigation of the effects of topography on Colorado Front Range winter storms. Phd Dissertation, Dept.of Atmospheric Science, Colorado State University, Fort Collins, CO, 201 pp.

Wesley, D. A. and R. A. Pielke, 1990: Observations of blocking-induced convergence zones and effects on precipitation in complex terrain, *Atmospheric Research*, **25**, 235-276.

Wesley, D. A., J. F. Weaver, and R. A. Pielke, 1990: Heavy snowfall during an extreme arctic outbreak along the Colorado Front Range. *Natl. Wea Dig.*, **15**, 2-19.

Whiteman, C. D., 1973: Some climatological characteristics of seedable upslope cloud systems in the High Plains. NOAA Tech. Rep. 268 -APCL-27 (NTIS-COM-73-50924/2GI), 43 pp.

Wolfsberg, D. G., K. A. Emanuel, and R. E. Passarelli, 1986: Band formation in a New England winter storm. *Mon. Wea. Rev.*, **114**, 1552-1569.

APPENDIX A

Station Identification and Location Table

APPENDIX A

Station Identification and Location

Below are the station callsigns, World Meteorological Organization station numbers (if assigned), station name, state Identification, country identification, latitude, longitude (- indicates west longitude) and elevation in meters. Radar sites, wind profilers, and CLASS stations are indicated after the station name. All stations, except CHL and MHR had recorded surface weather data.

1K5	724600	Elkhart	KS	US	3700	-10188	1102
4LJ	724630	Lamar	CO	US	3811	-10260	1103
AFF	745310	Colorado Springs (USAF Academy)	CO	US	3891	-10481	1999
AKO	724698	Akron (-Washington Co AP)	CO	US	4017	-10322	1422
ALS	724620	Alamosa (San Luis Valley Reg AP)	CO	US	3745	-10586	2299
APA	724666	Centennial Airport	CO	US	3957	-10483	1789
ARV	99999	Arvada PROFS	CO	US	3980	-10510	1635
ASE	724676	Aspen (-Pitkin Co/Sardy Field AP)	CO	US	3921	-10686	2379
AUR	99999	Aurora PROFS	CO	US	3977	-10487	1608
BFF	725660	Scottsbluff (Wm B Heilig AP)	NE	US	4187	-10360	1206
BGD	99999	Briggsdale PROFS	CO	US	4065	-10434	1480
BJC	724699	Broomfield (Jefferson Co AP)	CO	US	3990	-10512	1722
BKF	724695	Aurora (Buckley AP)	CO	US	3972	-10478	1726
BOU	99999	Boulder PROFS	CO	US	4001	-10525	1611
BRI	99999	Brighton PROFS	CO	US	4000	-10480	1512
BYE	99999	Byers PROFS	CO	US	3974	-10413	1554
C96	99999	Winter Park	CO	US	3989	-10582	2615
CAG	725710	Craig (-Moffat AP)	CO	US	4052	-10755	1915
CAO	723600	Clayton (Muni AP)	NM	US	3645	-10315	1515
CHL	99999	CSU CHILL Radar	CO	US	4045	-10464	1420
COS	724660	Colorado Springs (Muni AP)	CO	US	3881	-10471	1881
CYS	725640	Cheyenne (AP)	WY	US	4115	-10482	1872
DEN	724690	Denver (Stapleton AP)/Profiler	CO	US	3975	-10487	1625
EGE	724675	Eagle (Co AP)	CO	US	3965	-10691	1985
ELB	99999	Elbert PROFS	CO	US	3923	-10463	2135
EPK	99999	Estes Park PROFS	CO	US	4037	-10556	2395
ERI	99999	Erie, PROFS	CO	US	4005	-10501	1584
FCL	724697	Fort Collins	CO	US	4058	-10508	1524
FCS	724680	Fort Carson (Butts AAF)	CO	US	3868	-10477	1779
FOR	99999	Fort Collins PROFS	CO	US	4059	-10515	1603
FTM	99999	Fort Morgan PROFS	CO	US	4033	-10380	1370
GCK	724515	Garden City (Muni AP)	KS	US	3793	-10071	878
GLD	724650	Goodland (Renner Fld-Muni AP)	KS	US	3937	-10170	1124
GLY	99999	Greeley PROFS	CO	US	4042	-10463	1415
GXY	99999	Greeley (-Weld Co AP)	CO	US	4042	-10470	1437
ISG	99999	Idaho Springs PROFS	CO	US	3968	-10549	3455
KIM	99999	Kimball Mobile CLASS	NE	US	4122	-10467	1488
KNB	99999	Keensburg PROFS	CO	US	4007	-10451	1519
LAK	99999	Lakewood PROFS	CO	US	3970	-10516	1825
LAR	725645	Laramie (Gen Brees Fld)	WY	US	4132	-10568	2217
LBF	725620	North Platte (Lee Bird Fld)	NE	US	4113	-10068	849
LGM	99999	Longmont PROFS	CO	US	4017	-10516	1536
LHX	724635	La Junta (Muni AP)	CO	US	3805	-10353	1285
LIC	724665	Limon (Muni AP)	CO	US	3930	-10370	1696
LTN	99999	Littleton PROFS	CO	US	3957	-10496	1739
LVE	99999	Loveland PROFS	CO	US	4041	-10504	1513
MHR	99999	NOAA MHR Radar	CO	US	3987	-10478	1585
NUN	99999	Nunn PROFS	CO	US	4080	-10476	1638
P01	99999	Tie Siding PAM	WY	US	4106	-10554	2387
P02	99999	Burns PAM	WY	US	4118	-10436	1668
P03	99999	Kimball PAM/CLASS	NE	US	4119	-10367	1494
P04	99999	Sidney PAM	NE	US	4110	-10298	1307
P05	99999	Rist Canyon PAM	CO	US	4061	-10530	2210
P06	99999	Owl Canyon/Lew Grant Farm PAM	CO	US	4077	-10509	1657
P07	99999	Carr PAM	CO	US	4090	-10488	1743

P08	99999	Hereford/Poly Berger PAM	CO	US	4097	-10429	1615
P09	99999	Battle Canyon PAM	CO	US	4095	-10368	1526
P10	99999	Stoneham PAM	CO	US	4070	-10369	1361
P11	99999	Sterling PAM	CO	US	4061	-10321	1202
P12	99999	Berthoud PAM/CLASS	CO	US	4032	-10514	1577
P13	99999	Masters PAM	CO	US	4029	-10424	1369
P14	99999	Wiggins PAM/CLASS	CO	US	4029	-10405	1384
P15	99999	Midway PAM	CO	US	4022	-10340	1356
P16	99999	Akron PAM/CLASS	CO	US	4017	-10321	1420
P17	99999	Nederland PAM	CO	US	3995	-10551	2589
P18	99999	Bettasso/Boulder Filter PAM	CO	US	4001	-10534	1951
P19	99999	North of Bennett PAM	CO	US	3991	-10440	1564
P20	99999	Hoyt PAM	CO	US	4002	-10413	1460
P21	99999	Woodrow PAM	CO	US	3999	-10357	1359
P22	99999	Stapleton PAM	CO	US	3977	-10487	1606
P23	99999	Front Range Airport PAM	CO	US	3979	-10456	1672
P24	99999	South of Bennett PAM	CO	US	3956	-10445	1795
P25	99999	Last Chance/Lusto SP PAM	CO	US	3961	-10358	1570
P26	99999	Anton PAM	CO	US	3972	-10312	1457
P27	99999	Sedalia Dawson Butte PAM	CO	US	3937	-10497	1881
P28	99999	Elizabeth PAM	CO.	US	3943	-10462	1981
P29	99999	Bijou Saum Ranch PAM	CO	US	3941	-10424	1852
P30	99999	Agate PAM	CO	US	3946	-10394	1664
P31	99999	Monument PAM	CO	US	3909	-10486	2146
P32	99999	Elbert PAM/CLASS	CO	US	3923	-10463	2135
P33	99999	Matheson PAM	CO	US	3905	-10398	1874
P34	99999	Limon PAM	CO	US	3918	-10370	1694
P35	99999	Flagler PAM/CLASS	CO	US	3936	-10304	1480
P36	99999	Elicott PAM	CO	US	3887	-10441	1876
P37	99999	Truckton/Yoder PAM	CO	US	3877	-10417	1803
P38	99999	Punkin Center PAM	CO	US	3884	-10388	1692
P39	99999	Wild Horse PAM	CO	US	3891	-10298	1408
PLV	99999	Platteville Mobile CLASS	CO	US	4022	-10480	1515
PTL	99999	Platteville PROFS/Wind Profiler	CO	US	4026	-10487	1449
PUB	724640	Pueblo (Mem AP)	CO	US	3828	-10451	1439
RAY	99999	New Raymer Mobile CLASS	CO	US	4061	-10384	1430
ROL	99999	Rollinsville PROFS	CO	US	3991	-10549	2748
RWL	725745	Rawlins (Muni AP)	WY	US	4180	-10720	2055
SNY	725610	Sidney (Muni AP)	NE	US	4110	-10298	1312
TAD	724645	Trinidad	CO	US	3725	-10433	1750
WRD	99999	Ward PROFS	CO	US	4004	-10554	3004
ZZZ	99999				99999	99999	99999

APPENDIX B

Summary of Data Display Development

APPENDIX B

Summary of Data Display Development

The GEneral Meteorological data assimilation, analysis and display software PAcKage (GEMPAK) developed by the National Aeronautics and Space Administration (NASA) was used extensively in the analysis of meteorological data particularly, conventional surface and upper air meteorological data (desJardins and Peterson, 1985; Koch *et al.* 1983). The breadth and utility of GEMPAK programs saved considerable time in analysis since virtually any data type or parameter can be analyzed and displayed with only minor modifications to the GEMPAK command files (desJardins *et al.* 1991). Most of the figures in this thesis showing conventional data were prepared using GEMPAK. This required writing FORTRAN programs to convert a wide variety of data formats to GEMPAK format as well as initializing and organizing GEMPAK data files. The primary data source was NCAR. Their WISP 91 Data Catalog (NCAR, 1991) gives a complete description of data collected during the experiment. Conversion programs were written for the following data sets:

Portable Automated Mesonet (PAM) surface observations

Prototype Regional Operational Forecast System (PROFS) surface observations

Cross-chain Loran Atmospheric Sounding System (CLASS) rawinsonde observations

National Weather Service rawinsonde observations

30 second U. S. Geological Survey topographic data

Wind profiler observations

Data was also analyzed and displayed using the PLOT GKS graphics package developed at Oregon State University and later modified and expanded at Colorado State University. Time - height series, Scorer parameter, stability analyses, and some radar data displays were plotted with this program. FORTRAN programs were written to put the the following into network common data format - netcdf files used by the PLOT GKS program:

PAM pressure data

Profiler data

30 second U. S. Geological Survey topographic data

Extended Vertical Azimuth Display (EVAD) data

Time-height cross sections of EVAD derived divergence, vertical velocity, Doppler radial velocity, and reflectivity fields

Dual Doppler analyses of vertical velocity, horizontal velocity, divergence, and reflectivity fields

In addition to PLOT GKS, other programs were used to edit and display radar data obtained from the CSU CHILL radar and the Mile High Radar (MHR). Raw data were checked for folded Doppler velocities and unfolded if necessary interactively using the NCAR developed Research Data Support System (RDSS) editing software on UNIX® based SUN® workstations. Vertical cross sections were also prepared and examined using this software. After completion of editing, data were converted from radar spherical coordinates to Cartesian coordinates with the Sorted Position Radar INTerpolation (SPRINT) software package. Finally, the Custom Editing and Display of Reduced Information in the Cartesian Space (CEDRIC) Doppler radar analysis program was used for single- and dual-Doppler data analysis and creation of netcdf data

files. See Mohr *et al.* (1986) for more information on SPRINT and CEDRIC. The netcdf files generated by SPRINT and CEDRIC were called by PLOT GKS for data display. Control of the displays was accomplished through manipulation of a command file called on execution of PLOT GKS.

RDSS was used in conjunction with the X-Windows XWD, San Diego Supercomputer Center IMCONV, and Wavefront IMF_DSPL programs, on a Silicon Graphics Iris® Personal Work Station to generate loops of MHR reflectivity and velocity fields at the Colorado State University Visualization Laboratory. The loops were then written to a video disk for subsequent recording on videotape. Also, an overlay of terrain contours obtained from the 30 second U. S. Geological Survey terrain height data was included on the loop. This provided insight into location and movement of echoes with respect to major terrain features.

APPENDIX C

Colorado State University CHILL and Mile High Radar Specifications

CSU-CHILL Radar Characteristics in WISP91

System:	
Doppler Capability	yes
System Gain (dB) [Assumed to be antenna gain minus waveguide loss. Also CHILL virtually never operates w/o the radome]	
ZDR Mode	39
Bypass Mode	41
Polarisation [can vary from pulse to pulse]	Xmit H Rec H Xmit V Rec V
Antenna:	
Shape	parabolic
Feed	center
Diameter (m)	8.5
Beamwidth (H/V deg)	.96
Antenna Gain (dB)	43.3 dB
First Sidelobe (1 way db)	-25 [radome on]
Scan Rate (deg/s)	
Asimuth	0–24
Elevation	0–15
Noise Temperature (k) [including waveguide]	≈ 100
Transmitter:	
Wavelength (cm)	11
Frequency (MHs)	2725
Peak Power (kW)	600
Pulse Width (micro-sec)	1.0
PRF (Hs)	1050 [WISP91 average]

CSU-CHILL Radar Characteristics – continued

Receiver:	
Noise temp (K)	≈ 420
Noise Figure (dB)	4.0
Transfer function	
Doppler	linear
Intensity	linear
Log Channel [Did not exist in WISP91]	
Linear channel	
Bandwidth (MHz)	5
Dynamic Range (dB)	50
Noise Power (dBm)	-111.1
Min detectable Signal (dBm)	≈ −125
Min Det Refl. Factor	
[rain @ 50 km, dBZ	-15 [based on S/N of -15 dB]
Data Acquisition:	
No. of range gates	500–1400
Range gate spacing (m)	150
No. of Samples	55–128 [range for WISP91]
Recorded (R) and Displayed (D) Data Fields:	
Log Power hor.	R, D
Normalised Coherent Power	R, D
Spectrum Width	R, D
Mean radial velocity	R, D

Capabilities

	MHR
System	
Doppler Capability	yes
System Gain (dB)	
Radome on	43
Radome off	—
Polarization	Xmt Rec H
Antenna	
Shape	parabolic
Feed	center
Diameter (m)	8.2
Beamwidth (H/V deg)	0.9
Antenna gain	44
First Sidelobe (1 way dB)	
Radome on	-25
Radome off	
Scan rate (deg/s)	
Azimuth	0-30
Elevation	0-15
Noise temperature (K)	≈ 100
(includes waveguide)	
Transmitter	
Wavelength (cm)	10
Frequency (MHz)	
Peak Power (kW)	700
Pulse Width (us)	1.6
PRF (Hz)	250-1250
Receiver	
Noise temp. (K)	400
Noise figure (dB)	3.8
Transfer function	
Doppler	IF linear
Intensity	IF linear
Log Channel	
Bandwidth (MHz)	—
Dynamic Range (dB)	—

	MHR
Noise power (dBm)	—
Linear Channel	
Bandwidth (MHz)	0.6
Dynamic Range (dB)	100
Noise power (dBm)	-107
Min. Det. Signal (dBm)	-122
Min. Det. Refl. Factor (Rain @ 50 km, dBz)	-18
Data Acquisition	
No. of range gates (intervals of 256 gates)	256-1024
Range gate spacing (m)	225-900
No. of samples	45, 14
Recorded (R) and Displayed (D) Data Fields	
Log Power, hor.	R, D
Coherent power, hor.	
Spectrum width	R, D
Velocity	R, D
Log Power, circ. main power	
Log Power, circ. cross polar.	
Coherent Power, circ. main	
CDR	
Correlation	